Aus dem
Mannheim Zentrum für Translationale Neurowissenschaften (MCTN)
der Medizinischen Fakultät Mannheim
Institut für Neuroanatomie (Leiter: Prof. Christian Schultz)

Plasticity of the axon initial segment in the mouse barrel cortex

Inauguraldissertation
zur Erlangung des medizinischen Doktorgrades
der
Medizinischen Fakultät Mannheim
der Ruprecht-Karls-Universität
zu
Heidelberg

vorgelegt von
Nora Jamann

aus
Berlin
2020

Dekan: Prof. Dr. med. Sergij Goerdt
Referent: Prof. Dr. med. Christian Schultz

CONTENTS

Page

LIST OF ABBREVIATIONS

AcD – axon-carrying dendrite

AIS – axon initial segment

ankG – Ankyrin G

AP – action potential

Ca_v – voltage gated calcium channel

IF – immunofluorescence

K_v – voltage gated potassium channel

MBP – myelin basic protein

Na_v – voltage gated sodium channel

NF-186 – neurofascin-186

PFA – paraformaldehyde

PoM – posteriomedial nucleus of the thalamus

SD – standard deviation

STED – stimulated emission depletion

STORM – stochastic optical reconstruction microscopy

S1BF – primary somatosensory cortex, barrel field

VPM – ventroposteromedial nucleus of the thalamus

WB – Western blot

1 INTRODUCTION

The axon initial segment (AIS) is a molecular microdomain located at the proximal axon of mammalian neurons and is characterized by unique protein scaffolds and a high density of sodium channels. It has been shown to be the main site of action potential (AP) initiation. Recent evidence has uncovered a remarkable structural plasticity of this microdomain, which has direct implications for neuronal excitability and firing properties. Here, I will introduce the different structural components of the AIS scaffold and their role at the AIS. I will then summarize the current evidence on AIS plasticity and the effect it has on neuronal function. Lastly, I will introduce the model systems used in this study to investigate AIS plasticity.

1.1 AIS structure – early EM studies

In electron microscopy studies, it was discovered more than 50 years ago that the AIS is structurally distinct from the somatodendritic compartment (Laatsch and Cowan, 1966; Palay et al., 1968; Peters et al., 1968; Westrum, 1966) as well as the rest of the axon. Ultrastructurally, three key features of the AIS were identified. First, it is characterized by a dense undercoating located directly underneath the plasma membrane but not connected to it, leaving a small gap of a few micrometers. This granular layer has a sharp onset right after the axon. Interestingly, this undercoating can also be found at nodes of Ranvier (noR) (Peters, 1966). However, in distinction to noR, the AIS also contains two unique organelle distributions that make it ultrastructurally easily distinguishable from other neuronal compartments: scattered clusters of ribosomes and microtubule fascicles (Palay et al., 1968). The density of the ribosome clusters appears to be lower than in Nissl substance of the soma or dendrites and it decreases gradually along the AIS. The ribosomes are often localized at tubules of the endoplasmatic reticulum (ER) and they disappear with the onset of myelination. The microtubules are organized in parallel bundles and appear to be crosslinked via “bars” or “arms” (a structure later to be identified as Trim 46 (Harterink et al., 2019)). Depending on the type of neuron, these fascicles contain 3-5, or in some cases up to 22 microtubules per bundle (e.g. in layer V pyramidal neurons). The number of fascicles per AIS can vary between one and 6. Interestingly, mitochondria and neurofilaments also start to be oriented more in parallel once entering the AIS.

1.2 Ankyrin G – master organizer and regulator of neuronal polarity

The main scaffolding protein at the AIS is Ankyrin G (ankG). It belongs to the ankyrin family, a group of scaffolding proteins unified by their role as adaptors between membrane proteins and the submembranous spectrin cytoskeleton of various tissues. They are encoded by three genes: ank1 or ankR ("restricted"), ank2 or ankB ("broad") and ank3 or ankG ("giant"). AnkR is part of the membrane scaffold of erythrocytes, but it can also be found at muscle cells and neurons (Bennett et al., 1985). Ankyrin B (ankB) was first characterized in the brain, where it is localized at axons (Kunimoto, 1995), however it is also found in the peripheral nervous system (Engelhardt et al., 2013). Ank3, the gene encoding ankG, was found to be expressed in several tissues, including the brain (Kordeli et al., 1995). Ankyrins share a similar structure with highly conserved domains (Jenkins and Bennett, 2001). They consist of an N-terminal head domain (Davis and Bennett, 1994) that contains a membrane binding domain with 24 "ank repeats" as well as a spectrin binding domain (Davis and Bennett, 1990; Michaely and Bennett, 1992). The ank repeats form 4 subdomains, which each contain 6 homologous repeats (Michaely and Bennett, 1993). The C-terminal tail domains vary between the different isoforms.

In neurons, three different ankG isoforms can be found. The full-length protein encoded by ank3 has a size of 480 kDa and is therefore termed "giant ankG". Additionally, a shorter 270 kDa brain-specific isoform exists, which lacks most of the 2200 amino-acid tail domain (Kordeli et al., 1995). Both isoforms consist of a serine-threonine-rich domain as well as o-linked n-acetyl glucosamine residues at these sites, which distinguish them from other ankyrins (Zhang and Bennett, 1996). Immunofluorescent stainings revealed localization of the two isoforms at noR in rat sciatic nerve and spinal cord white matter as well as at the AIS of various neuronal cell types (Kordeli et al., 1995). Another splice variant of 190 kDa lacking the serine-rich tail domain is expressed at the AIS. It is non-specific to the brain as it is also found in murine lung and kidney (Kordeli et al., 1995).

Several binding partners of ankG have been identified. As stated above, ankyrins bind spectrins. The isoform present at the AIS is ßIV-spectrin (Berghs et al., 2000). Additionally, ankG has binding sites for voltage-gated sodium (Bennett and Baines, 2001; Srinivasan et al., 1998) and potassium channels (Pan et al., 2006) as well as cell adhesion molecules like neurofascin-186 (NF-186), and neuron glia-related CAM

(NrCAM) (Michaely and Bennett, 1995). Hence, a role of ankG as major scaffolding protein at the AIS was proposed early on (Kordeli et al., 1995).

Indeed, region specific knockdown of ankG revealed its fundamental role in recruiting the components of the AIS scaffold (Jenkins and Bennett, 2001; Zhou et al., 1998): After region specific cerebellar ankG knockdown, Purkinje cells failed to cluster voltage-gated sodium channels (VGSC) and NF-186 at the AIS properly (Sobotzik et al., 2009; Zhou et al., 1998). Additionally, AP waveform was altered, although surprisingly APs could still be fired, and mice developed an atactic gate indicating disruption of normal cerebellar function (Zhou et al., 1998). Accordingly, voltage-gated potassium channels KCNQ2/3 were lost after knockdown of cerebellar ankG (Pan et al., 2006). Further studies revealed that giant ankG is the main splice variant responsible for clustering of the AIS protein complex (Jenkins et al., 2015): In cultured hippocampal neurons from ankG null mice, which completely lack an AIS, transfection of cultured cells with a plasmid containing the 480 kDa cDNA could restore AIS clustering of ßIV-spectrin, VGSC and NF-186, whereas transfection with the 270 kDa cDNA only lead to a partial rescue. Surprisingly, genetic deletion of the 480 kDa isoform produces a phenotype that survives until weaning age as opposed to total ankG null mice that die after birth. Structurally however, AIS and noR are severely disrupted in giant-exon-null mice. Also, AP firing frequency is reduced, yet still intact (Jenkins et al., 2015). Possibly, the upregulation of the 190 kDa isoform as well as a 210 kDa splice variant observed in these mice could compensate for the loss of AIS by clustering VGSC outside of the AIS. Another unexpected finding from this study was that a mutation in the spectrin-binding domain did not affect the ability of ankG to cluster ßIV-spectrin to the AIS, suggesting a non-canonical interaction site for spectrin clustering. Generally, giant ankG has been termed the “master organizer” of the AIS (Rasband, 2010).

In addition to being important for AIS assembly, a role of ankG for maintenance of neuronal polarity has been proposed. When ankG is either silenced with short hairpin RNA *in vitro* (Hedstrom et al., 2008) or knocked down *in vivo* (Sobotzik et al., 2009), neurons lose their inherent polarity with a somatodendritic compartment on one side and the axonal compartment on the other. Instead, axons begin to establish dendritic features such as spine-like protrusions containing postsynaptic densities. The characteristic undercoating of the AIS and the microtubule bundles disappear and are

replaced by somatodendritic proteins such as MAP2 and the K^+/Cl^- cotransporter KCC2.

The fact that the presence of the AIS scaffold keeps somatodendritic proteins from invading the axons led to the hypothesis of the AIS serving as a diffusion barrier. This had been already indicated by earlier studies, where lateral mobility of membrane proteins and lipids was found to be markedly reduced at the AIS (Kobayashi et al., 1992; Winckler et al., 1999).

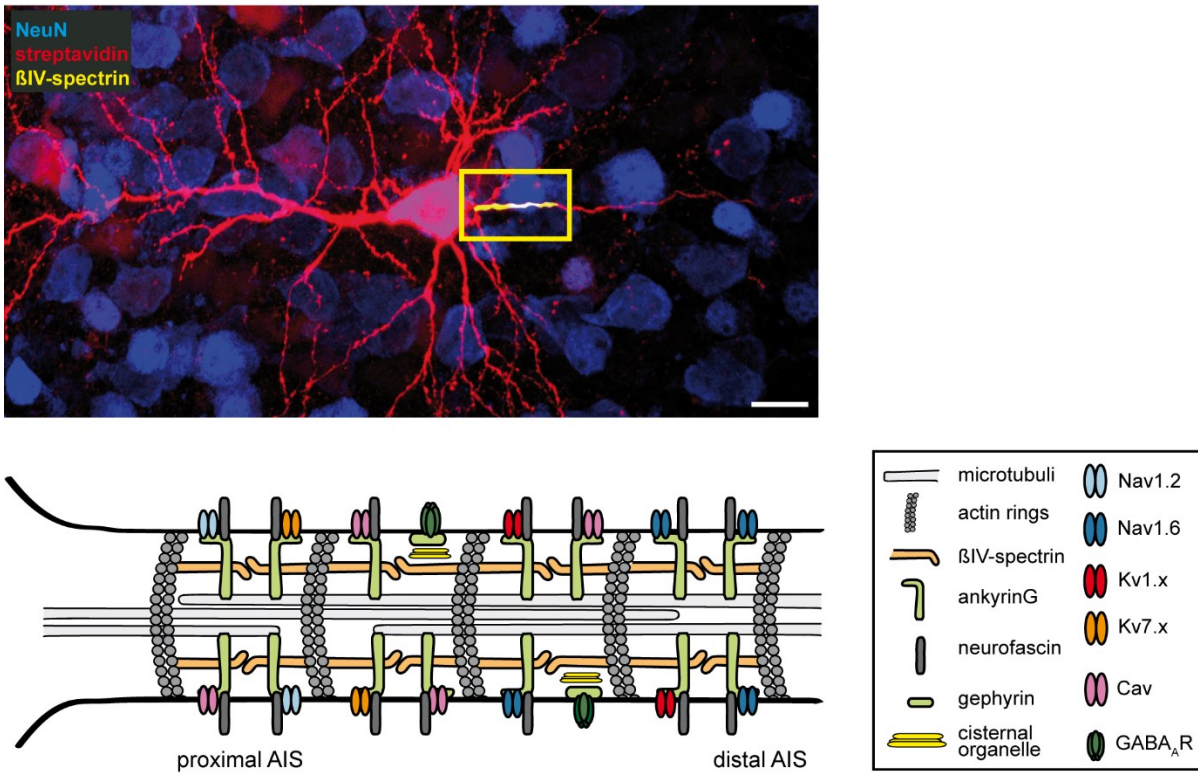

Figure 1 Ultrastructure of the AIS
***Top*: IF image of a pyramidal neuron filled with biocytin and counterstained for streptavidin, NeuN (neuronal somatic marker), and ßIV-spectrin to detect the AIS at the proximal axon. *Bottom*: Illustration depicting the proposed molecular scaffold at the AIS based on superresolution microscopy: Ankyrin G (ankG) (light green) is the major scaffolding protein that tethers various channels to the AIS. It binds to ßIV-spectrin, which links it to the actin-ring-cytoskeleton as well as to microtubules. Besides ion channels, $GABA_A$ receptors ($GABA_AR$) are expressed at the AIS. They open upon GABA release from nearby axo-axonic synapses and are localized close to the cisternal organelle, an intracellular calcium store. Adapted from published figure in Engelhardt et al., 2019**

1.3 Ultrastructure of the AIS – periodicity

The recent development of superresolution microscopy techniques such as stochastic optical reconstruction microscopy (STORM) and stimulated emission depletion

(STED) microscopy revealed a remarkable periodicity of the AIS scaffold. It came to light that throughout the axon, actin is organized in evenly spaced rings, which are about 180 nm to 190 nm apart and form a periodic submembranous lattice (D'Este et al., 2015; Schlüter et al., 2019; Xu et al., 2013) (Fig. 1). The actin periodicity is also present in dendrites as well as at noR (D'Este et al., 2015).

Additionally, actin patches and long actin fibers can also be found in the axon, whereas in the somatodendritic compartment, actin is rather organized in bundles. Developmentally, actin rings appear 2-3 days *in vitro* (DIV) before other AIS specific proteins (D'Este et al., 2015).

Strikingly, at the AIS, key structural proteins such as ankG, ßIV-spectrin, and sodium channels follow this periodicity. Colocalization analyses revealed that ßIV-spectrin colocalizes with NF-186 and sodium channels at its C-terminus, whereas the N-terminus colocalizes with the actin rings (Leterrier et al., 2015; Xu et al., 2013). Additionally, antibodies against the spectrin binding domain of ankG detected a periodicity, whereas antibodies against the tail domain at the N-terminus failed to do so (Leterrier et al., 2015). This led to an updated viewpoint of the structure of the AIS scaffold: ßIV-spectrin serves as an adaptor protein between the actin rings and ankG (Fig. 1). AnkG clusters sodium channels and NF-186 in between actin rings and extends its tail end into the cytosol, where it interacts with microtubules. At the distal axon, a similar actin-spectrin lattice is formed by ankyrin B (ankB) and ßII-spectrin (Xu et al., 2013). Remarkably, the ßII-spectrin periodicity is ubiquitously found in axons as well as a subset of dendrites and glial processes of various neuronal cell types, including inhibitory and excitatory cells. It has also been found in different brain regions and across various species (He et al., 2016), suggesting a ubiquitous expression. The periodicity of the scaffold at the AIS appears to be remarkably stable even after depolymerization of actin (Leterrier et al., 2015) or knockdown of the actin-binding protein adducin (Leite et al., 2016), whereas the distal axon is strongly disorganized after actin depolymerization (Leterrier et al., 2015).

Functionally, the role of a periodic submembranous protein lattice is less understood. In erythrocytes, where an actin-spectrin-based hexagonal submembranous lattice was first described (Byers and Branton, 1985; Yu et al., 1973), this interaction is thought to increase stability as well as flexibility of the erythrocyte membrane in order to allow passage through narrow spaces such as capillaries, where the membrane is subjected to a high level of mechanistic stress. Hence, one hypothesis is that the periodic actin

rings provide mechanical support in a long thin tubular structure such as the axon and thus help protect axons from shear forces (Leite and Sousa, 2016). This would explain why in dendrites, the periodic lattice can rarely be encountered, since they are shorter and thicker and therefore more resistant to shear forces. Another hypothesis states that actin could serve as docking stations during cargo transport through the axon (Gallo, 2013). Further studies are necessary to investigate the exact role of AIS and axon protein periodicity and a possible involvement in AIS plasticity (see below).

1.4 Channels at the AIS

1.4.1 Sodium channels

The mammalian sodium channel family consists of 9 different isoforms ($Na_v1.1$ -1.9). Due to their similar protein structure, which is >50% homologous, and the resulting similarities in channel kinetics, they are, unlike potassium and calcium channels, all counted as members of the same family. They were therefore labelled $Na_v1.x$ in the nomenclature (Goldin et al., 2000), x indicating a number according to the order of gene discovery. At the AIS, three isoforms are present: $Na_v1.1$, 1.2 and 1.6. Structurally, VGSC consist of two major subunits: the pore-forming, 260 kDa alpha subunit and the auxiliary ß-subunit. The latter interacts with cell adhesion molecules such as contactin, NrCAM, and NF-186 (McEwen and Isom, 2004) as well as molecules of the extracellular matrix (Srinivasan et al., 1998), implicating an important role in channel targeting (Catterall et al., 2005).

Expression patterns of the sodium channel subunits at the AIS highly depend on brain region and neuronal subtype. Nav1.1. has been described in a number of different neuron types, including motoneurons, retinal ganglion cells, and hippocampal granule cells (Table 1). In most cases, they appear to be highly concentrated at the proximal AIS (Lorincz and Nusser, 2008; Wart et al., 2007); however, in short-axon cells of the olfactory bulb, they are evenly distributed. Interestingly, they are absent in excitatory pyramidal neurons of the cortex, while they are expressed by GABAergic interneurons. Since firing properties between these two populations are very distinct, differential isoform expression most likely plays a role in shaping neuronal output parameters.

Table 1 Channels at the AIS

Isoform	Neuron type	Location at AIS	Localisation other than AIS	References
$Na_v1.1$	IN, OB, RGC, MN, HC, PC	proximal AIS in cortical and cerebellar IN, MN; uniform distribution in short-axon cells of	dendrites, soma, noR	(Duflocq et al., 2008; Lorincz and Nusser, 2008; Wart et al., 2007)
$Na_v1.2$	RGC, PYR, HC	proximal AIS	unmyelinated axons, noR (development)	(Boiko et al., 2001, 2003; Hu et al., 2009; Jarnot and Corbett, 1995)
$Na_v1.6$	RGC, HC, PYR, IN, MN, DG, PC	distal location in RGC, HC, PYR, IN; uniform distribution in PC	noR, proximal dendrites	(Boiko et al., 2003; Catterall, 1981; Hu et al., 2009; Inda et al., 2006; Kress et al., 2010; Kuba et al., 2006; Lorincz and Nusser, 2008; Royeck et al., 2008; Wart et al., 2007)
$K_v1.1$	PYR, IN, MNTB	distal AIS	juxtaparanode, presynaptic terminals	(Dodson et al., 2002; Goldberg et al., 2008; Inda et al., 2006; Kole et al., 2007; Lorincz and Nusser, 2008; Rasband et al., 1998)
$K_v1.2$	PYR, IN, MC, RGC, MNTB	distal AIS	soma, dendrites in PYR, presynaptic terminals of cerebellar basket cells	(Dodson et al., 2002; Goldberg et al., 2008; Inda et al., 2006; Lorincz and Nusser, 2008; Rasband et al., 1998; Wart et al., 2007)
$K_v7.2$	PYR, MN, HC	uniform	noR	(Battefeld et al., 2014; Devaux et al., 2004; Pan et al., 2006)
$K_v7.3$	PYR, MN, HC, PC	uniform	noR, soma of PC	(Devaux et al., 2004; Pan et al., 2006)
T/R type Ca_v	PYR, PC, CWC	unknown	presynaptic terminals, dendrites	(Bender and Trussell, 2009)
P/Q type Ca_v	PYR, PC	unknown	presynaptic terminals, dendrites	(Callewaert et al., 1996; Yu et al., 2010)

Abbreviations: IN = interneuron, OB = olfactory bulb, RGC = retinal ganglion cell, MN = motoneuron, HC = hippocampal pyramidal cell, PC = Purkinje cell, PYR = pyramidal neuron, DG = dentate gyrus, MNTB = medial nucleus of the trapezoid body, CWC = cartwheel cells

The $Na_v1.2$ isoform is expressed solely in the proximal region of retinal ganglion cells, hippocampal granule cells, and cortical pyramidal neurons (Boiko et al., 2001, 2003; Jarnot and Corbett, 1995). It seems to predominantly play a role during development, where it is for example present at noR. Interestingly, a developmental switch from $Na_v1.2$ to $Na_v1.6$ has been described (Boiko et al., 2001). Also, $Na_v1.2$ is expressed in unmyelinated axons, e.g. in axons of shiverer mice, a mouse line that completely lacks myelin due to a mutation of myelin basic protein (MBP; (Chernoff, 1981)).

$Na_v1.6$ is the most ubiquitously expressed channel isoform at the AIS. It is expressed in all types of neurons including myelinated and unmyelinated neurons, inhibitory and excitatory neurons of the cortex, hippocampal pyramidal cells, motoneurons and Purkinje cells (Table 1). In most cases, the distribution along the AIS follows a proximal to distal gradient, with the highest expression being at the distal AIS. The differential expression of different sodium channels along the AIS helps explain why AP initiation occurs at the distal AIS although overall sodium channel expression is uniform: Using outside-out recordings from axonal membranes at various distances from the soma, Hu et al. found that the progressive shift in the activation voltage of sodium channels towards distal locations could be explained by a low-threshold activation of the distally expressed $Na_v1.6$ compared to the high threshold of $Na_v1.2$ at the proximal AIS (Hu et al., 2009). Therefore, the authors proposed a role for $Na_v1.6$ in AP initiation and forward propagation, whereas $Na_v1.2$ promotes backpropagation to the soma (Fig. 2A). Lastly, a recent study suggested that Na_vs at the AIS might be also permeable to calcium ions (Hanemaaijer et al., 2020). Using high-speed calcium imaging, the authors found that the largest fraction of AIS calcium transients during depolarisations were sensitive to the Na_v blocker tetrodotoxin, suggesting that small amounts of calcium enter through Na_vs, which could in turn activate calcium release from intracellular calcium stores.

Taken together, differential localization and expression of various Na_v subtypes in different neuronal populations strongly influences cellular excitability and firing properties.

1.4.2 Potassium channels

Voltage-gated potassium channels (K_vs) are a large group of channels, encoded by 40 genes grouped into twelve different families (Gutman et al., 2003). Just like sodium channels, the alpha subunit consists of six transmembrane segments with the pore domain formed by segment 5 and 6 and the voltage sensing unit formed by segment 4 (Yellen, 2002). The pore structure is highly conserved between the families and

allows a rapid yet selective passage of a high number of potassium ions in order to rapidly repolarize the membrane potential during an AP (Doyle et al., 1998). Additionally, several different auxiliary beta subunits have been described, although their exact contribution to channel function is yet to be determined (Gulbis et al., 2000; Knaus et al., 1994). At the AIS, the most abundant isoforms are $K_v1.1$, $K_v1.2$, $K_v7.2$ and $K_v7.3$ (Table 1).

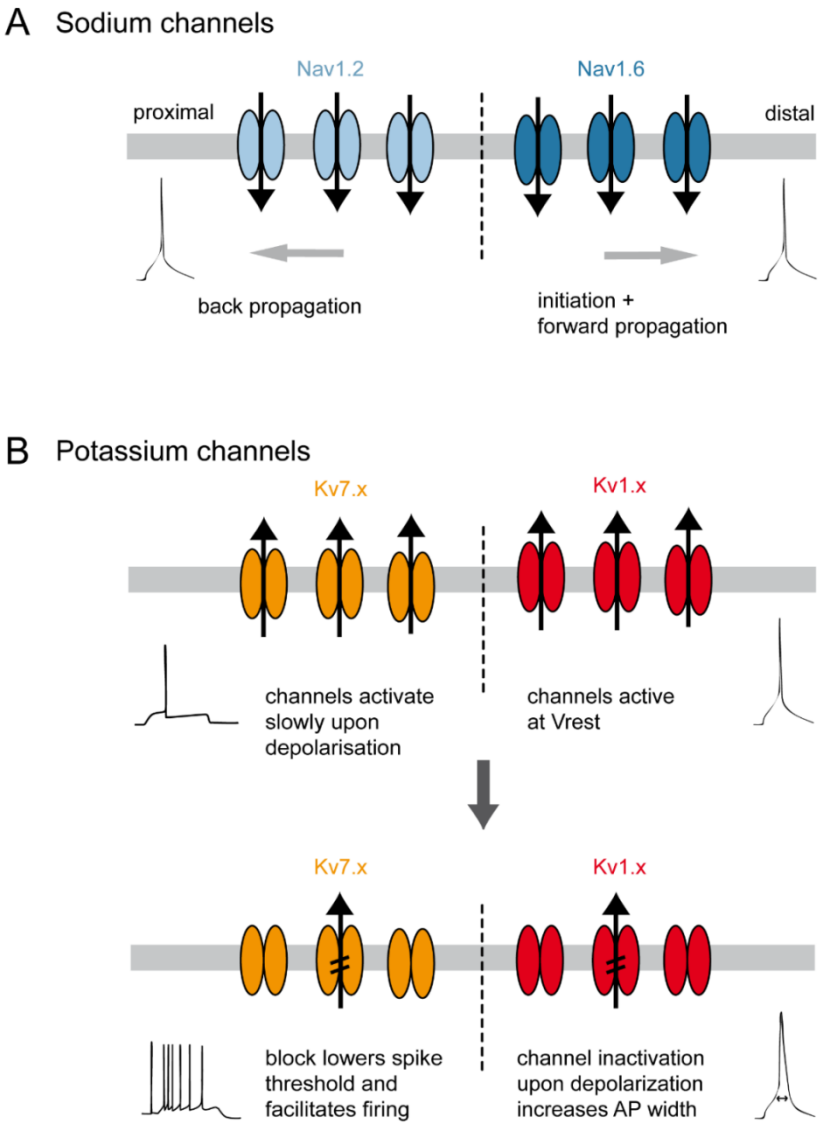

Figure 2 Channel function at the AIS
A The two types of Na_vs at the AIS have different functions: The distally located $Na_v1.6$ isoform has a lower voltage activation threshold. It therefore facilitates AP initiation at the distal AIS. On the other hand, the proximally located $Na_v1.2$ has a higher voltage threshold and is thought to mediate backpropagation of the AP to the somatodendritic compartment. **B** The main K_v channel subtypes located at the AIS are K_v7 and K_v1 channels. K_v7 channels activate slowly close to threshold and generate the “M-current”. When blocked, repetitive firing is facilitated. K_v1 channels are active at resting membrane potential. When they are inactivated upon

subthreshold depolarization, AP width is increased which in turn increases neurotransmitter release at the distal axon. Published in Engelhardt et al., 2019

K_v1.1 and 1.2 are the predominant isoforms expressed at the AIS. In the cortex, they can be found at both pyramidal cells and interneurons (Table 1). They activate at a low threshold and mediate a fast-activating, slowly-inactivating outward potassium current that counterbalances depolarizations (Goldberg et al., 2008; Kole et al., 2007). Like Na_vs, they are expressed in a gradient along the AIS, with a maximum intensity at a distal location just after the onset of Na_v1.6 expression (Lorincz and Nusser, 2008). Not all neuron types express all K_v1 type channels: Mitral cells and retinal ganglion cells only express K_v1.2 and Purkinje cells completely lack K_v1 channels. This differential expression most likely contributes to the distinct firing patterns of neuronal populations since several studies have shown how strongly the K_v1 current influences AP waveform and repetitive firing. A study on K_v1 channels conducted by Kole et al. showed that their inactivation through slow subthreshold depolarizations leads to a broadening of the AP in layer V pyramidal neurons (Fig. 2B (Kole et al., 2007)). Strikingly, this also had an effect at the distal axon, increasing synaptic release onto the postsynaptic neuron as measured by an increase in excitatory postsynaptic potential (EPSP) amplitude. Furthermore, Goldberg et al. found that K_v1.1 dampens excitability at slow depolarizations (Goldberg et al., 2008). However, if depolarizations are fast, K_vs do not activate fast enough to counteract the inward current and AP initiation is unhindered. Thus, interneurons respond preferentially to large and fast inputs that “outrun” the potassium current, whereas slowly rising inputs are suppressed by K_v1.

Another important channel type at the AIS is K_v7.2/7.3, sometimes also termed as KCNQ2/3, which describes the encoding gene. They have been described to localize at the AIS and noR in the CNS and PNS (Pan et al., 2006). Similar to Na_v 1.6, expression at the AIS follows a proximal to distal gradient (Battefeld et al., 2014). K_v7 channels mediate the so called “M current” (M=muscarine), a slow non-inactivating potassium current that activates just below AP threshold (Halliwell and Adams 1982). Several functions have been attributed to K_v7 channels. In general, the M-current alters AP threshold and resting membrane potential, which has implications for intrinsic firing properties of an individual neuron (Shah et al., 2008). Since they activate close to threshold, K_v7 channels can suppress repetitive firing. The hyperpolarization resulting from the outward potassium current, which is activated at the first AP of a spike train,

counteracts the depolarizing sodium influx, thus preventing further APs from initiating. If K_v7 channels are blocked, repetitive firing is enhanced and spike frequency is increased (Aiken et al., 1995). K_v7 also control intrinsic burst firing. If they are blocked in hippocampal CA1 pyramidal neurons, afterdepolarization is increased and the firing mode upon brief current injections switches from single spiking to burst firing (Yue and Yaari, 2004) (Fig. 2B). A detailed electrophysiological study by Battefeld et al. carried out in cortical pyramidal neurons demonstrated that these functions most likely play a role in the somatodendritic compartment (Battefeld et al., 2014). In the axon and noR, K_v7 channels mainly play a role in shaping the AP waveform: By stabilizing the resting membrane potential, steady-state Na_v availability is increased and because of the larger current upon depolarization, AP amplitude is increased.

1.4.3 Calcium channels

The family of mammalian voltage-gated calcium channels (Ca_vs) has ten members, which can be grouped into three subfamilies each serving distinct functions in the brain (Catterall, 2011). They consist of a five-subunit complex with a pore-forming alpha subunit, a dimer of an alpha 2 and delta subunit, an intracellular ß subunit, and a transmembrane γ subunit. Electrophysiologically, they are sorted into groups according to the current they mediate (e.g. “L-type” for long-lasting). Only few studies have investigated the role of Ca_vs at the AIS. So far, expression of P/Q type and T/R type Ca_vs has been described at the AIS (Bender and Trussell, 2009; Yu et al., 2010). Bender et al. studied Ca_vs in cartwheel interneurons of the dorsal cochlear nucleus of mice as well as Purkinje cells and cortical pyramidal neurons. Using 2-Photon imaging, they detected T- and R-type Ca_vs colocalized with AIS Na_vs (Bender and Trussell, 2009). Pharmacological blockage of this channel subtype revealed that it shapes the waveform of so-called “complex spikes”, which are generated by the simultaneous activation of fast sodium currents and slow calcium currents. Moreover, blocking these channels led to a reduced spike probability (Bender and Trussell, 2009). Yu et al. were the first to describe the presence of P/Q type Ca_vs at the AIS of cortical pyramidal neurons (Yu et al., 2010). They observed an increase in baseline intracellular calcium concentrations at subthreshold depolarizations. If P/Q type Ca_vs were blocked, AP repolarization was slowed, and excitability was increased (Yu et al., 2010). This might seem counterintuitive since influx of a positively charged ion should not contribute to repolarization. The authors could show that this effect is probably mediated by a reduced calcium-dependent potassium current.

1.5 AIS plasticity

1.5.1 Structural plasticity

Given that the AIS as a structure was described over half a century ago, the discovery that it can exhibit structural plasticity is still a relatively new concept.

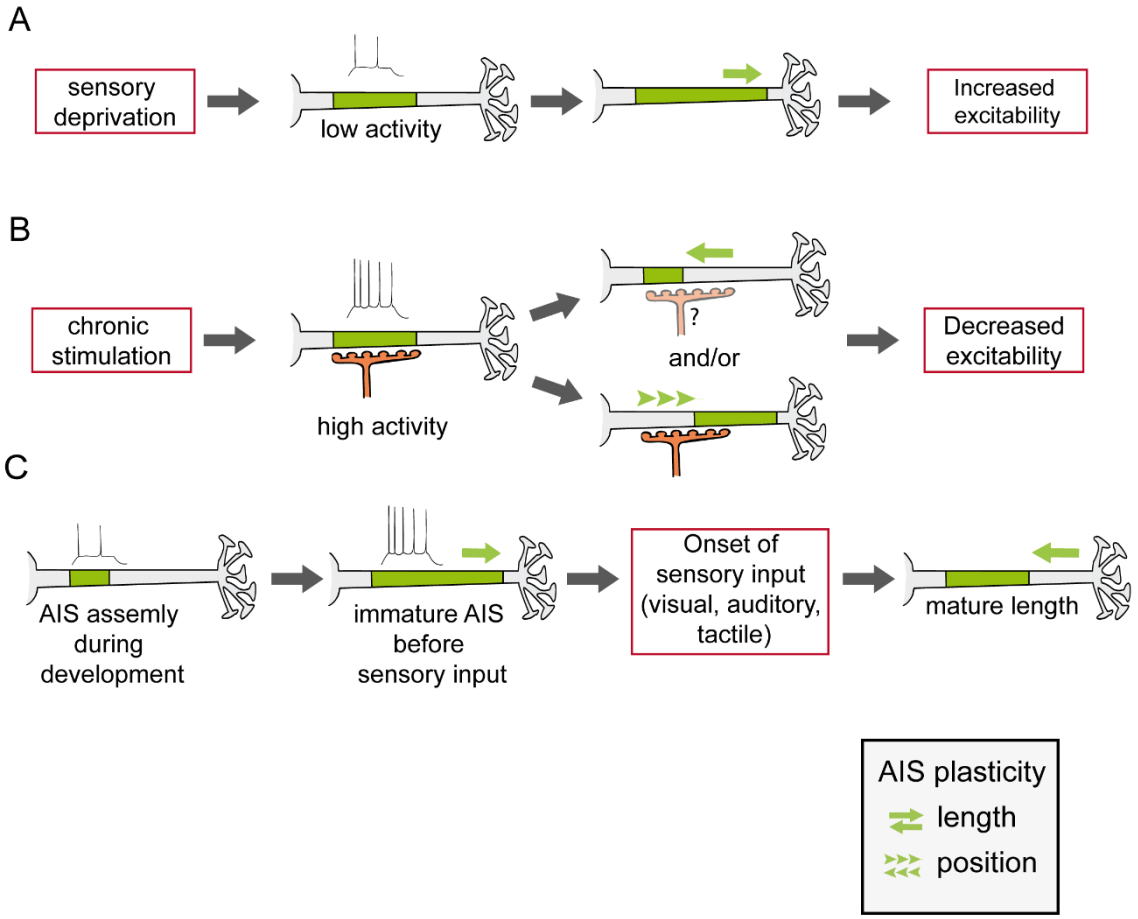

Figure 3 Forms of AIS plasticity
A After long-term sensory deprivation by removal of the cochlea and resulting low activity in auditory brainstem neurons, AIS length increases. This in turn leads to an increase in excitability (Kuba et al., 2010). **B** After chronic stimulation of cultured hippocampal neurons, AIS either shorten rapidly (hours) or shift to a distal location (days) (Evans et al., 2015; Grubb and Burrone, 2010). Chandelier cell synapses (orange) however do not change their location at the AIS under similar conditions *in vitro* (Wefelmeyer et al., 2015) **C** AIS maturation during visual cortex development follows a triphasic profile: Initially, AIS length increases after birth. After the onset of sensory input through eye-opening, AIS length rapidly shortens. It subsequently stabilizes at an intermediate, mature length (Gutzmann et al., 2014; Schlüter et al., 2017)

First evidence that the length and location of the AIS influence neuronal firing patterns came from studies in sensory systems (Fried et al., 2009; Kuba and Ohmori, 2009; Kuba et al., 2006). In avian auditory brainstem nuclei, such as the nucleus laminaris,

neurons function as coincidence detectors in order to compute interaural time differences at characteristic frequencies (CF). These neurons are arranged in a tonotopic order, with high, middle and low CFs along a rostromedial to caudolateral axis. Between these different populations, AIS size and location scale with each CF: Low CF neurons have a long and proximal AIS whereas middle and large CF neurons have a short and distally located AIS (Kuba et al., 2006). Computational analysis indicates that this variation exists in order to achieve the lowest possible spike threshold and thus optimal firing rates at the individual frequency. A similar observation was made in retinal ganglion cells, where AIS size and location vary between different ganglion cell types (Fried 2009). In 2010, two hallmark publications were the first to describe structural plasticity of the AIS, in terms of length and position changes, as a response to changes in neuronal activity: Kuba et al. applied auditory deprivation in chickens by removing their cochlea right after birth (Kuba et al., 2010). This resulted in a significant increase in AIS length (about 1.7-fold) in auditory brainstem neurons after about a week of sensory deprivation (Fig. 3A). This structural change was accompanied by an increase in excitability as measured by a lowering of AP threshold and increase of spontaneous firing in the deprived neurons. Thus, the authors were the first to propose AIS plasticity as a homeostatic mechanism at single neuron level in response to changes in presynaptic input. Complementarily, Grubb and Burrone (Grubb and Burrone, 2010) conducted *in vitro* experiments to induce an increase rather than a decrease in neuronal activity. The authors employed two approaches: either cultured hippocampal neurons were exposed to a high level of extracellular potassium or were triggered to repeatedly evoke AP bursts via expression of the light activated cation-channel channelrhodopsin. Instead of length changes, in this study, the proximal AIS onset shifted farther away from the soma. Again, AIS plasticity was accompanied by a change in intrinsic excitability: Neurons showed an increase in minimum current needed to generate an AP (rheobase), and thus reduced intrinsic excitability. A similar study later revealed that elevating extracellular potassium *in vitro* can also lead to very rapid length changes, with a significant AIS shortening observed after only a few hours of increased activity (Evans et al., 2015). Wefelmeyer et al. made an intriguing observation using organotypic slice cultures under the same experimental conditions (high extracellular potassium or light-evoked stimulation): Whereas almost all components of the AIS shift distally in the chronic depolarization model of AIS plasticity, the GABAergic synapses at the AIS remain in place (Wefelmeyer et al.,

2015) (Fig. 3B). These synapses are formed by parvalbumin-positive interneurons in the cortex and hippocampus termed axo-axonic cells (AAC in hippocampus) or Chandelier cells (ChC in neocortex). These interneurons exhibit a large axonal arborization, which spans several cortical columns and specifically targets hundreds of AIS of cortical pyramidal neurons, granule cells or mossy cells (Howard et al., 2005; Kosaka, 1983; Somogyi, 1977; Somogyi et al., 1983; Soriano and Frotscher, 1989). The specific role of these cells and their synapses for neuronal output is still largely unknown and under investigation (Woodruff et al., 2010). Whether the effect on the AIS is mainly excitatory or inhibitory is a subject of debate (Khirug et al., 2008; Szabadics et al., 2006; Woodruff et al., 2011). Modeling studies suggest that the distal relocation of the AIS further away from the input of the ChC synapses decreases excitability (Wefelmeyer et al., 2015). Developmentally, the formation of ChC synapses onto the AIS coincides with a period of a shift in intrinsic excitability in cortical pyramidal neurons (Maravall et al., 2004; Pan-Vazquez et al., 2020). Voltage imaging suggests that ChC activity is depolarizing during this period, but later switches to an inhibitory effect in adult mice (Pan-Vazquez et al., 2020). Overall, ChC most likely play an important role in the development and maintenance of a physiological excitation/inhibition balance in neuronal networks and it comes at little surprise that ChC maldevelopment and manifested dysfunction has been implicated in neuropsychiatric diseases such as schizophrenia (Lewis et al., 2005).

AIS remodelling has also been shown to occur during development of sensory systems (Gutzmann et al., 2014; Kim et al., 2019; Kuba et al., 2010). As outlined above, in the mouse visual cortex, a triphasic length change can be observed: Initially, AIS length gradually increased during the first two postnatal weeks. Then, after P15 a sudden and substantial reduction until P21 occurs (Fig. 3C). The shortening coincides with the time point of eye opening at P14, which implies an activity-dependent mechanism as a response to the massive increase in presynaptic input. At adult stages AIS length then reaches a “mature” intermediate length. If mice are reared in the dark until adulthood, the reduction of AIS length is completely abolished, further underlining the dependence of normal AIS development on sensory input (Gutzmann et al., 2014). However, it remains elusive whether the observed developmental plasticity is a general feature of sensory systems. Also, it has not yet been investigated whether AIS plasticity during development will lead to changes in intrinsic excitability and firing properties. AIS plasticity has also been described to occur during hibernation (León-Espinosa et al.,

2018), indicating the possibility that AIS plasticity could also be a physiological mechanism in more mature brains during phases of altered sensory input or neuronal activity. There have been no studies to date investigating in detail whether AIS plasticity is confined to the developmental period or could also be a homeostatic mechanism in the adult brain.

1.5.2 Functional AIS plasticity

An important question is, why a long and proximal AIS seems to be preferable in terms of increasing an individual neurons excitability. In general, it has been suggested that the AIS is the optimal site of AP initiation because it is close to the soma and at the same time small in size compared to the somatodendritic compartment. Thus, capacitance is far lower at the AIS and a much smaller sodium current is needed to generate an AP. Also, a small capacitance favours rapid changes to membrane voltage, as occur during AP generation (Kole and Stuart, 2012). Hence, moving this optimal site of spike initiation further away from the soma isolates it from the large capacitive current sink generated by the soma.

On the other hand, moving the AIS far away from the soma reduces the amount of current reaching the initiation site and therefore reduces the number of events where threshold will be reached. This would explain why a distal shift results in a decrease in excitability in some populations (Grubb and Burrone, 2010). Indeed, experimental and modeling studies have confirmed that AIS location and size covaries with the size and complexity of the somatodendritic compartment in order to normalize the somatic AP across different neuronal morphologies (Gulledge and Bravo, 2016; Hamada et al., 2016; Thome et al., 2014). Gulledge and Bravo computed a model that took into account the size of the dendritic tree in different neuronal populations (Gulledge and Bravo, 2016). They then varied either size or location in these models and examined the effect on rheobase (the minimum current needed to elicit an AP). In general, as mentioned above, shifting the AIS distally resulted in a decrease of the capacitive load of the soma, thus promoting excitability. In small neurons on the other hand, this also produced a reduction in local input resistance and an increase in the membrane time constant, both being factors that limit excitability (Kole and Brette, 2018). In large neurons, this effect is the opposite. In conclusion, small neurons have their lowest threshold with an AIS adjacent to the soma, whereas in large neurons a distal AIS location is more beneficial. This could be an explanation why some neurons, such as dopaminergic interneurons in the olfactory bulb, display an “inverted” structural

plasticity. A subset of these neurons has been shown to possess an AIS which, under baseline conditions, locates distally (Chand et al., 2015). After 24 hours of depolarisation, AIS lengthen and shift more proximal to the soma, which is the opposite of AIS plasticity normally described in the literature (Grubb and Burrone, 2010). Hence, according to modeling and experimental data, a long AIS length is optimal in large neurons and an intermediate or shorter length is preferable in small neurons (Goethals and Brette, 2020; Gulledge and Bravo, 2016). Interestingly, modeling suggested that AIS length variation has a higher impact on excitability, whereas experimental data has suggested location as the main contributing factor (Gulledge and Bravo, 2016; Hamada et al., 2016). Another factor contributing to this complex matter is the "rediscovery" of the fact that axons do not always originate from the soma, but that in some cell populations, axons directly emanate from a basal dendrite. These "axon-carrying dendrite" (AcD) cells had already been described by pioneering neuroscientist Simon Ramon y Cajal (Cajal, 1911) and early EM studies (Palay et al., 1968; Peters et al., 1968), however, the knowledge about these cells had moved into the background over time. A series of recent studies revealed that AcD cells are far more abundant than previously assumed. Depending on the region and species studies, they make up to 30% of layer V cortical pyramidal neurons, 60% of hippocampal pyramidal neurons, 40% of cerebellar granule cells, 40% of basket cell interneurons, 60% of Martinotti cells, and up to 75% percent in substantia nigra dopaminergic neurons (Blythe et al., 2009; Gentet and Williams, 2007; Hamada et al., 2016; Häusser et al., 1995; Höfflin et al., 2017; Thome et al., 2014).

What is the electrical significance of positioning the onset of the axon on a dendrite rather than adjacent to the soma? According to resistive coupling theory, the amount of Na current needed to generate an AP at the AIS is inversely proportional to the axial resistance between AIS and soma (Brette, 2013). The axial resistance is determined by the geometry of the dendritic or axonal branch that spans the gap between the AIS and soma (Kole and Brette, 2018). Consequently, theory predicts that if the AIS emanates from a dendrite or in general a more distal location, axial resistance is higher and therefore rheobase would be lower. Experimentally, however, it was shown that AIS-soma distance was not a strong predictor of AP threshold (Hamada et al., 2016; Thome et al., 2014). Further studies are needed to disentangle the effect on intrinsic excitability. Another proposed crucial consequence of an AcD might be for dendritic integration. If the dendrite carrying the axon receives synaptic input, in contrast to

regular dendrites, this input does not have to travel along a possibly large somatodendritic compartment before reaching the axon and is thus more likely to elicit an AP in the axon. This “privileged” input has for example been observed in hippocampal neurons, where AcDs were more excitable following dendritic input and generated APs that had a lower threshold due to the shorter electrotonic distance from input to output (Thome et al., 2014). Similarly, a study in dopaminergic substantia nigra neurons showed that synaptic input onto the AcD would often elicit APs, which stayed in many cases confined to the axon and failed to backpropagate into the somatodendritic compartment (Gentet and Williams, 2007). Another study correlated *in vivo* firing rates of these neurons with AIS length and onset position (Meza et al., 2018). Interestingly, the authors found that according to their experimental and modeling data, AIS length and not onset position would drive firing rates.

1.5.3 Rapid AIS modulation

Structural plasticity of the AIS has been observed on a timescale from hours to weeks. There are, however, several rapidly acting mechanisms that could potentially alter AIS function within a matter of seconds. These have been most attributed to neuromodulatory effects of neurotransmitters locally released onto the AIS. One striking example is the effect of dopamine in the dorsal cochlear nucleus of the auditory pathway (Bender and Trussell, 2009; Bender et al., 2010). The local inhibitory glycinergic neurons (cartwheel cells), express T-type Ca_Vs, which can trigger burst-firing. The authors proposed the following pathway through which dopamine could influence the firing mode of these neurons: Upon dopamine release, D3 receptors at the AIS are activated, which in turn triggers intracellular protein kinase C (PKC). PKC then inhibits T-type Ca_Vs within seconds. This inhibition leads to a switch from burst-firing to single-spiking mode and delays spike timing (Bender et al., 2010). Another example are granule cells in the dentate gyrus (DG). They are innervated by cholinergic fibres from the septum. If acetylcholine (ACh) is locally released by high frequency stimulation, activation of the muscarinic acetylcholine receptor M1 promoted Ca_V3 activation (Martinello et al., 2015). The increase in Ca^{2+} concentration in the AIS then reduces the K_V7 generated M current, which decreases threshold and increases firing frequency of the DG neurons. Thus, ACh can increase excitability within seconds with a sustained effect lasting at least 30 minutes. Two studies have also investigated the effect of serotonin (5-HT) on the AIS (Cotel et al., 2013; Yin et al., 2017). In the prefrontal cortex, activation of the serotonin receptor 5-HT_{1A} receptor selectively blocks

$Na_V1.2$ and therefore backpropagation of APs into the somatodendritic compartment, whereas orthodromic spiking remains unaffected (Yin et al., 2017). This might possibly have an effect on synaptic integration since backpropagating APs usually shunt the dendritic membrane and hence reduce the temporal summation of EPSCs (Stuart and Häusser, 2001). In motoneurons, serotonin has been shown to inhibit both $Na_V1.2$ and $Na_V1.6$ and, consequently, both anti- and orthodromic spike propagation (Cotel et al., 2013). The authors proposed a possible role in motor fatigue, which occurs to protect the muscle from damage during repeated muscle contractions. Another “protective” effect could be caused by glutamate. If local glutamate levels are increased, K_V7 channels and $Na_V1.2$ are endocytosed rapidly and irreversibly (Benned-Jensen et al., 2016). Since glutamate levels rise during general ischemia, channel internalisation might be a way to protect the AIS from destruction after a pathological insult. Additionally, Ca^{2+} influx through NMDA receptors activates Calpain, a protease involved in AIS proteolysis during an ischemic insult (Schafer et al., 2009).
In conclusion, several neurotransmitters have been shown to rapidly and effectively influence neuronal firing and function mediated by their respective receptor effects at the AIS.

1.5.4 The molecular basis of plasticity

One key question in the field remains unanswered to date: What is the mechanism or pathway behind structural AIS plasticity? How does this large protein complex elongate or shift its position, sometimes within hours? So far, several studies have hinted at possible key players in regulating AIS plasticity, however, the exact molecular basis remains unknown. Current evidence strongly points to the importance of posttranslational modifications, especially phosphorylation by kinases and respectively dephosphorylation by phosphatases. One of the first pieces of evidence was the study by Garver et al. showing that cell adhesion molecules of the L1CAM family, such as NF-186 and NrCAM, possess a highly conserved intracellular tyrosine domain (Garver et al., 1997). This domain, when phosphorylated, impairs the binding to ankG and increases lateral mobility of these cell adhesion molecules. However, the responsible proteins for the posttranslational modifications have not been identified. Two candidates working in opposite directions are the phosphatase calcineurin and the cyclin-dependent kinase Cdk5. Calcineurin has been shown to be necessary for rapid as well as sustained plasticity after elevated activity *in vitro*, since a block of calcineurin abolished AIS plasticity (Evans et al., 2013, 2015). Accordingly, rapid AIS plasticity

also depends on the function of L-type Ca_Vs. On the contrary, Cdk5 inhibition leads to a shortening of the AIS even without increased firing rates (Chand et al., 2015; Evans et al., 2015). In *Drosophila melanogaster* mushroom body neurons, where an axonal accumulation of Ankyrin 1 resembles the vertebrate AIS, an increase in cyclin-dependent kinase 5 (Cdk5) activity leads to an elongation of AIS length (Trunova et al., 2011). Cyclin-dependent kinases have also been shown to phosphorylate the auxiliary ß-subunit of K_V1 channels, leading to a decreased interaction with the microtubule-associated protein EB1 (Vacher et al., 2011). Inhibition of CDK leads to the relocalization of K_V1 and EB1 to the soma. There is also evidence for regulation of Na_V binding via phosphorylation: Casein-kinase 2 (CK2), another kinase highly enriched at the AIS, phosphorylates $Na_V1.2$ channels, which in turn increases their binding affinity to ankG (Bréchet et al., 2008). If CK2 activity is inhibited, the accumulation of Na_Vs and ankG at the AIS is reduced (Bréchet et al., 2008; Sanchez-Ponce et al., 2011). Upon complete inhibition of CK2, axonal growth and microtubule formation are also impaired (Sanchez-Ponce et al., 2011). Another frequently investigated kinase is glycogen synthase kinase 3 (Gsk3). Gsk3 is a ubiquitously expressed kinase in the CNS with an excessive number of downstream targets and hence has been implicated in numerous cellular functions (Beurel et al., 2015). Tapia et al. showed that Gsk3 and its downstream target ß-catenin are highly enriched at the AIS and noR (Tapia et al., 2013). Inhibition of Gsk3 leads to a decrease in ankG and Na_Vs at the AIS, which reduced excitability and sodium current amplitude *in vitro*. Gsk3 has also been shown to phosphorylate fibroblastic growth factor 14 (FGF14) (Shavkunov et al., 2013). FGF14 influences Na_V kinetics by forming a complex with the channel. If GKS3 is inhibited, the interaction of FGF14 and Na_Vs is reduced, resulting in an altered Na_V function (Shavkunov et al., 2013). Thirdly, Gsk3 phosphorylates the tubulin deacetylase HDAC6 (Chen et al., 2010). The AIS seems to be selectively spared from deacetylation, since a high number of acetylated microtubules are specifically found at the AIS, whereas microtubules are deacetylated in the distal axon (Tapia et al., 2010). The idea is also supported by the fact that upon inhibition of HDAC6, ankG clustering at the AIS is lost (Tapia et al., 2010; Tsushima et al., 2015). Similarly, cell polarity is lost upon Gsk3 inhibition (Yoshimura et al., 2005). The exact involvement of the Gsk3-HDAC6 interaction in AIS assembly and plasticity remains yet to be explored.

Finally, CaM-Kinase II (CaMKII) has been shown to be at least partly involved in AIS plasticity. It has been shown to colocalize with ßIV-spectrin in cerebellar Purkinje neurons and phosphorylates Na_Vs (Hund et al., 2010). Inhibition of CaMKII reduced, but not completely abolished AIS plasticity upon high extracellular potassium concentration (Evans et al., 2015). A range of other common kinase pathways, such as the PKC, PKA, PI3K, and MAPK pathway do not seem to play a role in AIS plasticity (Evans et al., 2013). Taken together, the AIS appears to be a hotspot for phosphorylation with a palette of different kinases and phosphatases involved that play different roles depending on the protein and neuron type.

1.6 The barrel cortex

The barrel cortex is an extremely well characterized mammalian sensory system (Feldmeyer et al., 2013). It is the part of the primary somatosensory cortex of rodents and integrates tactile stimuli relayed from the whisker pad on the contralateral snout. Sensory information, generated by passive deflection or active movement of the whiskers, is transmitted by pseudo-unipolar neurons of the infraoptic nerve, a branch of the trigeminal nerve (Szwed et al., 2003). The somata of these neurons reside in the trigeminal ganglion (Fig. 4). The first synapse of the pathway is in the principal trigeminal nucleus in the brainstem, from where the pathway crosses over to the contralateral side. The second relay station is in the thalamus. Here, the information is processed and relayed both by the ventral posteromedial nucleus (VPM) via the “lemniscal” pathway and the posteromedial complex (PoM) via the “paralemniscal” pathway (Pierret et al., 2000; Veinante et al., 2000). VPM then projects to the main input layer of the primary somatosensory cortex, barrel field (S1BF), layer IV, but also sends axonal branches to layer V. PoM on the other hand mainly projects to layers I and V in S1BF.

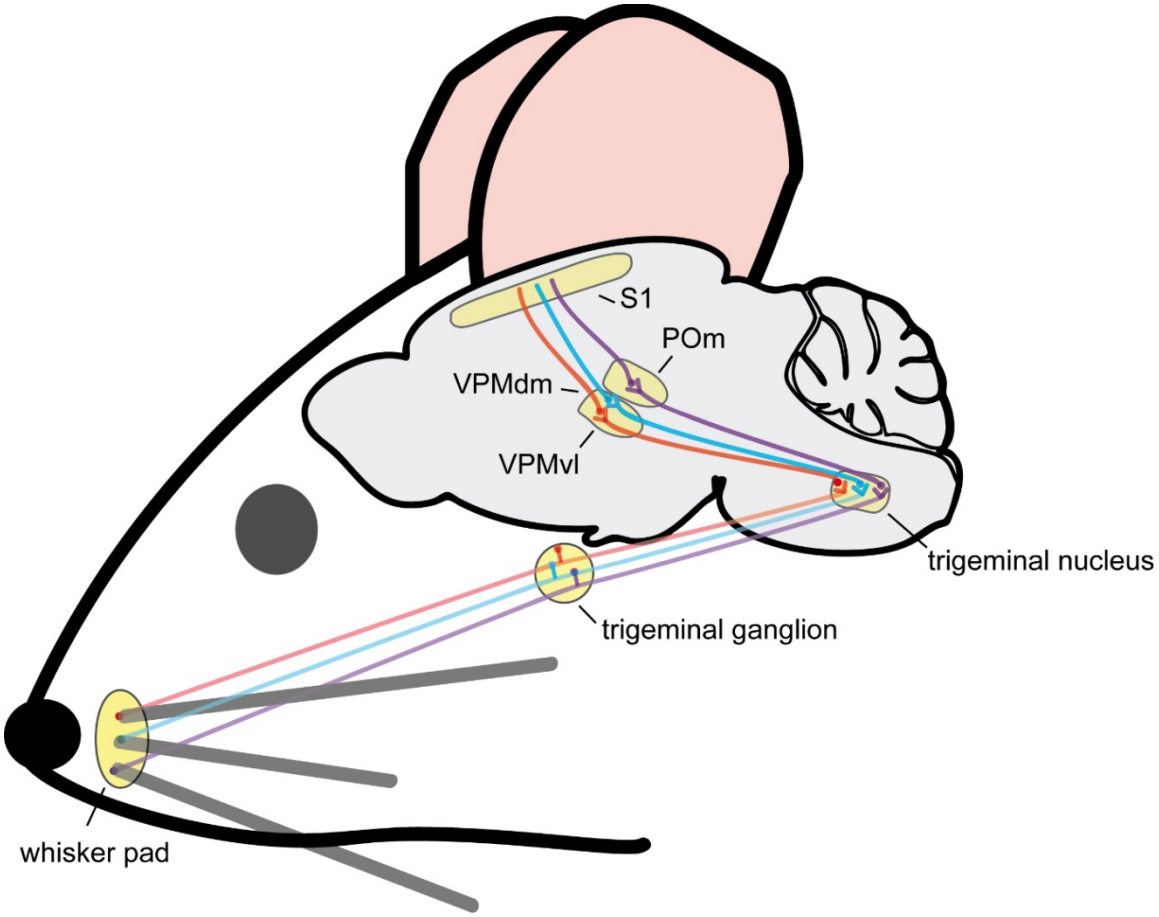

Figure 4 The whisker to barrel pathway
Sensory information is transformed into an electrical signal at the whisker follicles, which are innervated by sensory neurons. Upon touch, action potentials are generated. These are transmitted by the trigeminal nerve to the brainstem. The first synapse is located at the principal trigeminal nucleus (PrV). From here, information is propagated to the dorsomedial and ventrolateral ventral posteromedial nucleus (VPMdm and VPMvl) and posteromedial complex (PoM) of the thalamus, which subsequently relay the information to different layers in primary somatosensory cortex (S1).

The S1BF, often termed the “barrel cortex”, has become a well-studied cortical region because of its characteristic organization: The cortical circuit is organised in columns spanning the entire cortex (Woolsey and Loos, 1970). Each column represents a single whisker. Thus, the barrel cortex is a prime example for somatotopy, a neuronal organizational principle where the location at which sensory information reaches the cortex mimics the location in the periphery, forming a spatial map of representation at the cortical surface. The term “barrel cortex” was chosen because of the organization of layer IV, which, when brain slices are cut in a tangential angle resembles the shape of a barrel. The “walls” of these barrels are composed of excitatory spiny stellate neurons (Lübke et al., 2000). Their dendrites are oriented towards the middle of the barrel, where they form synaptic contacts with thalamocortical afferents that extend

their terminal arbours to layer IV. It was later discovered that a similar organization pattern could also be found downstream of the cortex in the brainstem and the thalamus, where neurons form “barrelettes” and “barreloids” respectively (Loos, 1976; Veinante and Deschênes, 1999). The barrel cortex as a model system offers the advantage to study activity-dependent plasticity by modulating the sensory input from the periphery and knowing quite well, where cortical processing is localized. One can for example increase activity by subjecting mice or rats to an enriched environment, which triggers explorative behaviour via active whisking (Staiger et al., 2000). On the other hand, countless studies have investigated the impact of reducing or completely abolishing sensory input by manipulating the whisker pad. Early studies used cauterization of the infraoptic nerve or the whisker pad, which lead to the complete loss of the area representation of single whiskers or whisker rows (Loos and Woolsey, 1973; Woolsey and Wann, 1976). Though these pioneering studies were extremely important to understand the (re-)organization of somatotopic regions, whisker cauterization has a few disadvantages and thus has been replaced by other methods. Firstly, the manipulation is quite extreme in its effect, which makes it impossible to study more subtle and more natural effects of sensory deprivation on cortical plasticity. Secondly, the manipulation will most likely cause local damage and alterations due to the activation of afferent pain receptors cannot be excluded. Finally, it does not offer the possibility of restoration of sensory input to study the reversibility of observed effects. A less invasive method and reversible is whisker plucking, where whiskers can regrow. However, again such removal of whiskers might damage local sensory receptors, leading lead to an altered outcome. Hence, the least invasive method is hence whisker trimming, where whiskers are cut and kept short with a fine scissor. In fact, it is closest to a natural situation, since rodents can loose and regrow whiskers during their lifespan and whisker trimming by mothers or littermates has been observed in laboratory environments (Garner et al., 2004). In this thesis, whisker trimming was chosen as a method of sensory deprivation as it is easy to apply and the least invasive method of choice. Additionally, it offers the possibility to regrow whiskers, allowing studying the effect of restoration of sensory input after periods of deprivation.

Several so called “critical periods” of S1BF development were identified through deprivation studies (Erzurumlu and Gaspar, 2012). Critical period is a term for a specific time window during development, were sensory input is necessary for normal

brain development (Hensch, 2005). Thus, when the cortex is deprived of such sensory input during this period, distinct structural and/or functional alterations can be observed. However, these alterations will not occur if deprivation is applied during other developmental periods. For example, establishment of the typical columnar organization of S1BF is only disturbed by neonatal whisker lesions during P0 – P4 (Durham and Woolsey, 1984). If lesions are applied later, anatomical somatotopy remains intact. Another critical period is the end of the second postnatal week (P10 to P16), where local cortical circuits are established and sensory maps are formed (Maravall et al., 2004; Stern et al., 2001; Wen and Barth, 2011). Hence, whisker deprivation paradigms allow the determination of distinct critical periods during early development. In this study, whisker trimming was used to investigate possible critical periods of AIS length changes and maturation of neuronal excitability during S1BF development.

1.7 Objectives

As outlined in the introduction, AIS plasticity is a potential key homeostatic regulator of neuronal input-output relations. However, it is still largely unknown if and in what way it occurs during development and in the adult brain. In a previous study in the visual cortex, a triphasic AIS remodelling during development was observed, which was shown to be dependent on sensory input (Gutzmann et al., 2014). Based on these finding, it was hypothesized that AIS plasticity is a general feature of developing sensory cortices.

The following questions were addressed with this thesis:

- Can AIS plasticity be observed in cortical layers II/III and V in developing S1BF?
- Is the observed plasticity be dependent on sensory input?
- Does AIS plasticity affect intrinsic cellular excitability in S1BF?
- Does AIS plasticity also exist in the mature mouse brain?

Taken together, the presented results demonstrate that AIS plasticity in S1BF occurs during development as well as in the adult brain. Sensory deprivation altered AIS length. Restoration of sensory input led to a rescue of AIS length to control levels. Finally, electrophysiological data suggests that AIS plasticity closely correlates with

parameters of intrinsic excitability, indicating a homeostatic role for the regulation of neuronal firing *in vivo*.

2 MATERIALS AND METHODS

Parts of the materials and methods section are excerpts from Jamann et al., 2020 (under review at the time of submission of this thesis, see list of publications).

2.1 Animals

All animal procedures were carried out in accordance with the recommendations of the Animal Research Council of the Medical Faculty Mannheim, Heidelberg University and were approved by the State of Baden-Württemberg under EU guidelines (35-9185.81/G-67/16, 35-9185.81/G-290/16). Mice of mixed gender from the wildtype C57BL/6JRj strain (Janvier Labs, France) were maintained with food and water *ad libitum* on a regular 12 /12 hours light/dark cycle.

2.2 Experimental groups

2.2.1 Developmental study

For the investigation of AIS development in S1BF, a total of 5-6 brains were analyzed in 12 age groups (Table 2). The maturation of AIS length is a robust indicator of developmental progression (Gutzmann et al., 2014; Kuba et al., 2010) and was therefore chosen as the key parameter in this study.

Table 2 Experimental groups for the developmental study

Age	IF	WB
E20	n=6	n=3
P1	n=6	n=3
P3	n=6	n=3
P7	n=6	n=3
P10	n=6	n=3
P13	n=6	n=3
P15	n=6	n=3
P21	n=6	n=3
P28	n=6	-
P35	n=6	-
P45	n=6	n=3
P180	n=6	-

Abbreviations: IF = immunofluorescence, WB = western blot

To ensure a true representation of the population, at least 100 AIS per animal were analyzed in S1BF in layers II/III and V, respectively. In early developmental stages, individual layers could not yet be identified. Thus, in the embryonic group, AIS were

analyzed in the intermediate zone. At P1 and P3, AIS from the cortical plate were analyzed for the layer II/III group and AIS from the subventricular zone were analyzed for the layer V group. For some of the age points, an additional three animals were sacrificed for Western blot analysis of AIS scaffolding protein expression (Table 2).

2.2.2 Deprivation study

For sensory deprivation experiments, animals were subjected to daily bilateral whisker trimming from P0 to different endpoints (Table 3). Whisker trimming was performed under a binocular microscope with a curved eye scissor (Fig 5). Whisker growth was monitored daily and constantly kept below 1 mm of length. In some experimental groups, whiskers were allowed to regrow (Table 3, Groups 2 and 3). Pups were trimmed without anaesthesia since they showed no sign of distress and could be handled easily. Animals older than P15 were briefly anesthetized with isoflurane prior to trimming. Adult mice (> P100) were anesthetized with 40 mg/kg BW Ketamine/ 5 mg/kg BW Xylazine i.p to minimize stress during trimming. To exclude any effects of handling or anesthesia on AIS plasticity, control experiments were performed (Table 4, Fig. 17B).

Table 3 Experimental groups deprivation

Group	Deprivation period	End Point	Control	IF	WB
1a	P0-P15	P15	P15	n = 6	n = 3
1b	P0-P21	P21	P21	n = 6	n = 3
1c	P0-P45	P45	P45	n = 6	n = 3
2	P0-P21	P45	P45	n = 6	/
3a	P10-P15	P15	P15	n = 6	/
3b	P10-P15	P21	P21	n = 6	/
4	16 days	> P100	> P100	n = 6	/

Abbreviations: IF = immunofluorescence, WB = western blot

Table 4 Control groups deprivation

Group	Treatment	End Point	IF
1	P0-P15 only handling, no trimming	P15	n = 3
2	16 days, only anaesthesia, no trimming	>P100	n = 3

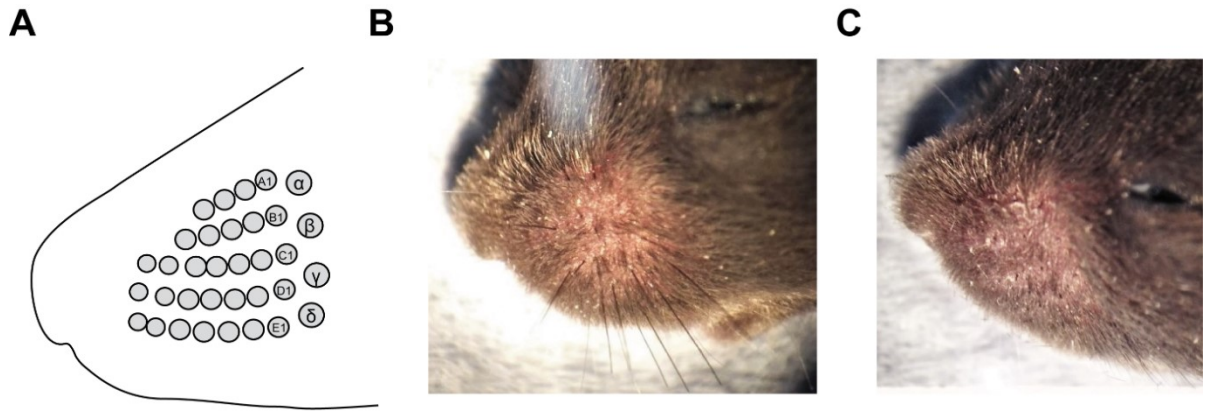

Figure 5 Whisker deprivation paradigm
A Schematic of whisker organization. Lateral view of the snout carrying five rows of principal whiskers (A-E). Additionally, three submandibular and two supraorbital whiskers were trimmed. **B** Image taken with binocular microscope, depicting the snout of a P15 mouse before whisker trimming. **C** Snout of a P15 mouse after whisker trimming. Whiskers were trimmed to less than 1 mm length and kept below this length via daily bilateral trimming.

2.3 Immunofluorescence

2.3.1 Fixation

Following previously established fixation and staining procedures (Gutzmann et al., 2014), a brief fixation protocol was used in order to improve AIS specific antibody stainings. For the developmental and deprivation studies, P0 – P7 animals were decapitated and brains were dissected in ice-cold 0.1 M phosphate buffer (PBS), fixed for 5 minutes by immersion in 4% paraformaldehyde (PFA, in 0.1 M PBS, pH 7.4) at 4°C and cryoprotected in 10% sucrose (overnight), followed by 30% sucrose (overnight) at 4°C. Animals P10 and older were exsanguinated with 0.9% NaCl under deep anaesthesia with Ketamine (120 mg/kg BW)/Xylazine (16 mg/kg BW) (Table 5). Subsequently, the brains were perfusion-fixed with cooled 4% PFA for 5 minutes. Brains were then removed from the skull with no additional post-perfusion fixation step. They were cryoprotected in 10% sucrose (overnight), followed by 30% sucrose (two times overnight) at 4 °C. The tissue was then trimmed to a coronal block including S1BF, embedded in Tissue Tek (Sakura Finetek) and snap frozen in liquid nitrogen. These samples were stored at 20°C until sectioning. Sectioning was carried out with a cryostat. Briefly, the block was trimmed in rough steps up to the desired region. Then, at least ten object slides containing four brain slices of 20 µm each were collected. Out of these ten, two object slides from different regions of S1BF were chosen for subsequent staining and microscopy.

Acute slices were fixed free floating for 20 minutes in 4% PFA (RT) and stored in 1x PBS at 4°C until further processing.

Table 5 Anesthetics

Anesthetic	Concentration	Source
Ketamin	10%	WDT, Garbsen, Germany
Xylazin	2%	Medistar, Ascheberg, Germany
Isoflurane	-	CP Pharma, Burgdorf, Germany
NaCl	0.9%	B. Braun Melsungen AG, Melsungen, Germany

2.3.2 Stainings

Table 6 Comparison of staining procedures for cryosections and acute slices

Step	Cryosections	Acute slices
Fixation	4% PFA 5 min via transcardial perfusion	4% PFA 20 min free floating
Preincubation with 0.2% Triton X-100	-	2 h
Blocking	1 h	2 h
1°AB incubation	1x ON	2x ON
1st washing step	3x 5 min	3x 20 min
2° AB incubation	90 min	1x ON
2nd washing step	3x 5 min	3x 20 min
Drying before mounting	-	min 3 h, max ON

Abbreviations: PFA = paraformaldehyde, ON = overnight, min = minutes, h = hours, AB = antibody

For cryosections, multichannel immunofluorescence (IF) staining was performed on 20 µm sections collected directly onto the object slides (see above). Slices were incubated in blocking buffer (1% BSA, 0.2% fish skin gelatine, 0.1% Triton in 1x PBS, Table 8) for at least 60 minutes to block all nonspecific binding sites and remove background staining. Subsequently, the slices were incubated in primary antibodies overnight (Table 9). After washing three times for 5 minutes in 1x PBS to remove any remaining unbound primary antibody, slices were incubated for at least 90 minutes in secondary antibodies (Table 10), protected from light. Afterwards, another washing step of 3 times 5 minutes was included to remove excess antibody. Finally, slices were immersed in mounting medium and protected by a cover slip for confocal microscopy. For preservation of IF, slices were mounted in a mounting medium with anti-fading effect (Roti-Mount FluorCare, Carl Roth, Table 7). After omission of the primary antibodies

and application of only secondary antibodies, no specific immunolabeling was observed.

For staining of acute slices after electrophysiology, an alternative staining procedure was carried out due to the increased thickness of the tissue (Table 6). Prior to blocking, penetration of antibody into the tissue was increased by incubating in PBS containing 0.2 % Triton-X100 for 2 hours. Blocking time was increased to at least 2 hours in a blocking buffer (1% BSA, 0.2% fish skin gelatine, 0.2% Triton).

Primary antibody incubation was increased to two times overnight at 4°C and followed by an extensive washing step of three times 20 minutes. Incubation time in the secondary antibody was increased to an overnight step and followed by another washing step for three times 20 minutes. Slices were then pulled onto an object slide and allowed to dry for several hours prior to mounting to avoid floating of the cover glass due to residual liquid. The mounted slices were dried at least a day before imaging so that no lateral movement would occur during imaging. A comparison of the two protocols is outlined in Table 6.

Table 7 Chemicals IF

Chemical	Name	Source
Embedding medium	Tissue Tek	Sakura Finetek, Alphe, Netherlands
Mounting medium	Roti® -Mount FluorCare	Carl Roth, Karlsruhe, Germany
Isopentan		AppliChem, Darmstadt, Germany

Table 8 Solutions IF

Solution	Composition	Source
Blocking/dilution buffer standard IHC	In 1x PBS: 1% normal fish skin gelatine 0.1% Triton X-100	Sigma-Aldrich, St. Louis, USA Carl Roth, Karlsruhe, Germany
Blocking/dilution buffer acute slices	In 1x PBS: 1% normal fish skin gelatine 0.2% Triton X-100	Sigma-Aldrich, St. Louis, USA Carl Roth, Karlsruhe, Germany
NaCl	In ddH_20: 0.9% NaCl	Carl Roth, Karlsruhe, Germany
PBS	In ddH_2O: 10 mM $Na_2HPO_4*2H_2O$ 1.47 mM KH_2PO_4	All chemicals: Carl Roth, Karlsruhe, Germany

	130 mM NaCl 2.68 mM KCl pH 7.4	KCl: AppliChem, Darmstadt, Germany
PFA	In 1x PBS: 4% PFA Filtered, ph 7.4 Stored at -20°	Merck, Darmstadt, Germany
Sucrose	In 1x PBS: 10%/30% Sucrose	Sigma-Aldrich, St. Louis, USA

Abbreviations: PBS = phosphate-buffered saline, PFA = paraformaldehyde

2.3.3 Analysis

Confocal imaging was carried out on a C2 Nikon confocal microscope (Nikon Instruments, laser lines: 642, 543, and 488 nm) with a 60x objective (oil immersion, numerical aperture of 1.4) and a SP5 confocal microscope (Leica, Mannheim; laser lines: Ar 488 nm/ 20 mW and 514 nm / 20 mW, DPSS 561 nm/ 20 mW, HeNe 633 nm /10 mW) with a 63x objective (oil immersion, numerical aperture of 1.4). To increase the number of AIS for analysis, stacks of images were acquired and merged for analysis (maximum intensity projection). The thickness of single optical sections was 0.5 µm. Stacks ranged from 10–20 µm in total depth for cryosections and were to 40 µm in z in acute slices. The confocal *x*-*y*-resolution was 0.21 µm per pixel. Images for qualitative analysis were evaluated and enhanced for contrast in Photoshop C4 (Adobe Systems). AIS length was measured using a self-written macro (Gutzmann et al., 2014; Höfflin et al., 2017) as well as the morphometrical software AISuite (Roos and Engelhardt; github.com/jhnnsrs/aisuite2). Both tools apply the well-established and widely used method of defining AIS start and end points. In brief, AIS start and end are located by the pixels where a predefined fluorescence threshold (relative to the maximum fluorescence intensity along a line drawn over an individual AIS) is surpassed (Grubb and Burrone, 2010; Gutzmann et al., 2014)). A straight line was drawn between these two points and thus defined AIS length. The threshold was adjusted depending on the individual staining quality and ranged from 10 – 30% of maximum fluorescence intensity. Both analysis tools were tested for inter-method reliability. This comparison revealed a robust consistency of results.

Table 9 Primary Antibodies

Antibody (host species)	Dilution	Target	Epitope/Sequence	Type	Source
Actin (rabbit)	1:5000 WB	Western blot loading control	C-terminus of human actin	Poly-clonal	Santa Cruz Biotechno-logy, Santa Cruz, USA
Ankyrin G (mouse)	1:500 IF 1:100 WB	AIS scaffold	Fusion protein, ~1000 amino acids of ankG, clone N106/36	Mono-clonal	UC Davis/NIH NeuroMab Facility, CA, USA
Ankyrin G (rabbit)	1:500 IF 1:100 WB	AIS scaffold	amino acids 4163-4377 at the C-terminus of ankG of human origin, clone H-215	Poly-clonal	Santa Cruz Biotechnology, Santa Cruz, USA
ßIV-spectrin (rabbit)	1:1000 IF 1:2000 WB	AIS scaffold	Recombinant protein corresponding to Human ßIV-spectrin, amino acids 2237-2256	Poly-clonal	selfmade, Biotrend Chemikalien GmbH, Cologne, Germany
MPB (rat)	1:250 WB	Myelin sheath	amino acids 82-87	Mono-clonal	Abcam, Cambridge, UK
Pan NaV (rabbit)	1:500 IF 1:1000 WB	Sodium channels	synthetic peptide CTEEQKKYYNAMKKLGSKK from the intracellular III-IV loop of Na+ channels, clone K58/35	Mono-clonal	Sigma, Saint Louis, USA
NaV 1.6 (rabbit)	1:500 IF	AIS specific sodium channel	amino acid residues 1042-1061 of rat Na$_V$1.6. Intracellular loop between domains II and III	Polyc-lonal	Alomone Labs, Jerusalem, Israel
NeuN (mouse)	1:1000 IF	Soma	IgG, Purified cell nuclei (mouse brain)	Mono-clonal	Millipore, Temecula, USA
NeuN (guinea pig)	1:1000 IF	Soma	N-terminus of Neu-N, GST-tagged recombinant protein corresponding to ms NeuN	Poly-clonal	Millipore, Temecula, USA

Abbreviations: IF = immunofluorescence, WB = western blot, IgG = Immunoglobulin G, GST = Glutathione S-transferase

Table 10 Secondary antibodies

Antibody (host species)	Dilution	Coupled to	source
ToPro3	1:1000	To-Pro-3-iodide	Life Technologies, Carlsbad, USA
Anti-rb IgG (goat)	1:1000	Alexa Fluor® 488	Life Technologies, Carlsbad, USA
Anti-ms IgG (goat)	1:1000	Alexa Fluor® 488	Life Technologies, Carlsbad, USA
Anti-rb IgG (goat)	1:1000	Alexa Fluor® 568	Life Technologies, Carlsbad, USA
Anti-ms IgG (goat)	1:1000	Alexa Fluor® 568	Life Technologies, Carlsbad, USA
Anti-rb IgG (goat)	1:1000	Alexa Fluor® 647	Life Technologies, Carlsbad, USA
Anti-ms IgG (goat)	1:1000	Alexa Fluor® 647	Life Technologies, Carlsbad, USA
Anti-gp IgG (goat)	1:1000	Alexa Fluor® 647	Life Technologies, Carlsbad, USA
anti-rb IgG (goat)	1:2000 (WB)	Horseraddish peroxidase	Dako Products, Santa Clara, USA
anti-ms IgG (goat)	1:2000 (WB)	Horseraddish peroxidase	Dako Products, Santa Clara, USA
anti-rat IgG (goat)	1:2000 (WB)	Horseraddish peroxidase	Dako Products, Santa Clara, USA

Abbreviations: rb = rabbit, ms = mouse, gp = guinea-pig, WB = western blot

2.4 Western Blot

For the developmental and deprivation study, 3 mice per selected time point were analyzed for protein expression (Table 2, 3). For mice from E20 – P3, processed samples included the entire cortex, to ensure sufficient amounts of material. For all older animals, brains were cut into 1 mm slices using a tissue matrix slicer (Zivic instruments). Then, single sections were placed in PBS and visualized using a binocular microscope in order to carefully dissect only S1BF for further sample preparation. Additionally, animals older than P10 were perfused transcardially with ice cold 0.9% NaCl as outlined above before removing the brain. Samples were diluted in a homogenization buffer (20 mM Tris, 0.5 M NaCl, 8 mM CHAPS, 6.4 mM EDTA, pH 7.5) containing Phosphatase and Protease Inhibitors (Sigma-Aldrich). Samples were then homogenized via ultrasonication, lysed for 60 minutes and centrifuged at 13.000 rounds per minute (rpm) for 45 minutes at -4°C. Protein quantification via a Bradford assay was performed and 20 µg samples containing Laemmli-buffer (2% SDS, 60 mM Tris-Cl, 10% glycerol, 5% ß-mercaptoethanol, 0.01% bromphenol blue) were heated for 10 minutes at 70°C.

Table 11 Chemicals WB

Component	Name	Source
Tris-Acetate gradient gel	NuPage® 3-8% Tris-Acetate Gel	ThermoFischer Scientific, Waltham, USA
High molecular weight protein ladder	HiMark™ Pre-stained Protein Standard	ThermoFischer Scientific, Waltham, USA
Bradford quantification solution	Roti®-Quant	Carl Roth, Karlsruhe, Germany

Table 12 Solutions WB

Solution	Composition	Source
Homogenisation buffer	in ddH_2O: 20mM Tris pH 0.5 M NaCl 0.5 % CHAPS 6.4 mM EDTA pH 7.5, stored at -20°C Protease and Phosphatase Inhibitor	 BioRad, Hercules, USA Carl Roth, Karlsruhe, Germany ApliChem, Darmstadt, Germany Serva, Heidelberg, Germany ThermoFischer Scientific, Waltham, USA
Tris-Tricine running buffer	In ddH_20 50 mM Tris-base 50 mM Tricine 0.1% SDS Store 10x stock at 4°C	 BioRad, Hercules, USA BioRad, Hercules, USA Carl Roth, Karlsruhe, Germany
Tris-Glycine buffer 1	In dd H_20 25 mM Tris-base 192 mM Glycine 20% methanol	 BioRad, Hercules, USA BioRad, Hercules, USA AppliChem, Darmstadt,Germany
Tris-Glycine buffer 2	In dd H_20 25 mM Tris-base 192 mM Glycine 15% methanol 0.05% SDS	 BioRad, Hercules, USA BioRad, Hercules, USA AppliChem, Darmstadt,Germany Carl Roth, Karlsruhe, Germany
Tris-Glycine buffer 3	In dd H_2O 25 mM Tris-base 192 mM Glycine 0.1% SDS	 BioRad, Hercules, USA BioRad, Hercules, USA Carl Roth, Karlsruhe, Germany
Laemmli buffer (2x)	4% SDS 20% glycerol 0.004% bromphenol blue 0.125 M Tris-HCl, pH 6.8 10% 2-Mercaptoethanol	Carl Roth, Karlsruhe, Germany Carl Roth, Karlsruhe, Germany Carl Roth, Karlsruhe, Germany BioRad, Hercules, USA Carl Roth, Karlsruhe, Germany
PBST	In 1x PBS: 0.1% Triton X-100	 Carl Roth, Karlsruhe, Germany
Blocking buffer	In 1x PBST 5% BSA	 PAN Biotech, Aidenbach, Germany
ECL kit	Advansta WesternBright ECL HRP substrate	Advansta, San Jose, USA

In order to be able to transfer and visualize large proteins such as the 480 kDa isoform of ankG as well as small proteins such as the 40 kDa loading control actin on the same membrane, a new protocol was developed (see Results). Following this protocol, gradient gels (3%-8% Tris-Acetate protein gels, Thermo Fisher Scientific) were loaded with the lysates and run for 55 minutes at 150 V in Tris-Tricine buffer (50 mM Tris, 50 mM Tricine, 0.1% SDS, Table 12). Blotting was performed at 550 pA in a Tris-Glycine buffer (25 mM Tris-Base, 192 mM Glycine, Table 12) under constant cooling. Solutions contained 20% methanol for 30 minutes, 15% methanol and 0.05% SDS for 30 minutes and only 0.1% SDS for another 90 minutes. After each step, membrane strips already containing smaller proteins were removed. Then, membranes were blocked for 60 minutes in PBST containing 5% BSA (Table 12). For the ankG antibody, a protein-free block with PBST was used due to non-specific interactions of the antibody when using the BSA-solution, which resulted in high background stainings. Primary antibodies were incubated overnight (Table 9) at 4°C under agitation. Membrane strips where then washed for 3 times 5 minutes each and incubated in the secondary antibodies (Table 10) for 90 minutes at room temperature. Another 3 times 5 minutes wash followed. Finally, protein signal was revealed with an ECL Kit (Western Bright ECl HRP substrate, Advansta) and imaged (Fusion solo, Vilber Lourmat). Analysis was carried out with Image J software (Supplementary Table 9). Samples were normalized against the internal loading control (actin). Additionally, in order to be able to compare several gels, a standardized sample with a consistent protein concentration was run on each gel. Samples were normalised to the βIV-Spectrin band of this sample.

2.5 Electrophysiology

Animal age ranged from P13 to P16 for the “P15” group and from P19-P22 for the “P21” group to enable the use of several animals per litter. This was done in accordance with the guidelines of 3Rs (reduce). Prior to slicing, mouse pups were briefly anesthetized with isoflurane (3%) and swiftly decapitated. The brain was quickly removed and placed in ice cold sucrose-based cutting solution (206 mM sucrose, 2.5 mM KCl, 1.25 mM NaH_2P0_4, 25 mM $NaHCO_3$, 25 mM Glucose, 3 mM MgCl, 1 mM $CaCl_2$, pH 7.4, Table 13), which was saturated with carbogen (95% O_2, 5% CO_2). A block containing S1BF was cut coronally, glued onto a slicing platform and immersed in ice-cold cutting solution which was constantly saturated with fresh carbogen. Then, 300 µm thick coronal sections containing S1BF were cut with a vibratome (VT 1200 S, Leica Biosystems). Acute slices were transferred to artificial cerebrospinal fluid (ACSF;

125 mM NaCl, 2.5 mM KCl, 1.25 mM NaH_2PO_4, 25 mM $NaHCO_3$, 1 mM $MgCl_2$, 2 mM $CaCl_2$, 25 mM glucose, pH 7.4, oxygen-saturated with 95% O_2, 5% CO_2, Table 13) and allowed to rest at room temperature for at least 30 minutes before recordings began. All recordings were carried out at room temperature. The number of cells or recorded neurons per group were n = 18 (P15 Ctrl), n = 20 (P15 Dep), n = 15 (P21 Ctrl) and n = 14 (P21 Dep). Slices were imaged with an upright Nikon Eclipse FN1 equipped with a DIC contrast filter (Supplementary Table 8). Layer II/III pyramidal neurons were visually identified and targeted for whole-cell recordings. Neuron type was confirmed online by the characteristic firing pattern and post-hoc by their characteristic morphology after biocytin filling. Patch pipettes were pulled from borosilicate glass (outer diameter 1.5 mm, inner diameter 0.8 mm, Science Products) to a tip resistance of 3.5 - 5.5 MΩ. The intracellular solution (140 mM K-gluconate, 3 mM KCl, 4 mM NaCl, 10 mM HEPES, 0.2 mM EGTA, 2 mM Mg-ATP, 0.1 mM Na_2-GTP) contained 3 mg/ml biocytin for post-hoc reconstruction and AIS colocalization analysis. Recordings were carried out using a HEKA EPC10 USB amplifier, which was controlled by Patchmaster Software (HEKA Electronics, Supplementary Figure 9). Signals were filtered with a 10 kHz (Filter 1) and 2.9 kHz (Filter 2) Bessel filter, digitized, and sampled at 50 kHz. The liquid junction potential was calculated to be –12 mV and corrected for post-hoc. Fast and slow capacitances were compensated for with the auto-functions of Patchmaster Software in cell-attached and whole-cell configuration, respectively. Series resistance (R_s) was repeatedly measured and monitored with a –10 mV step in voltage clamp mode. Neurons where R_s exceeding 30 MΩ during recordings were excluded from analysis to minimise voltage measurement errors. Additionally, R_s was measured for each neuron in current clamp mode (bridge balance) during step protocols and corrected for post-hoc. Input resistance (R_N) was calculated from the slope of the current/voltage relationship curve from a current clamp step protocol (3 steps, 50 pA, 500 ms). Resting membrane potential (RMP) was measured directly upon entering whole-cell configuration in current clamp at I = 0, when RMP had stabilised. AP properties were measured with a step protocol of 20 ms pulses, which were increased in 10 pA increments.

Table 13 Solutions electrophysiology

Solution	Composition	Source
ACSF	In ddH_2O 125 mM NaCl 2.5 mM KCl 1.25 mM NaH_2P0_4 25 mM $NaHC0_3$ 1 mM $MgCl_2$ 2 mM $CaCl_2$ 25 mM Glucose Approx. 300 mosmol, oxygenated constantly with 95% O_2/ 5% CO_2	 Carl Roth, Karlsruhe, Germany AppliChem, Darmstadt, Germany Carl Roth, Karlsruhe, Germany Carl Roth, Karlsruhe, Germany Merck, Darmstadt, Germany AppliChem, Darmstadt, Germany Carl Roth, Karlsruhe, Germany
Sucrose-based cutting solution	In ddH_2O 206 mM sucrose 2.5 mM KCl 1.25 mM NaH_2P0_4 25 mM $NaHC0_3$ 3 mM $MgCl_2$ 1 mM $CaCl_2$ 25 mM Glucose Approx. 300 mosmol, oxygenated constantly with 95% O_2/ 5% CO_2	 Carl Roth, Karlsruhe, Germany AppliChem, Darmstadt, Germany Carl Roth, Karlsruhe, Germany Carl Roth, Karlsruhe, Germany Merck, Darmstadt, Germany AppliChem, Darmstadt, Germany Carl Roth, Karlsruhe, Germany
Intracellular solution	In ddH_2O 140 mM K-Gluconate 3 mM KCl 4 mM NaCl 10 mM HEPES 0.2 mM EGTA 2 mM Mg ATP 0.1 mM Na_3 GTP 260-280 mosmol pH 7.2 with 1M KCl +3mg/ml Biocytin	 Carl Roth, Karlsruhe, Germany AppliChem, Darmstadt, Germany Carl Roth, Karlsruhe, Germany AppliChem, Darmstadt, Germany Carl Roth, Karlsruhe, Germany Sigma-Aldrich, St. Louis, USA Sigma-Aldrich, St. Louis, USA Carl Roth, Karlsruhe, Germany

Abbreviations: ACSF = artificial cerebral spinal fluid, Approx = approximately, mosmol = Milliosmol, HEPES = 4-(2-hydroxyethyl)-1-piperazineethanesulfonic acid, EGTA = ethylene glycol-bis(β-aminoethyl ether)-N,N,N′,N′-tetraacetic acid

For an analysis of firing patterns, 500-ms long current pulses, which were incremented in 50 pA steps, were used to trigger AP trains. From this, an input-frequency curve (*I-f* curve) was plotted. The maximum slope of the curve "*f*′(max)" as well as the current at maximum slope "*I f*′(max)" were analyzed and compared between groups. All current clamp protocols started starting from a holding current of *I* = 0 pA. Spontaneous postsynaptic currents (PSCs) were recorded for 2 minutes at –70 mV.

Analyses were carried out offline with either FitMaster Software (HEKA Electronics) or OriginPro 8 (Origin lab corporation). Current threshold was defined as the first current (20 ms) that reliably elicited an AP. Voltage threshold was measured at the point where the first time derivative of the phase plane plot (Fig. 12A, 22A, B) exceeded 50 V s^{-1}. AP amplitude was measured from voltage threshold to the AP peak voltage. AP half-width was defined as the width at the middle voltage of the rising phase between AP threshold and peak. For phase plot analysis, the first temporal derivative (V s^{-1}) was plotted against the voltage (V). The value at the first (AIS) and second (somatic) peak of the AP were then compared between groups. EPSCs were detected with the automatic event detection function of AxoGraph X (AxoGraph Scientific). Mean amplitudes and frequency were calculated for each neuron and average values were compared between groups.

2.6 Statistical analysis

Mean values and standard deviation (SD) of AIS length were calculated, plotted and analyzed in Sigma Plot 12.5 Software (Systat Software GmbH) or GraphPad Prism 8 software (GraphPad Software, Inc.) (for software see Supplementary Table 9). An unpaired *t*-test or Mann-Whitney test were applied for parametric and non-parametric comparison of two groups, respectively. A Two-way ANOVA followed by appropriate post-hoc correction was applied when comparing two or more groups over several time points (details are given in figure legends as well as the Supplementary Tables). In all graphs, box plots indicate the median (middle line) with min and max value (whiskers) and 25 and 75 percentiles (bottom and top border of box). P-values and number of samples are stated in each figure legend as well as Supplementary Tables for multiple comparisons.

3 RESULTS

3.1 AIS plasticity during barrel cortex development

In a previous study by Gutzmann et al., AIS length changes during development of the visual cortex were characterized (Gutzmann et al., 2014). A triphasic length change was observed, which began with an initial increase of AIS length after birth. After eye opening at P13-14, AIS length rapidly shortened and later returned to intermediate levels in adult animals. Deprivation studies with mice that were raised in the dark indicated that this triphasic developmental profile was dependent on sensory input from the eyes: In mice reared in darkness from birth to P28, the AIS remained elongated and did not shorten after P14. Based on these observations the question remained, whether this developmental plasticity was a unique feature of the visual cortex or whether developmental AIS plasticity is a common feature of sensory cortices. To address this question, AIS length changes during development of the somatosensory cortex were characterized.

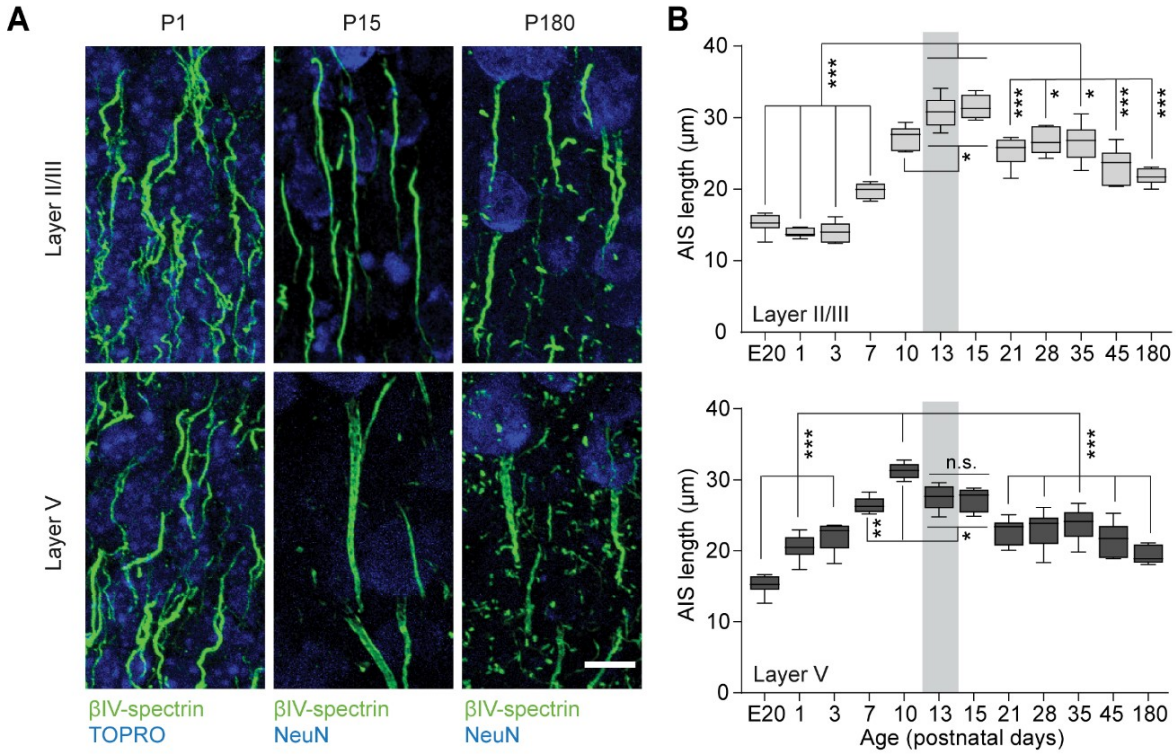

Figure 6 AIS length changes during S1BF development
A Representative confocal images of AIS length maturation for three postnatal ages (P1, P15, and P180) in cortical layers II/III and V. Immunostaining against ßIV-spectrin (green), TOPRO (blue) or NeuN (blue) as indicated. Note the long AIS at P15 in both layers. Scale bar 10 µm. **B** Population data of AIS lengths from E20 to P180 in layer II/III (top) and V (bottom). Initially, AIS length increases until P13-15,

after which it decreases. Gray bars indicate the onset of active exploration and whisking (P12–14). Adult animals maintain an intermediate AIS length throughout life (for layer II/III and layer V, One-way ANOVA $P < 0.001$, Holm-Sidak's post-hoc comparisons, >100 AIS per animal, n = 5-6 mice per age group; for all comparisons, $*P < 0.05$, $**P < 0.01$, $***P < 0.001$). Boxplots indicate median with 25 to 75% interval and error bars show min. to max. values. Only representative statistical results are depicted, all results of multiple comparisons can be found in Supplementary Table 1 and 2. Figure modified from Jamann et al., 2020.

As outlined in the introduction, primary somatosensory cortex, barrel field (S1BF) is unique in its somatotopic organization and therefore an ideal system to study neural plasticity induced by sensory input. In a first step, AIS length development during the first and second postnatal week of S1BF maturation was investigated. Additionally, juvenile and adult animals were included to detect AIS length changes over time into adulthood. The embryonic stage E20 was also included to determine AIS length *in utero*. As outlined in the introduction, several "critical periods" for barrel cortex maturation have been described (Erzurumlu and Gaspar, 2012). The chosen time points coincide with various significant critical periods of cortical development, e.g. lesion-induced structural plasticity of barrel organization (P0-P4,(Durham and Woolsey, 1984), the establishment of layer IV to II/III synapses (P10-P14, (Stern et al., 2001)) and horizontal layer II/III to II/III connections (P13-P16, (Wen and Barth, 2011)). Additionally, the chosen time points coincide with the onset of active whisking and explorative behavior in mouse pups from P10-P14 (Arakawa and Erzurumlu, 2015). A total of 6 animals per group at 12 time points (E20, P1, P3, P7, P10, P13, P15, P21, P28, P35, P45, P180, Fig. 6) were included in this study. After transcardial perfusion of the animals at the given time points, coronal sections containing S1BF were subjected to immunohistochemistry using antibodies against the widely established AIS markers ßIV-spectrin or ankG. Using a confocal microscope, at least three image stacks per animal of both layers II/III and V of the barrel cortex were collected for further morphometrical analysis (Fig. 6A). Using a previously described semi-automated method for AIS length measurement (see Material and Methods), at least 100 AIS per animal and layer were analyzed. At the first two time points (E20, P1), mature cortical layers are not yet fully developed. Therefore, AIS from the cortical plate and the subplate were included as surrogates for the supra- and infragranular layers that the sub- and cortical plate would later develop into. For E20, data was pooled and will be displayed in both graphs for comparison. For all other time points, layer II/III and layer V could be identified based on local cell density and the distance from the pial surface.

A striking pattern of developmental AIS length changes was observed, which was very similar to the developmental profile of the visual cortex: Initially, over the course of the first two weeks, AIS length increases steadily from 15.2 ± 1.4 at E20 to a peak of 31.5 ± 1.7 µm in layer II/III at P15 and 31.3 ± 1.1 µm in layer V at P10 (Fig. 6B). Interestingly, AIS appeared thin and contorted at early developmental stages. Later on, AIS had a straighter morphology with a characteristic proximal to distal diameter reduction (Fig. 6A). After the onset of active whisking and exploration of the environment ((Arakawa and Erzurumlu, 2015); P10 to P12), AIS length is reduced in both layers (25.3 ± 2.1 µm in layer II/III and 22.8 ± 1.9 µm in layer V, One-way ANOVA ***P < 0.0001, Holm-Sidak's multiple comparisons P15 vs P21 ***P <0.0001 for layer II/III, **P = 0.0042 for layer V). Then, AIS length steadily decreases in both layers, reaching a mature, intermediate length at P45 (23.3 ± 2.5 µm in layer II/III vs 21.6 ± 2.4 µm in layer V). Here, AIS length stabilizes and does not significantly differ from AIS length in older animals (Holm Sidak's multiple comparisons P45 vs P180, P = 0.80 for layer II/III and P = 0.5 for layer V). Interestingly there were some differences between the layers: Right after birth, layer V neurons start out with longer AIS (Layer II/III vs layer V at P1, unpaired *t*-test ***P < 0.0001). However, at mature age, AIS length in layer V is significantly shorter (Layer II/III vs layer V at P180, unpaired *t*-test **P = 0.007). Additionally, layer V starts shortening earlier than layer II/III and therefore already peaks at P10.

In a subsequent analysis of the data, the frequency distribution of AIS length on the population level was compared (Fig. 7). Key developmental age points (P1, P15, P21 and P45) for both layer II/III (Fig. 7A) and layer V (Fig. 7B) were compared. A change in the distribution of AIS lengths during development was found: After birth, the distribution is relatively narrow (full width at half maximum 7.68 in LII/III, 10.86 in LV). At P15, where AIS are longest, the distribution is the widest, with lengths ranging from ~ 15 to as long as ~ 60 µm in layer II/III. Overall, the distribution is wider in layer V (FWHM 14.97 in LV, 11.91 in LII/III). Afterwards, coinciding with AIS shortening, AIS distribution also narrows down (FHWM ~ 10 at P21) and stays consistently narrow at adult stages, possibly reflecting a maturation process that leads to a more homogeneous AIS length within the population.

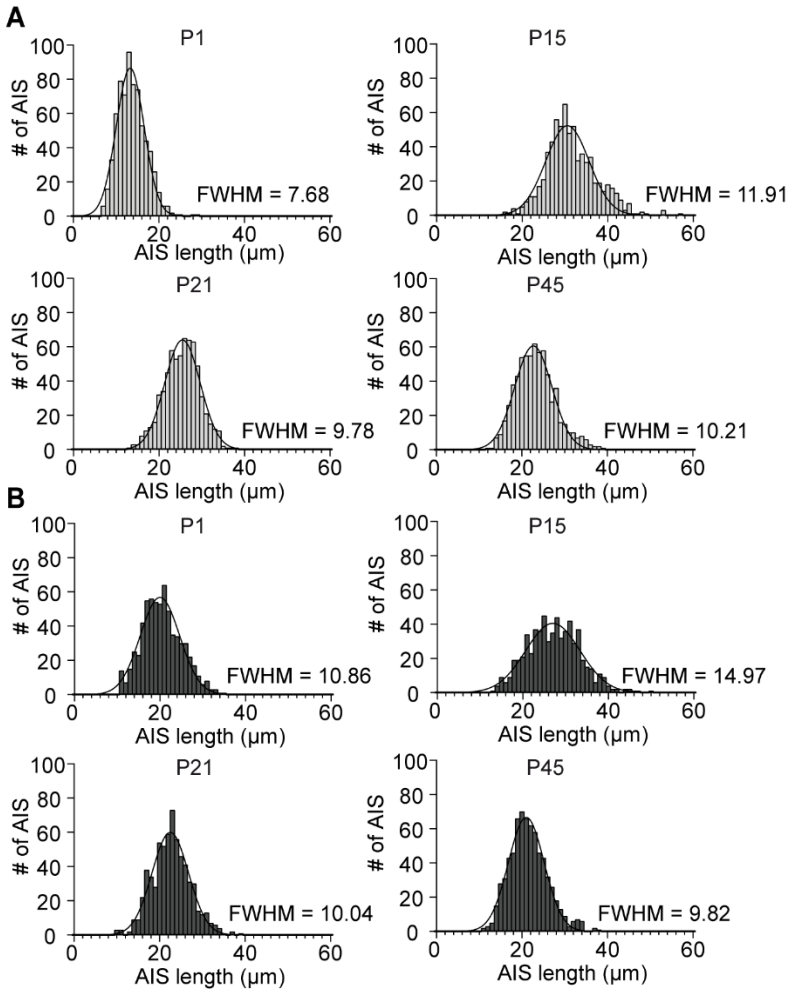

Figure 7 Population distribution of AIS length is highest at P15 in both layers
A Population histograms of AIS length with linear fit plotted for different ages (P1, P15, P21 and P45) in layer II/III. FWHM = full width at half maximum. At P1, AIS are short and the distribution is narrow. Note the increased distribution width for P15 AIS as expressed by the increased FWHM. At P21 the distribution resembles that of the mature population at P45. **B** In accordance with the layer II/III data, the variation of the length distribution is greatest at P15 and lowest at mature, post developmental levels (P45).

3.2 Establishment of a Western blot protocol for high molecular weight proteins

After observing AIS length changes during S1BF development the next question was, whether the observed structural plasticity was accompanied by changes in protein expression levels. As described in the introduction, the major AIS scaffolding proteins are ankG and βIV-spectrin. AnkG has three brain-specific isoforms (480 kDa, 270 kDa and 190 kDa). Initially, several technical challenges had to be overcome. First, using an 8% Tris-glycin gel, high molecular weight proteins such as the 480 kDa isoform of ankG cannot enter the gel during the standard electrophoresis time and therefore fail to be blotted (Fig. 8A). Second, especially at the early age time points during development, protein expression levels are low and therefore difficult to detect (Fig. 8B).

Table 14 Comparison of a standard and newly developed Western blot protocols

	Standard protocol	**High MW protocol**
Electrophoresis gel	8% Tris-glycine	3%-8% Tris-Acetate gradient gels
Blotting system	Semi-dry	Wet-blot
Blotting buffer	Tris-glycine, 20% methanol	Tris glycine, buffer 1: 20% methanol, buffer 2: 15% methanol, 0.05% SDS, buffer 3: 0% methanol, 0.1% SDS
Blotting time and current	45 mA, 90 min	500 mA, 30 min. (buffer 1), 30 min. (buffer 2), 90 min. (buffer 3)
Blotting temperature	RT	4°C

Abbreviations: min = minutes, RT = room temperature, SDS = Sodium dodecyl sulfate

Hence, a novel approach was applied to develop a protocol that would allow the analysis of protein expression of all isoforms across all ages. Table 14 summarizes the alterations that were made to the standard protocol. In order to resolve both high and low molecular weight (MW) proteins on the same gel, commercially available gradient gels were utilised. These have a gradual increase of tris-acetate along the gel so that low molecular weight proteins will stay in the gel at high concentrations and high molecular weight proteins will enter the gel at low concentrations. Next, the transfer process was modified, using a three step blotting procedure so that a step wise transfer of low to high molecular weight proteins onto the blotting membrane was achieved. After each step, a strip of membrane was removed and stored it in PBST so that the already blotted proteins would remain in the membrane and the higher MW proteins would continue to be blotted.

In order to facilitate the blotting, different concentrations of methanol and SDS were applied at each step, since methanol aids the low MW protein transfer and SDS increases transfer of high MW proteins. Finally, two membrane systems were tested with the new protocol (PVDF and nitrocellulose, Fig. 8C, D). In both cases, protein transfer was efficient enough to realiably detect proteins. The signal-to-noise ratio was better for the nitrocellulose membranes, where bands were clearly visible against the background. On the other hand, the bands also appeared crooked and diffuse in some

cases, which would make reliable analysis of protein expression difficult. Therefore, PVDF membranes were used for all Western blot analyses of AIS proteins. In order to facilitate band signal contrast, 20 µg instead of 10 µg protein was loaded (Fig. 8 C, D).

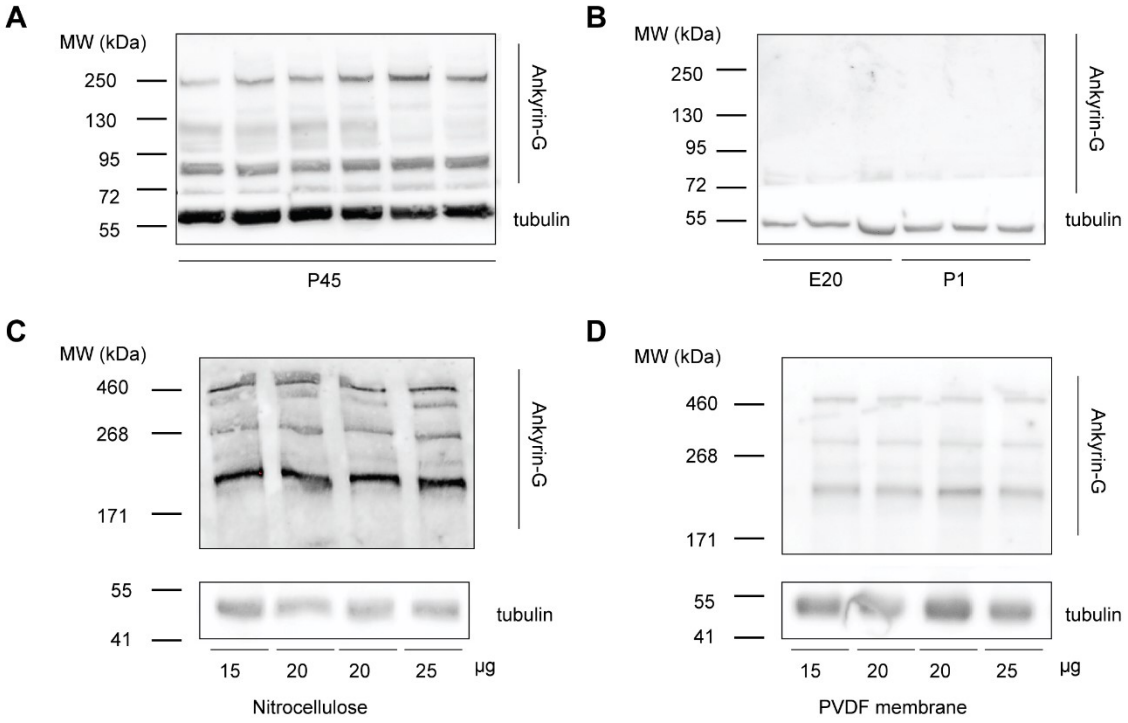

Figure 8 Establishment of a Western blot protocol to study large molecular weight (MW) proteins
A 8% Tris-glycin gel loaded with 20 µg protein samples excised from S1BF of P45 mice. With this standard gel preparation, the 270 kDa isoform is clearly visible, the large ankG isoform (480 kDa), however, is not transferred onto the membrane. **B** 8% Tris-glycin gel loaded with samples taken from of E20 and P1 mice. With the standard blotting time of 120 minutes in a semi-dry blotting system, proteins that are expressed in lower abundance in young animals will not be transferred sufficiently. **C, D** Comparison of newly developed protocol with three-step blotting process onto either nitrocellulose membrane (*left*) or PVDF-membrane (*right*). Note that in both conditions, all three brain-specific ankG isoforms are detectable (190 kDa, 270 kDa and 480 kDa). On the nitrocellulose membrane, bands show more contrast, yet appear more diffuse and aslant. On a PVDF-membrane, bands have less contrast, but are evenly shaped. With increasing amount of protein (15, 20 or 25 µg), detectability of bands increases.

3.3 Differential expression of Ankyrin G isoforms during development

Using the optimized immunoblot approach, AIS protein expression (480 kDa, 270 kDa, 190 kDa ankG and βIV-spectrin) during development was analyzed. Samples of 3 animals per group were collected and processed as described section 2.2.1. Actin was used as a loading control for protein sample concentration, since it has a lower MW

than tubulin (40 kDA) and is therefore located further away on the membrane from βIV-spectrin. This ensured a reproducible separation onto different membrane strips in the three-step protocol. Since several gels with samples from different time points were compared, each gel also contained a sample with constant protein concentration for normalization of fluorescence intensity variations across trials.

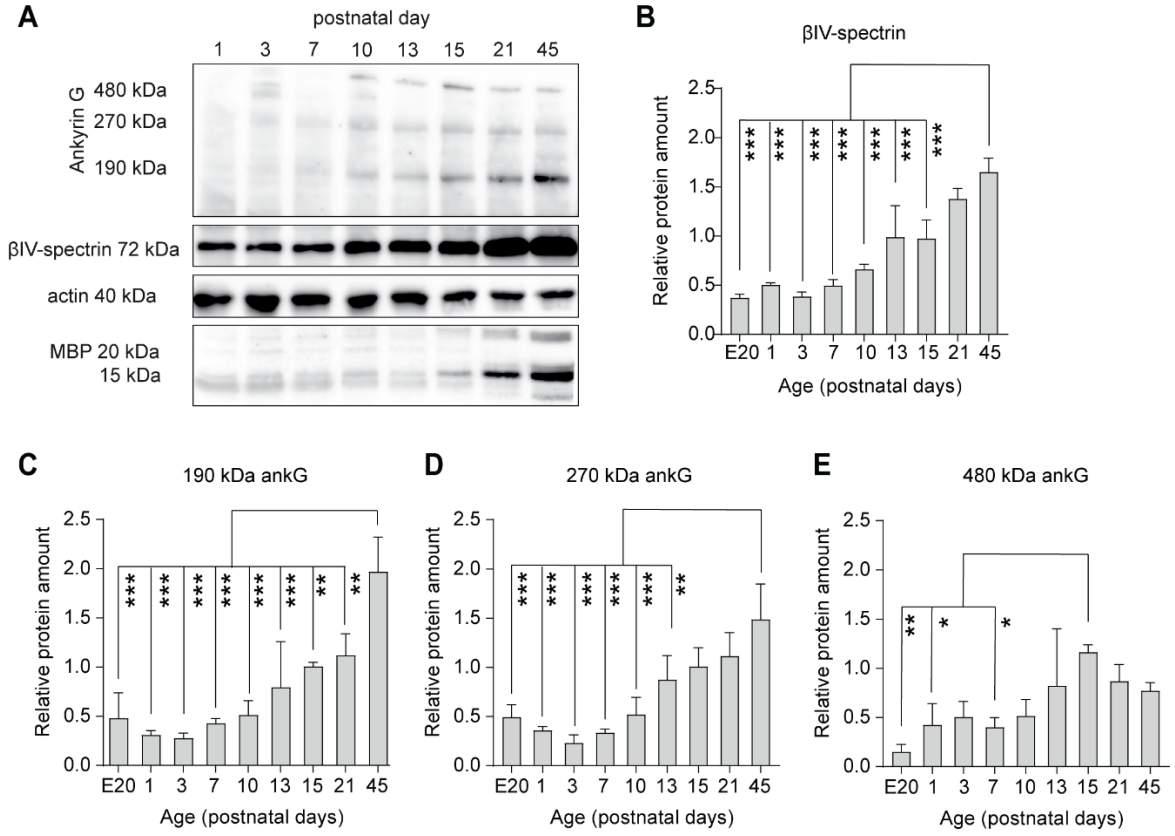

Figure 9 Differential expression of isoforms during S1BF development
A Representative immunoblot with protein samples of S1BF from different ages, stained for ankG, βIV-spectrin and MPB. Actin serves as loading control. Note the upregulation in the lower MW isoforms and βIV-spectrin as well as myelin basic protein (MBP) as a sign for increased myelination. **B** Quantification of βIV-spectrin over time reveals a significant upregulation in adulthood as compared to developmental stages (One-way ANOVA $P < 0.0001$, Tukey's multiple comparisons $^{*}P < 0.05$, $^{**}P < 0.01$, $^{***}P < 0.001$). **C** Quantification of the 190 kDa isoform over time shows a gradual upregulation until P21, followed by a significant upregulation in adult mice (One-way ANOVA $P < 0.0001$, Tukey's multiple comparisons $^{*}P < 0.05$, $^{**}P < 0.01$, $^{***}P < 0.001$). **D** Quantification of the 270 kDa ankG isoform over time shows an increase until the end of the second postnatal week. After P15, there is no significant increase compared to adult mice (One-way ANOVA $P < 0.0001$, Tukey's multiple comparisons $^{*}P < 0.05$, $^{**}P < 0.01$, $^{***}P < 0.001$) **E** Quantification of the 480 kDa ankG isoform over time shows a significant upregulation until P15 (One-way ANOVA $P = 0.0019$, Tukey's multiple comparisons $^{*}P < 0.05$, $^{**}P < 0.01$). **B – E** Only representative statistical results are depicted; all results of multiple comparisons can be found in Supplementary Table 3. Parts of figure included in Jamann et al., 2020.

A remarkable differential expression of the different AIS isoforms (Fig. 9A) was observed. Overall, all ankG isoforms as well as ßIV-spectrin are expressed at steadily increasing levels during early postnatal stages. After P15, a drastic increase of expression levels of all isoforms (with the exception of the 480 kDa isoform) until adult levels occurs (Fig. 9B – E). This could be explained in part by increased myelination, since AIS proteins are also expressed at nodes of Ranvier. Indeed, levels of myelin basic protein (MBP), a protein expressed at the myelinating membrane of oligodendrocytes, at P21 and P45 are notably increased (Fig. 9A). However, not all ankG isoforms follow the same pattern. The 190 kDa isoform only slightly increases after P21, and yet at adult stages, it is the most abundant isoform in S1BF. The 290 kDa isoform does not show a significant increase after P21, suggesting a stable expression already during development. The 480 kDa isoform shows a different expression pattern, reaching a peak expression at P15 and afterwards steadily declining to adult levels. Strikingly, this pattern reflects AIS length changes during development with an initial increase followed by a decrease after P15. Thus, AIS length changes mimic the expression profile of the 480 kDa isoform changes during development, with an initial increase followed by a decrease after P15.

3.4 Electrophysiological properties of layer II/III neurons change during development

After observing alterations of AIS structure and protein expression during development, it was next asked if these changes could have functional implications, hypothesizing that AIS length changes would go hand in hand with changes in intrinsic cellular excitability. To address this point, a series of electrophysiological experiments were carried out. Animals at three different ages (P15, P21, P28) were used for acute slice preparations. Then, whole-cell patch clamp recordings in layer II/III pyramidal neurons of S1BF were performed. In order to do so, pyramidal neurons were identified under the microscope based on their characteristic triangular appearance with a prominent apical dendrite. Additionally, pyramidal neuron identity was based on the characteristic regular spiking AP firing patterns evoked by injection of 500 ms current pulses into the soma (Fig. 10A). By using a stepwise increment of current pulses, an input frequency dependence curve was plotted (Fig. 10B). Strikingly, firing frequency was greatly reduced when comparing neurons at P15 and P28 (Two-way ANOVA $P < 0.0001$ for current injection, age and the interaction). This was especially true for the

lower current injections close to threshold (Bonferroni's multiple comparison test ***P < 0.0001 for 150, 200 and 250 pA for P15 vs P28 and P21 vs P28). P15 was, however, not significantly different from P21. Therefore, the strongest shift in excitability appears to happen after P21 (Fig. 10B). Overall, the P28 curve is shifted to the right. This was also reflected by the analysis of the slopes of the curve: Whereas the maximum slope was not significantly different between the groups (Fig 10C), the current of the maximum slope was significantly increased at P28 (Tukey's multiple comparisons *P = 0.023 for P21 vs P28, **P = 0.002 for P15 vs P28, Fig. 10D).

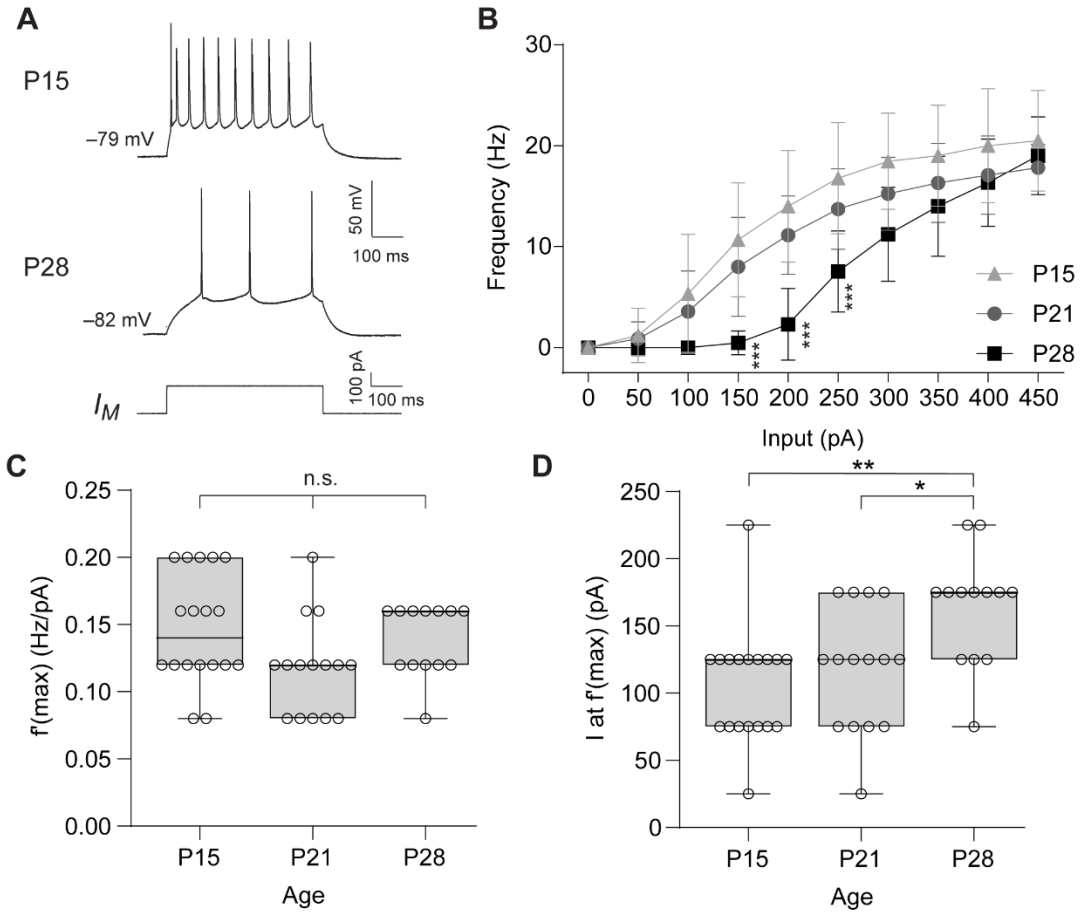

Figure 10 Neuronal firing frequency is reduced during S1BF development
A Representative traces of AP trains elicited by current injection (500 ms, 250 pA). Note the decreased firing frequency at P28. **B** Input/frequency relationship as determined by 500 ms injections of increasing currents. Firing frequencies are significantly reduced over time (Two-way ANOVA P < 0.0001 for current injection, age and the interaction. Bonferroni's multiple comparison test ***P < 0.0001, n = 15 cells P15, 14 cells P21, 13 cells P28). All results for multiple comparisons are summarized in the appendix, Supplementary Table 4. **C** Analysis of the maximum slope f'(max) of the input-frequency relationship. f'(max) was unchanged (One-way ANOVA P = 0.068). **D** Analysis of current at the maximum slope (I at f'(max)). I at f'(max) was significantly higher at P28 (One-way ANOVA P = 0.002, Tukey's multiple comparisons *P = 0.023, **P = 0.002). Parts of figure included in Jamann et al., 2020.

Previous studies had indicated that during early cortical development, passive properties of neurons change, e.g. with a hyperpolarization of the resting membrane potential (RMP) and a reduction of input resistance (R_N) (Maravall et al., 2004). Therefore, RMP and membrane resistance (R_M) changes over time were determined (Table 15). Indeed, RMP was hyperpolarized at P28 as compared to P15 (Table 15, Tukey's multiple comparisons P15 vs P28 $*P = 0.03$). This could be one contributing factor to the shift in firing frequencies, since with a more hyperpolarized RMP, more current would be needed to reach threshold. Additionally, R_N was significantly reduced over time, indicating a possible increase in soma size and dendritic complexity (Table 15, Tukey's multiple comparisons P15 vs P28 $*P < 0.0001$). Lastly, series resistance (R_S), a parameter used to monitor the quality of the electrical access to the cell during whole-cell recordings, was measured. R_S increases if parts of the cell membrane are clogging the pipette tip, leading to a divergence of the command holding voltage of the amplifier and the true membrane potential that the neuron is sitting at. R_S was significantly higher at P28 (Table 19, Tukey's multiple comparisons P15 vs P28 *P < 0.002). This is to be expected, since establishing a good seal and access to the cell is more challenging with higher age of cells, thus achieving high quality whole-cell patch clamp recordings becomes increasingly difficult. However, to minimize the possible error of the true voltage recording, only cells with $R_S < 25$ MΩ were included in the analysis according to good practice standards of this method.

Table 15 Passive properties change during development.

	P15 (n=15)	P21 (n=14)	P28 (n=13)	P
RMP (mV)	-81.76 ± 3.8	-82.22 ± 5.3	-86.59 ± 5.53	0.026
R_N (MΩ)	303.1 ± 73.98	202.9 ± 69.22	130.9 ± 38.07	< 0.0001
R_s (MΩ)	14.88 ± 2.6	12.70 ± 5.2	21.73 ± 5.9	< 0.0001

With increasing age layer II/III pyramidal neurons are more hyperpolarized at rest, have a decreased input resistance and a higher series resistance. P values depict results of One-way ANOVA. RMP = resting membrane potential, R_N = Input resistance, R_S = Series resistance. Data are indicated as mean ± SD.

Would the observed shift in intrinsic excitability also be reflected in the properties of single APs? To answer this, APs with brief increasing current pulses were elicited until reaching current threshold (Fig. 11A).

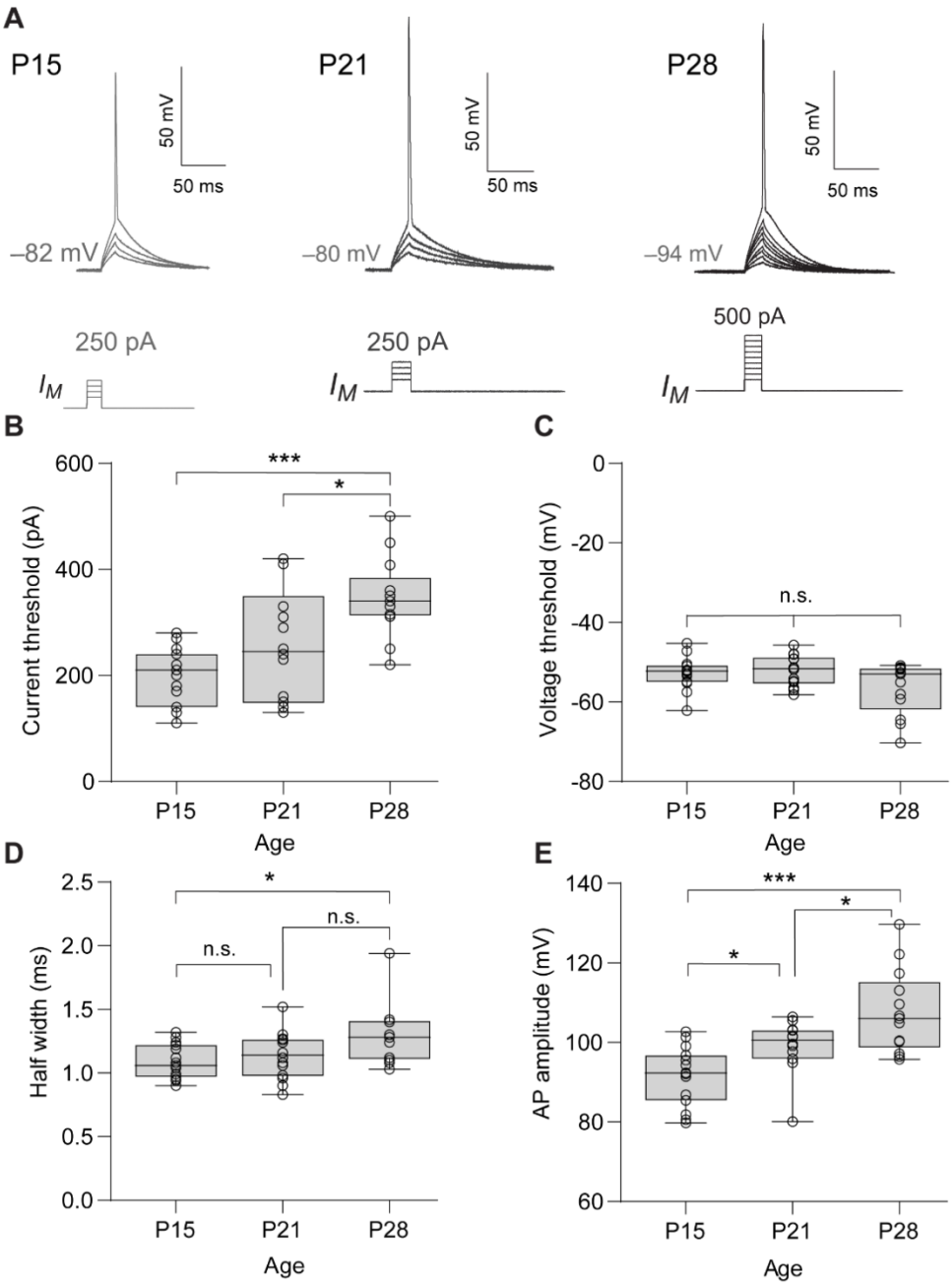

Figure 11 AP properties change during development
A Representative traces of single APs elicited by 20 ms current injections; injections at 10 pA increment to determine current threshold. Note the increased current threshold at P28. **B – D**: Analysis of AP properties for threshold APs. n = 15 cells for P15, 14 cells for P21, 13 cells for P28. **B** Current threshold significantly increases over time (One-way ANOVA $P = 0.0001$, Tukey's multiple comparisons $^*P = 0.021$, $^{***}P < 0.0001$). **C** Voltage threshold of threshold APs was unchanged (One-way ANOVA $P = 0.055$). **D** Half width was significantly higher at P28 (One-way ANOVA $P = 0.014$, Tukey's multiple comparisons $^*P = 0.014$) **E** AP amplitude significantly increases during development (One-way ANOVA $P = 0.0001$, Tukey's multiple comparisons $^*P < 0.05$, $^{***}P < 0.0001$). Parts of figure included in Jamann et al., 2020.

Current threshold (minimum current need to elicit the AP) and voltage threshold (as defined by the infliction point, where the first derivative of the volatge trace exceeds 50 Vs^{-1}) were determined next (Fig. 11B, 11C). In accordance with the *If*-curve data, current threshold was greatly increased at P28 (mean current P15 ~ 200 pA, P28 ~ 350 pA; 2 One way ANOVA ***P <0.0001, Tukeys multiple comparisons P15 vs. P28 ***P < 0.0001, P21 vs. P28 *P = 0.021). Voltage threshold, however, was remarkably constant throughout development (One-way ANOVA P = 0.054). Additionally, AP half width (width measured at mid voltage between threshold and peak) was slightly increased at P28 as compared to P15 (Fig. 11D mean AP half width P15 1.09 ms, P28 1.33 ms; P15 Tukey's multiple comparisons P15 vs P28 *P = 0.014). Lastly, a comparison of AP amplitude showed a significant increase with progressing age (mean AP amplitude P15 ~ 92 mV, P28 ~ 108 mV, One-way ANOVA P < 0.0001).

Next, it was determined whether these changes in threshold are accompanied by changes in AP shape. To address this question, phase plane plots of the development of the voltage trace over time were plotted (as represented by the first derivative; Fig. 12A). Next, the first and second peak of the curve, which had been previously demonstrated to reflect AP initiation kinetics in the AIS (first peak) and soma (second peak) (Kole et al., 2008), were measured. The data showed that both AIS and soma peak did not change during development (Fig. 12 C, 12D, AIS peak ~ 100 V/s, soma peak ~ 150 V/s, One-way ANOVA P > 0.05). Finally, it was addressed whether changes in synaptic input onto layer II/III neurons during S1BF development could be detected. To this end, spontaneous excitatory postsynaptic currents (EPSCs) were recorded at -70 mV (Fig. 12B). When comparing the mean frequency and amplitude of spontaneous synaptic events (Fig. 12 E – F), a significant increase in the frequency of EPSCs from P15 to P21 (Fig. 12E, Tukey's multiple comparison *P = 0.04 for P15 vs P21) was detected. However, the amplitude of these currents was not altered (Fig. 12F, Tukey's multiple comparisons P15 vs P21 P = 0.65). Instead, the opposite was observed in the P21 group. Here, the mean amplitude of the synaptic currents was unchanged after P21, but strongly decreased after P21 (Fig. 12F, Tukey's multiple comparisons P21 vs P28 ***P < 0.0001). Thus, synaptic input onto layer II/III neurons was drastically changed during S1Bf development, with an overall decrease in amplitude and increase in frequency.

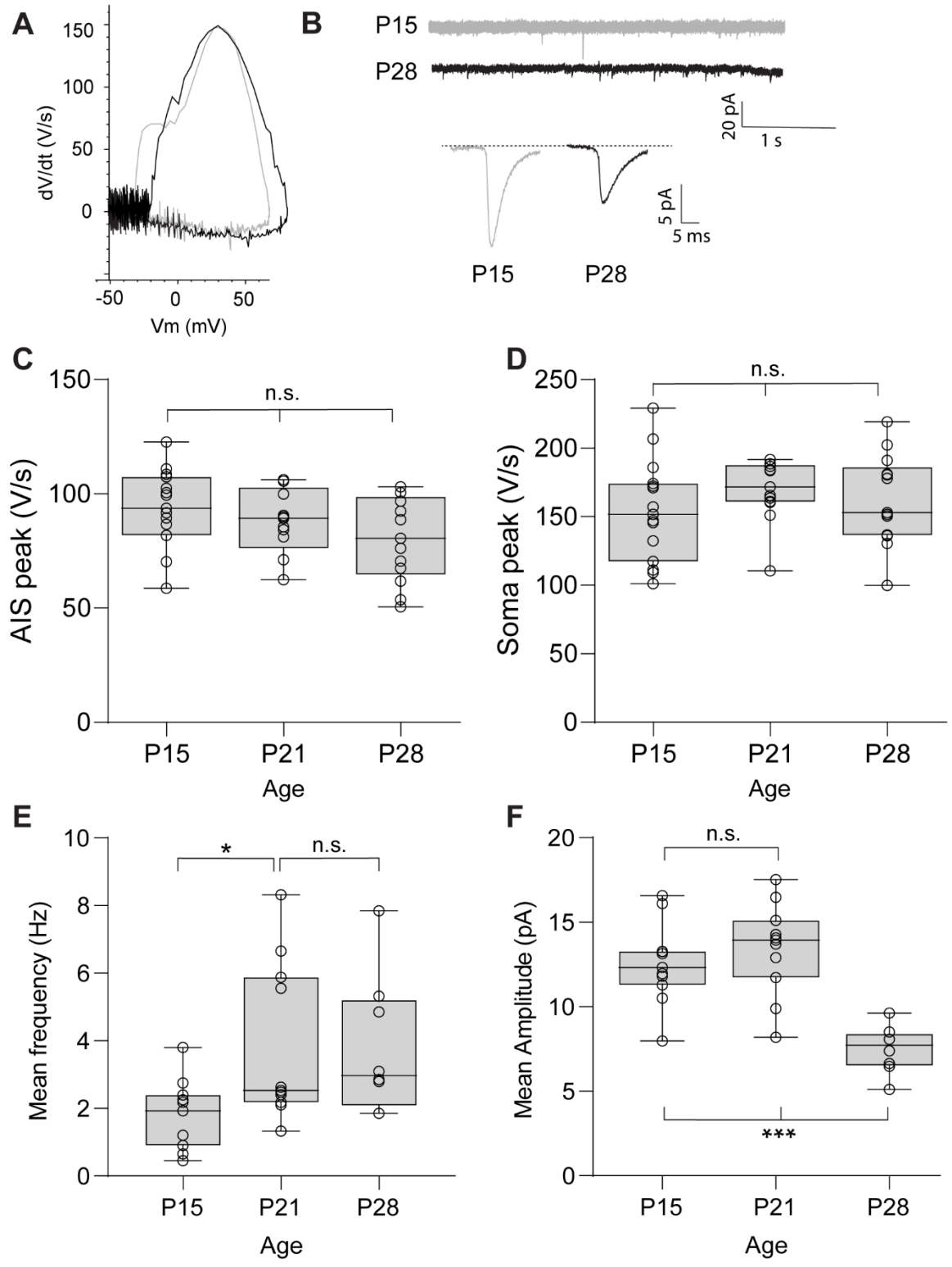

Figure 12 AP shape and synaptic transmission mature during development
A Representative phase plane plots of neurons at different ages demonstrate the change in AP shape (P15 light grey, P28 black). **B** Representative traces of spontaneous excitatory postsynaptic currents (EPSCs) recorded at -70 mV. Top trace shows 6 s of recording. Bottom trace depicts the averaged EPSCs across the entire recording session of 2 min for two sample cells. **C, D** Analysis of the first and second peak (AIS and soma peak, respectively) of the phase plane plot reveals no a significant increase at P28. C AIS peak (One-way ANOVA $P < 0.0001$, Tukey's

multiple comparisons ***P < 0.0001). D soma peak (One-way ANOVA P < 0.0001, Tukey's multiple comparisons ***P < 0.0001). **E** The mean frequency of EPSCs is significantly lower at P15 compared to P21 (One-way ANOVA P = 0.027, Tukey's multiple comparisons *P = 0.04. **F** Mean amplitude of synaptic events is significantly lower at P28 (One-way ANOVA P < 0.0001, Tukey's multiple comparisons ***P < 0.001). Parts of figure included in Jamann et al., 2020.

3.5 Long term deprivation increases AIS length in S1BF

3.5.1 Activity-dependent AIS plasticity during development

Based on the findings from the developmental study, it was next hypothesized that the shortening of AIS length after P15 and P10 in layers II/III and V, respectively, could be influenced or even triggered by an increase of peripheral sensory information, because it coincides with the onset of active whisking around P12 (Arakawa and Erzurumlu, 2015). This was tested by applying a sensory deprivation paradigm *in vivo*. As outlined in the introduction, there are several critical periods with windows of opportunity to deprive mice from tactile information that they usually receive via their whisker pad. In this study, it was decided to apply the least invasive method (manual whisker trimming), because it deprives stimuli within a physiological range of normal mouse behavior and restores sensory input after regrowth of whiskers. With whisker trimming, whiskers are kept short so that the amount of collected information is greatly reduced. However, tactile information is not completely abolished and thus the cortical columnar organization can develop normally. Changes to other neuronal compartments such as the dendritic domain have been shown to be restricted to the microscopic level only (Lee et al., 2009). Hence, it was deemed to be the appropriate deprivation model to study axonal plasticity.

In the first experimental approach, pups were deprived continuously, beginning with the day of birth (P0 – P45, Fig. 13A, Group 1). All whiskers, including supraorbital and submandibular whiskers, were trimmed daily from birth to P15, P21 and P28, respectively. AIS length analysis was carried out as described for the developmental study (representative confocal images depicted in Fig. 13B) in layers II/III and V. Daily deprivation from birth resulted in an overall increase in AIS length at P15, P21 and P45 (Fig. 13C, Two way ANOVA ***P < 0.0001 for the factor deprivation) in layer II/III. The mean increase was ~ 4.4 µm at P15, ~ 5.4 µm at P21 and ~ 3.1 µm at P45. Interestingly, AIS plasticity was only observed in layers II/III. Layer V AIS length remained unaffected by sensory deprivation (Fig. 13D, Two-way ANOVA P = 0.20 for

the factor deprivation). Of note, whisker deprivation did not abolish the developmental shortening observed previously (Fig. 6).

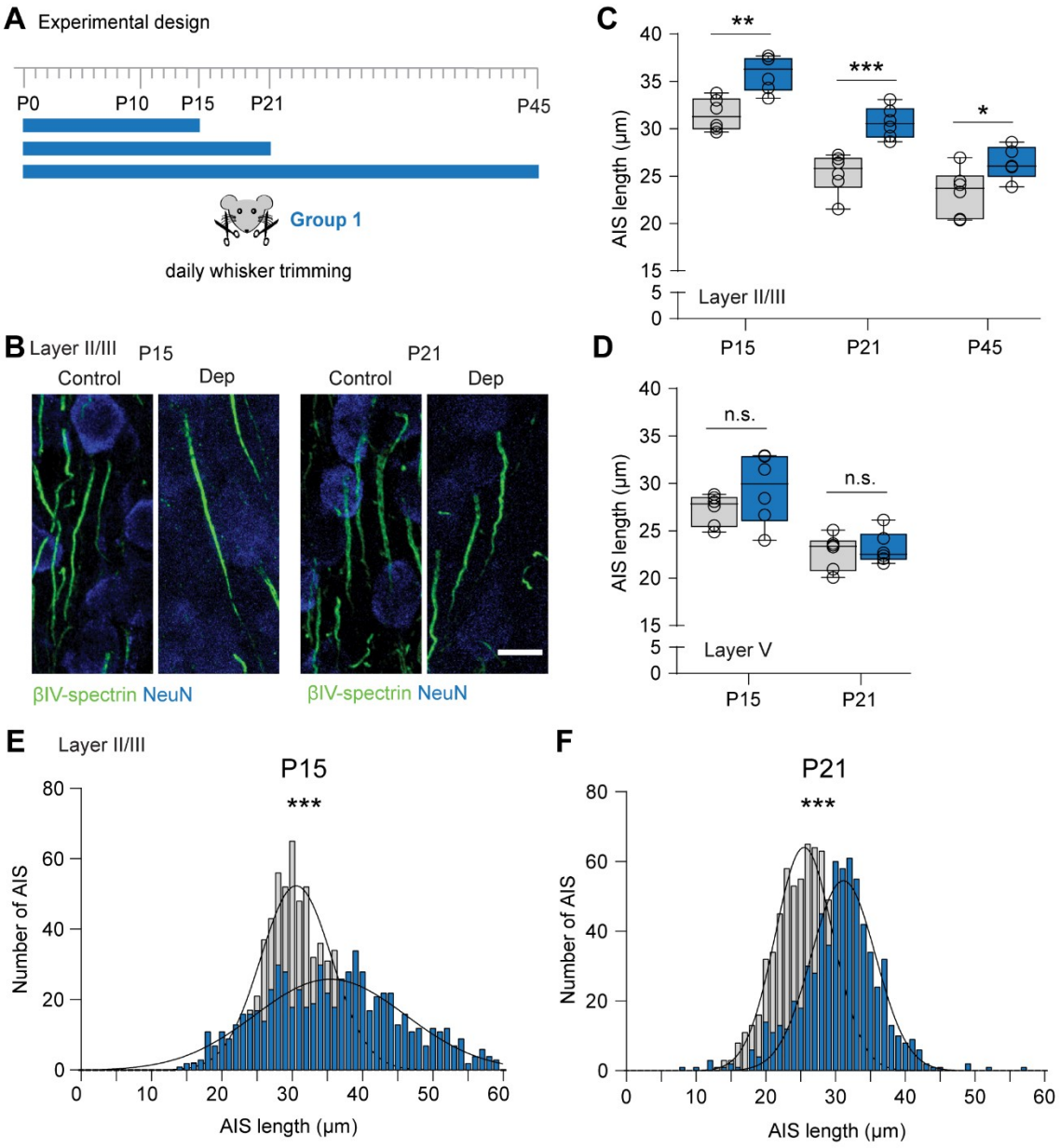

Figure 13 Long-term deprivation leads to an AIS length increase in S1BF
A Schematic of the experimental design. Whiskers were trimmed bilaterally and daily from date of birth until three respective end points (P15, P21 and P45). **B** Representative confocal images of layer II/III AIS stained for ßIV-spectrin (green) and NeuN (blue) in control and deprived mice. Scale bar 10 µm. **C** Population data for Group 1 for control (grey) and deprived (dark blue) animals in layer II/III of S1BF. Deprivation leads to longer AIS (Two-way ANOVA for both deprivation and time $P < 0.0001$, for the interaction $P = 0.417$, >100 AIS/animal, n = 5-6 mice, Sidak's multiple comparison tests $^{*}P = 0.0416$, $^{**}P = 0.002$, $^{***}P = 0.0002$). **D** Population data for Group 1 in layer 5 of S1BF. Deprivation (Dep) did not increase AIS length in layer V (Two-way ANOVA for deprivation $P < 0.0001$, for age $P = 0.20$, for the interaction $P = 0.38$, >100 AIS/animal, n = 5-6 mice, Sidak's multiple comparisons P15 Dep vs

Ctrl *P* = 0.24, P21 Dep vs Ctrl *P* = 0.94). **E** AIS length frequency histograms for the P15 and P21 time points for control (grey) and deprived (dark blue) animals (for P15 and P21 Dep vs Ctrl, >600 AIS per condition, Kolmogorov-Smirnov test P < 0.0001). Full width at half maximum P15 Ctrl 11.9 µm vs P15 Dep 25.3 µm; full width at half maximum P21 Ctrl 9.8 µm vs P21 Dep 10.9 µm). Parts of figure modified from Jamann et al., 2020

At P45, AIS were longer than in the control group, but also substantially shorter than in the P15 deprived group, suggesting that AIS shortening is in part mediated by intrinsic mechanisms that are independent of sensory input. However, deprivation did influence the extent of shortening from P15 to P21, reducing it from ~ 20% (control) to ~ 10% percent shortening (deprived) from P15 to P21 (Fig. 13C). This suggests that AIS development is at least partially influenced by sensory input from the whiskers. When plotting the frequency histograms of the whole AIS population, it became apparent that at P15 in both control and deprivation groups, a striking variability of AIS lengths was present. However, in the deprivation group, a large fraction of neurons had AIS lengths at the extremely long end of the spectrum (40 - 60 µm). This suggests that upon deprivation, a subpopulation of neurons elongate their AIS extensively while others remain within a physiological range. Interestingly, this difference was abolished in the P21 groups. Here, in the deprivation and control groups, the AIS population was more homogeneous, but the P21 neurons showed a median length shift of a few micrometers to the right (median AIS length ~ 25.6 µm (Ctrl) vs. 31 µm (Dep).

Next, it was investigated whether a shorter period (5 days) of deprivation would also lead to a significant increase in AIS length (Fig. 14A, Group 2). When animals were deprived for five days between P10 and P15 and whiskers were then allowed to regrow, no significant length change at P15, P21 or P45 in neither layers II/III (Fig. 14B, C, Two-way ANOVA for the factor deprivation *P* = 0.33) or layer V (Fig. 14D, Two-way ANOVA for the factor deprivation *P* = 0.26) was observed. This suggests that extensive deprivation periods (> 5 days) are necessary to induce lasting AIS length changes and thus deprivation induced AIS plasticity in the S1BF occurs on a slow timescale over several days to weeks.

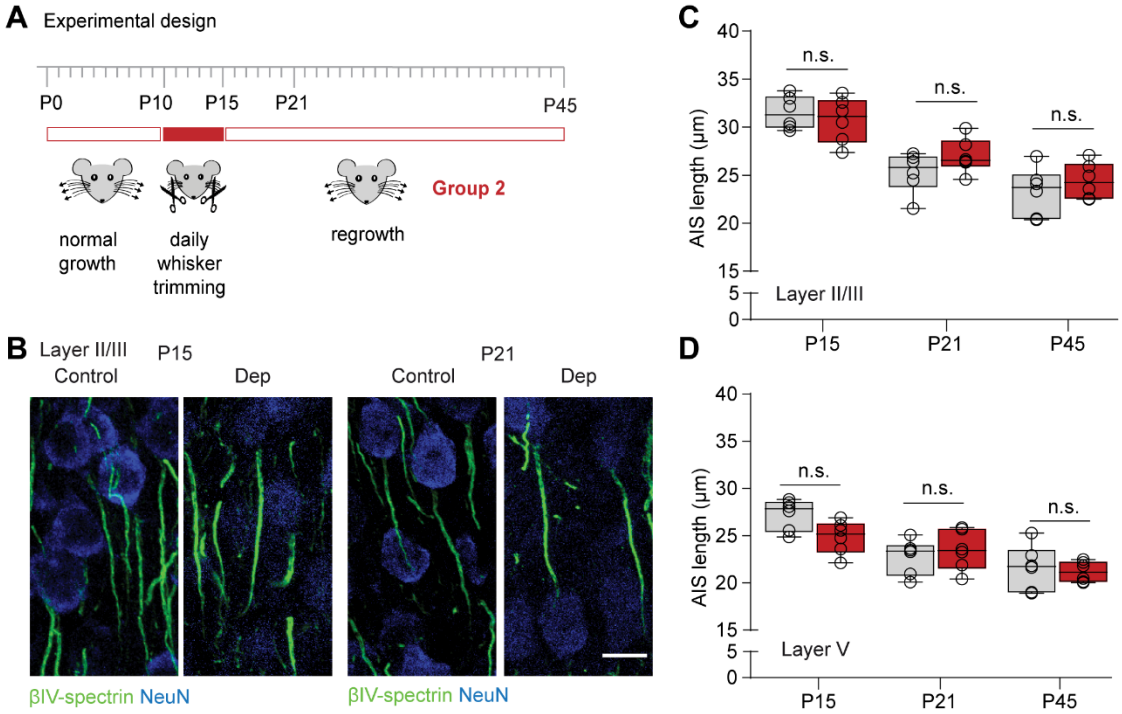

Figure 14 Short-term deprivation (5 days) does not lead to an AIS length increase
A Schematic of the experimental design. Whiskers were trimmed bilaterally and daily from P10 – P15 and were subsequently allowed to regrow until P15, P21 and P45 respectively. **B** Representative confocal images of layer II/III AIS stained for ßIV-spectrin (green) and NeuN (blue) in control and deprived mice. Scale bar 10 µm. **C** Population data for Group 2 for control (grey) and deprived (red) animals in layer II/III of S1BF. Short-term deprivation does not lead to longer AIS (Two-way ANOVA for deprivation P = 0.33, for age P < 0.0001, for the interaction P = 0.33, >100 AIS/animal, n = 5-6 mice). **D** Population data for Group 2 in layer V of S1BF. Short-term deprivation does not lead to longer AIS (Two-way ANOVA for deprivation P = 0.26, for age P < 0.0001, for the interaction P = 0.14, >100 AIS/animal, n = 5-6 mice). Parts of the figure modified from Jamann et al., 2020.

Based on the finding that activity-dependent AIS plasticity could be induced during development of S1BF, the question was asked whether there is a critical period for establishment of a mature AIS length. In this study, it was hypothesized that if there was a critical period for AIS maturation, AIS length would not “recover” to control levels even after restoration of sensory input. To answer this question, another group of animals was subjected to daily whisker deprivation until P21 (Fig. 15A). Following this period of deprivation, whiskers were allowed to regrow until the P45 endpoint. Surprisingly, AIS length returned to normal levels at P45 (Fig. 15B, C, P45 Dep vs Ctrl unpaired *t*-test P = 0.22). This suggests that even after prolonged periods of

deprivation, there is no developmentally defined critical period for AIS length, as shown by a complete reversal of the deprivation induced length changes.

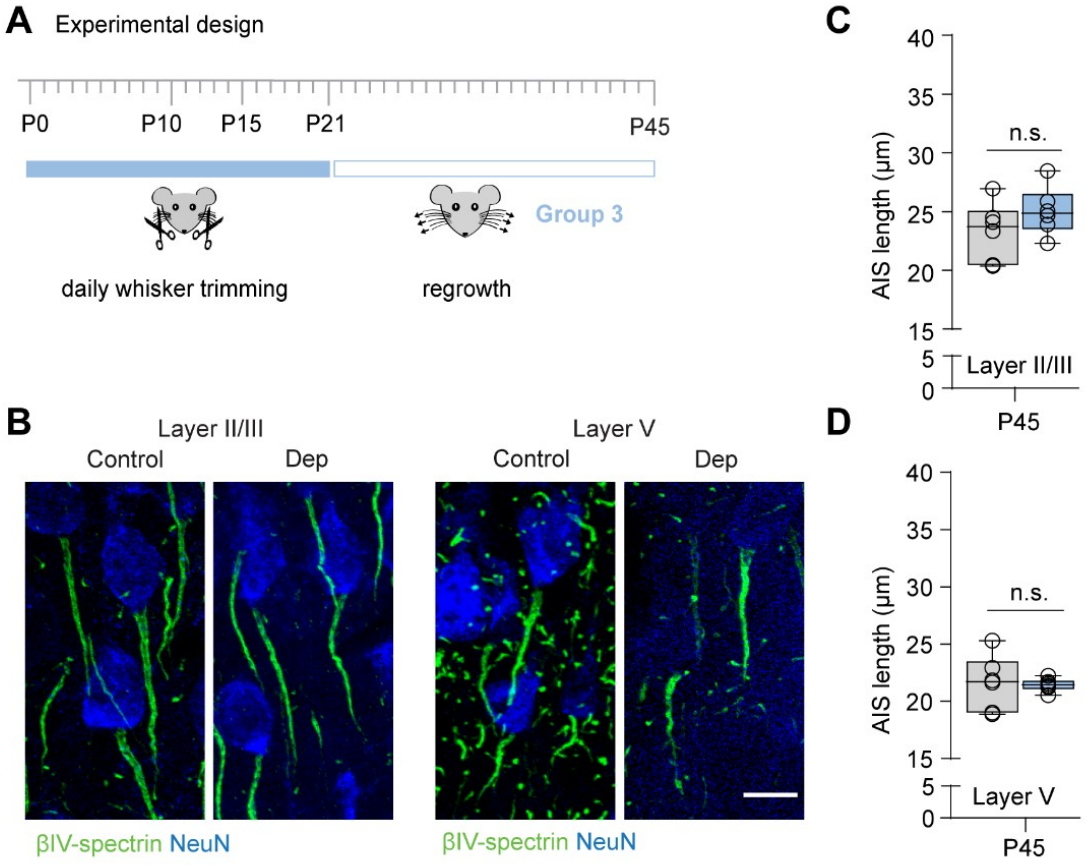

Figure 15 AIS length recovers after sensory input is restored
A Schematic of the experimental design. Whiskers were trimmed bilaterally and daily from P0 – P21 and were subsequently allowed to regrow until P45 **B** Representative confocal images of layer II/III and layer V AIS stained for ßIV-spectrin (green) and NeuN (blue) in control and deprived mice. Scale bar 10 µm. **C** Population data for Group 3 for control (grey) and deprived (light blue) animals in layer II/III of S1BF. AIS length returns to control levels after whisker regrowth (unpaired *t*-test $P = 0.22$). **D** Population data for Group 3 in layer V of S1BF. Layer V AIS length is unchanged (unpaired *t*-test $P = 0.88$). Parts of the figure modified from Jamann et al., 2020.

3.5.2 Activity-dependent AIS plasticity in adult mice

Up to this point, the present study had only focused on AIS plasticity in the developing brain. It remained unclear, whether AIS plasticity could also be a feature present in the adult brain.

Therefore, mice older than three months (>100 days) were subjected to a period of two weeks of whisker deprivation. AIS length in layer II/III and V of S1BF was then compared to control animals (Fig. 16A). To minimize stress during handling, adult mice

were anesthetized with 40 mg/kg BW Ketamine/ 5 mg/kg BW. Strikingly, AIS length in layer II/III increased from ~ 22 µm to 24 µm (Fig. 16B, C; unpaired *t*-test ***P* = 0.005). Although the length change was not as pronounced as during development (compare to Fig. 13), AIS plasticity was thus observed even in the adult neocortex. In agreement with data from the developmental experiment, layer V neurons did not undergo any measurable AIS length changes (Fig. 16B, D; unpaired *t*-test *P* = 0.95).

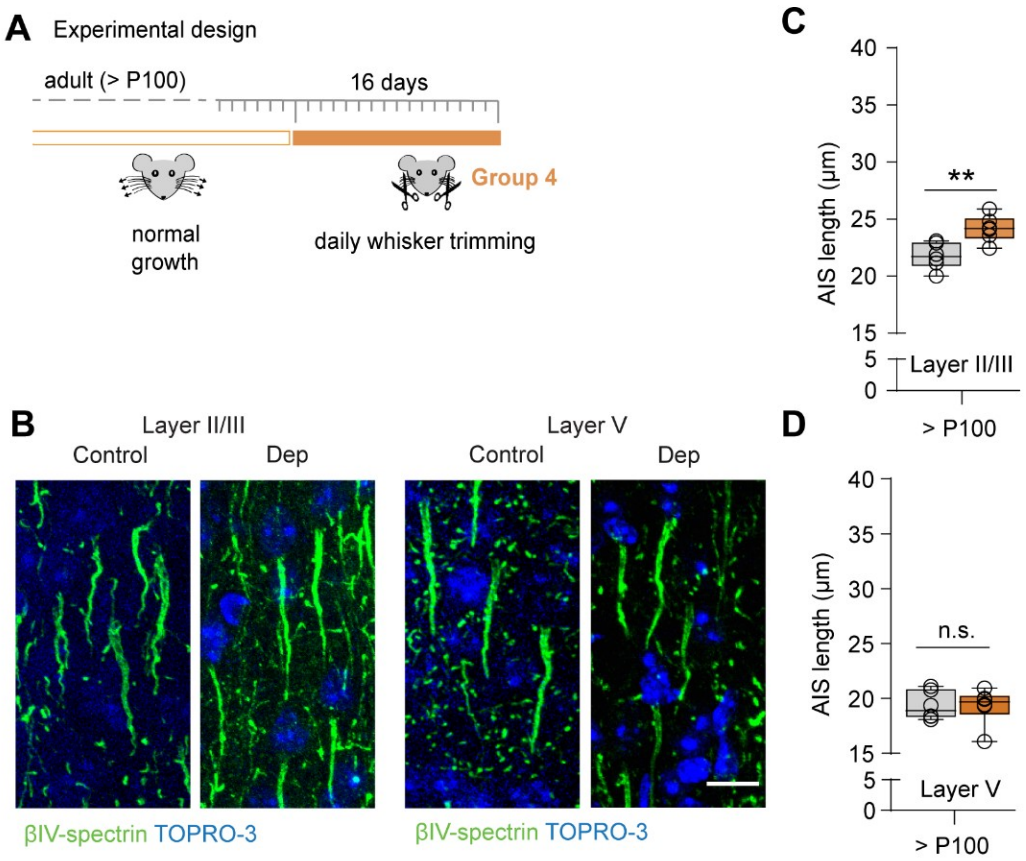

Figure 16 AIS plasticity can be triggered by sensory deprivation in adult mice
A Schematic of the experimental design. Whiskers were trimmed bilaterally and daily for 16 days in adult mice (> P100) **B** Representative confocal images of layer II/III and layer V AIS stained for ßIV-spectrin (green) and NeuN (blue) in control and deprived mice. Scale bar 10 µm. **C** Population data for Group 4 for control (grey) and deprived (orange) animals in layer II/III of S1BF. AIS length increases after 2 weeks of whisker deprivation (unpaired *t*-test *P* = 0.0046). **D** Population data for Group 4 in layer V of S1BF. Layer V AIS length remains unchanged (unpaired *t*-test *P* = 0.95). Parts of the figure modified from Jamann et al., 2020.

3.5.3 Control groups

To control for possible effects of the daily handling of pups on AIS length, a handling control group was included, in which pups were handled daily in a similar manner as

the deprivation group, but instead of trimming, whiskers were only gently ruffled. These animals showed no significant length change at P15 compared to the control group (Fig. 17A, unpaired *t*-test *P* = 0.15). Similarly, to exclude any effect of the anesthesia in adult mice, a control group that received daily anesthesia, but was not whisker trimmed, was included. These animals did not show significant AIS length alterations compared to controls (Fig. 17B, unpaired *t*-test *P* = 0.63).

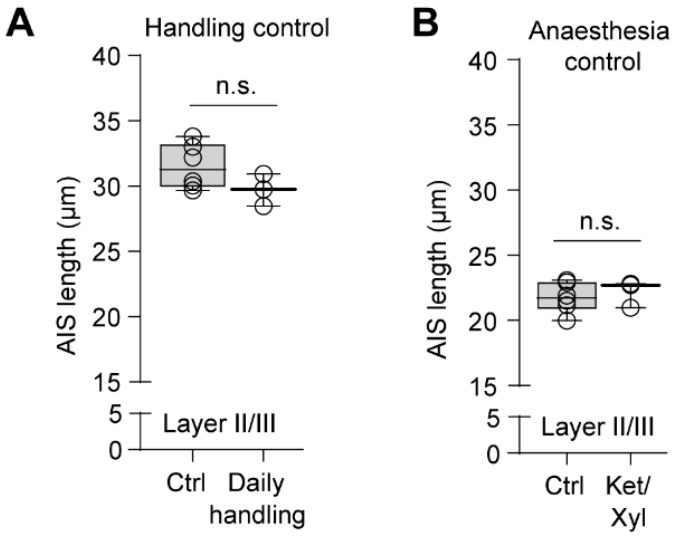

Figure 17 Control groups for deprivation experiments
A Daily handling of pups without whisker trimming does not lead to significant AIS length changes in layer II/III (unpaired *t*-test *P* = 0.15). **B** Daily anesthesia of adult mice without whisker trimming does not lead to significant AIS length changed in layer II/III (unpaired *t*-test *P* = 0.63). **A – B** n = 3 - 6 animals per group, >100 AIS per animal. Parts of the figure modified from Jamann et al., 2020.

3.6 Deprivation alters AIS protein expression

To determine, whether deprivation would affect protein expression, Western blot analysis of protein expression levels in the deprived groups was performed. Animals in the deprivation groups P0-P15, P0-P21 and P0-P45 were compared to controls (Fig. 18A). Similar to the immunoblot analysis performed during S1BF development (Fig. 9), the three ankG isoforms as well as ßIV-spectrin were investigated. Bands were normalised against actin as a loading control. Various effects were observed for the individual isoforms. AnkG 190 kDa was not significantly changed overall, although there was a transient upregulation at P21 (Fig. 18B Two-way ANOVA *P* = 0.08 for deprivation, Sidak's multiple comparisons **P* = 0.024 at P21 Dep vs Ctrl.). There were no significant changes in the expression of the 270 kDa isoform over time (Fig. 18B, Two-way ANOVA *P* = 0.08 for deprivation).

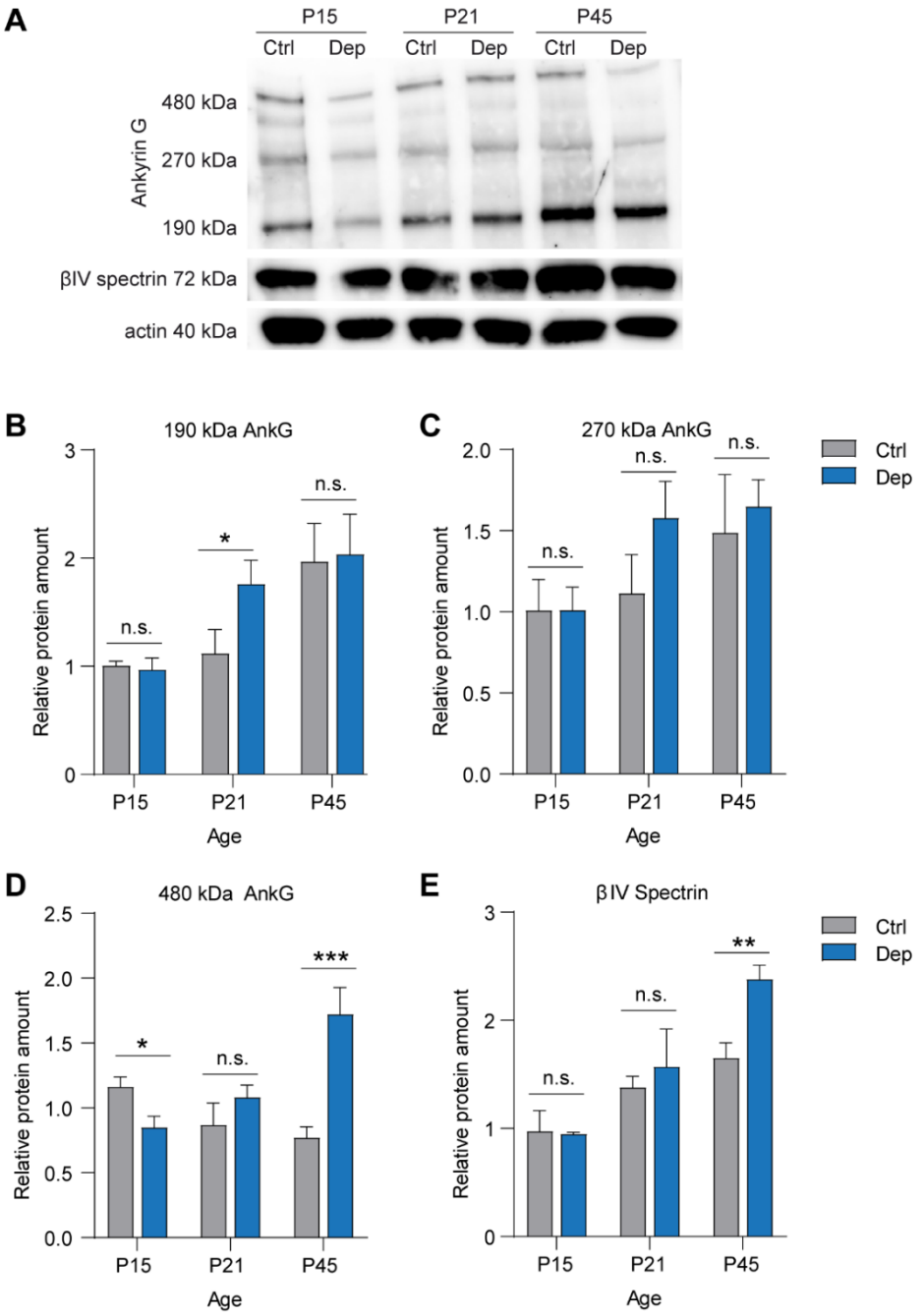

Figure 18 Deprivation alters protein expression levels during development
A Representative immunoblot with protein samples of S1BF from different ages from control and deprived animals (group 1), stained for ankG and βIV-spectrin. **B** Analysis of the 190kDa isoform shows that an intermediate upregulation occurs during development (P21), but returns to baseline at P45 (Two-way ANOVA $P = 0.08$ for deprivation, $^{***}P < 0.0001$ for age, $P = 0.07$ for the interaction, Sidak's multiple comparisons $^{*}P = 0.024$). **C** Analysis of the 270 kDa ankG showed no change in the expression of this isoform after sensory deprivation (Two-way ANOVA $P = 0.08$ for deprivation, $^{**}P = 0.004$ for age, $P = 0.24$ for the interaction). **D** Analysis of the 480 kDa reveals a differential expression. Initially, giant ankG is downregulated after sensory deprivation, however it is strongly upregulated in mature animals (Two-way ANOVA $^{***}P = 0.0005$ for deprivation, $^{**}P = 0.007$ for age, $^{***}P < 0.0001$ for the interaction, Sidak's multiple comparisons $^{*}P = 0.034$, $^{***}P < 0.0001$). **E** Sensory deprivation leads to an upregulation of βIV-spectrin in adult animals (P45), but not during development (Two-way ANOVA $^{**}P = 0.005$ for deprivation, $^{**}P < 0.0001$ for age, $^{*}P < 0.01$ for the interaction, Sidak's multiple comparisons $^{**}P = 0.001$)

The most striking development occurred in the expression of the 480 kDa isoform: initially, at P15 it is downregulated. Over time it appears to overshoot in the other direction and is strongly upregulated at P45 (Fig. 18C, Two-way ANOVA ***P = 0.0005 for deprivation, Sidak's multiple comparisons *P = 0.034 at P15, ***P < 0.0001 at P45). The upregulation of this 'giant' isoform is accompanied by an increase in the expression of βIV-spectrin at the P45 time point exclusively (Fig. 18E, Sidak's multiple comparisons **P = 0.001 at P45 Dep vs Ctrl). Thus, with prolonged deprivation, both 480 kDa ankG as well as ßIV-spectrin appear to be expressed increasingly.

3.7 Deprivation alters neuronal excitability

The deprivation experiments revealed that during development as well as in the adult brain, removing sensory input leads to a structural remodeling of the AIS and affects protein expression. However, it remained unanswered whether this structural plasticity would have consequences for neuronal function and would lead to altered intrinsic excitability. Therefore, whole-cell patch clamp experiments in the barrel cortex in acute brain slices from control and deprived animals were performed.

All measurements were performed in four groups: (I) P15 control animals with intact whiskers (P15 Ctrl), (II) P15 animals that underwent daily bilateral whisker trimming from birth (P15 Dep), (III) P21 control animals with intact whiskers (P21 Ctrl), and (IV) P21 animals that underwent daily bilateral whisker trimming from birth (P21 Dep). The numbers of cells measured per group are outlined in the legends of each figure and in section 2.5. Only layer II/III pyramidal neurons were measured; interneurons were excluded from the analysis.

First, the input/frequency relationship for the groups by 500 ms long current injections were determined (Fig. 19A). Then, the control vs deprived groups at P15 and P21, respectively, were compared. Overall and at both time points, deprivation had a significant effect on firing frequencies (Fig. 19B, D, Two-way ANOVA ***P < 0.0001 for the factor deprivation at P15 and P21). As predicted by both theoretical (Gulledge and Bravo, 2016) and experimental studies (Kuba et al., 2010), AIS elongation, here caused by the sensory deprivation, was accompanied by increased firing frequencies. At P15, this effect is especially pronounced at currents close to threshold, with firing frequencies twice as high in the deprivation group (Fig. 19B, frequency at 100pA ~ 5

Hz (Ctrl) vs ~ 10Hz (Dep), Holm-Sidak's multiple comparisons test **P = 0.0037). Overall the curve appeared to be shifted to the left, as indicated by a change of the current at the maximum slope whereas the maximum slope itself did not change (Fig. 19C, unpaired t-test P = 0.15 for f'(max), **P = 0.0028 for I at f'(max)). At P21, the effect seemed less pronounced and mainly restricted to higher firing frequencies (Fig. 19D). There was no change in the slope of the curve (Fig. 19E, Mann-Whitney test P = 0.35 for f'(max), P = 0.16 for I at f"(max)).

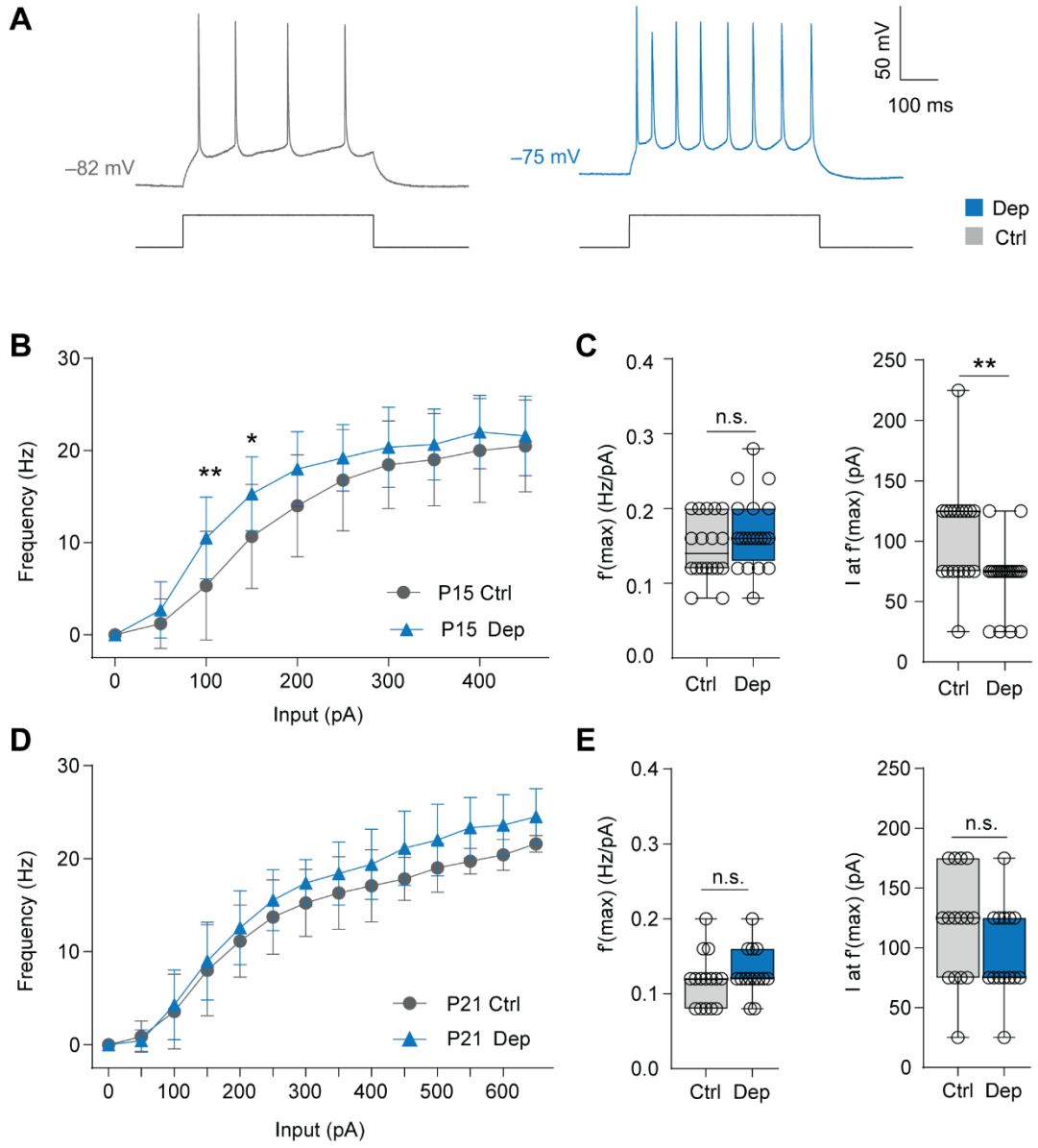

Figure 19 Sensory deprivation increases firing frequencies
A Representative traces of AP trains elicited by 100 pA current injections (500 ms pulse) at P15. Note the increased firing frequency in the deprived neurons (blue trace). **B** Input/frequency relationship for P15 as determined by 500 ms injections of increasing currents (Group 1). The deprivation group showed significantly increased firing frequencies (Two-way ANOVA ***P < 0.0001 for current injection and deprivation, Holm-Sidak's multiple comparison test *P = 0.0135, **P = 0.0037, n =

15 cells for Ctrl, 20 cells for Dep) **C** Analysis of the maximum slope f'(max) of the I-*f* curve and the current at the maximum slope (50 pA steps) I at f'(max) at P15. The current at the maximum slope was significantly lower in the deprivation group (Mann-Whitney test ***P* = 0.0028). The maximum slope was unchanged (unpaired *t*-test *P* = 0.15). *n* = 14 cells for Ctrl, 18 cells for Dep.
D Input/frequency relationship for P21 as determined by 500 ms injections of increasing currents. There was an overall increase in firing frequencies after deprivation (Two-way ANOVA *P* < 0.0001 for current injection and deprivation).
E Analysis of the maximum slope f'(max) of the I-*f* curve and the current at the maximum slope I at f'(max) at P21. The maximum slope was unchanged (Mann-Whitney test *P* = 0.35). The current at the maximum slope was unchanged (Mann-Whitney test *P* = 0.16). *n* = 15 cells for Ctrl, 14 cells for Dep. Parts of the figure modified from Jamann et al., 2020.

Next, properties of threshold APs were compared between the groups (Fig. 20A). A significant decrease in the current needed to elicit an AP was observed in the deprived neurons at P15 (Fig. 20B, unpaired t-test **P* = 0.015). On the contrary, there were no changes to the current threshold at P21 (Fig. 20C, unpaired *t*-test *P* = 0.56). Additionally, all other parameters (voltage threshold, AP half width and amplitude) remained unchanged between any of the groups (Fig. 20B, C).

Changes in the firing behavior have been shown to be influenced by passive properties of neurons, such as the membrane resistance (R_M) and RMP. Therefore, these parameters were measured to exclude a confounding effect on the data (Table 16) and found no differences between the groups. Additionally, the stability and quality of the recordings are crucial for reliable data acquisition. A measure for the quality of the electrical access to the cell is the input resistance (R_N). Comparison of this parameter between the groups showed no difference (Table 16).

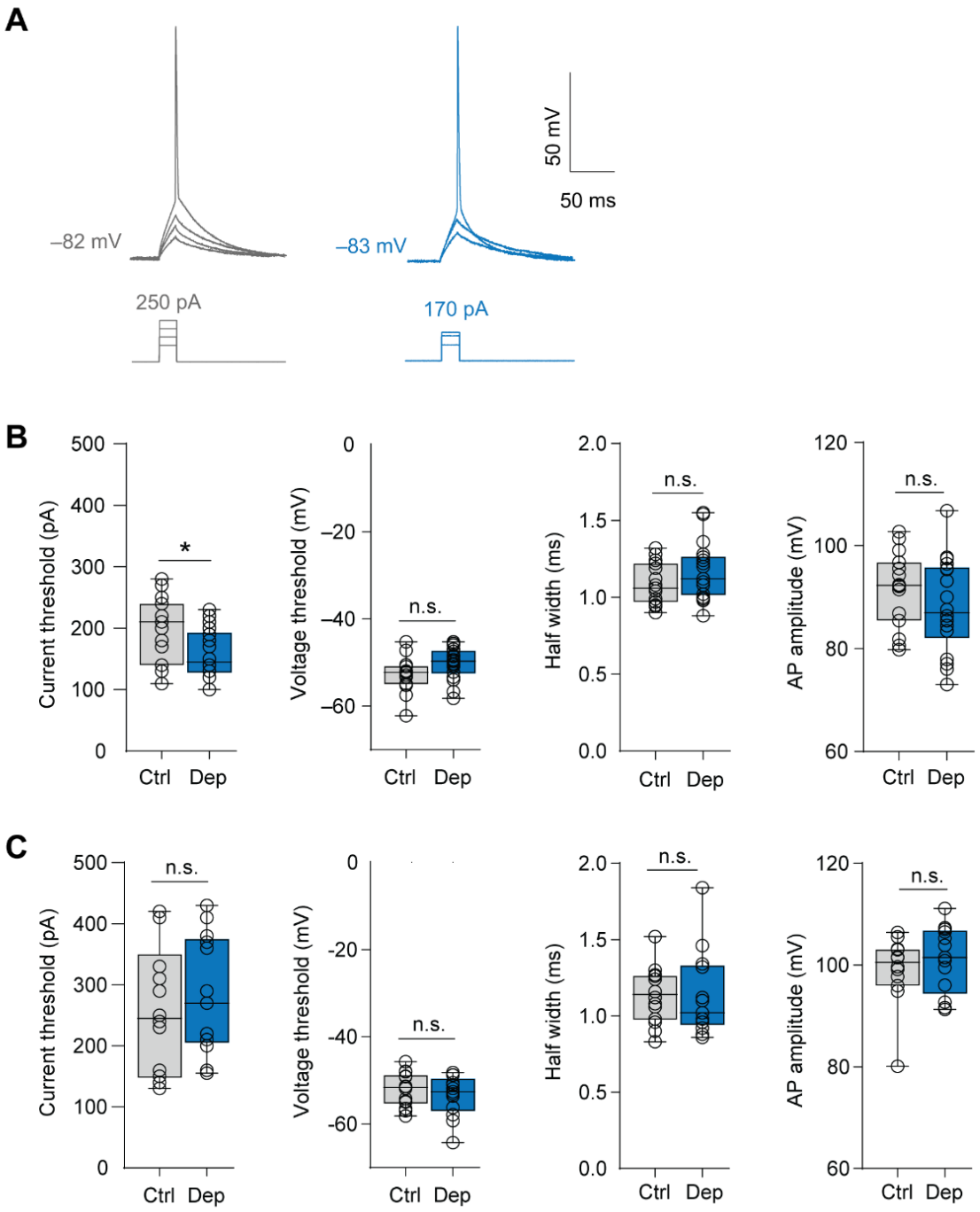

Figure 20 Sensory deprivation decreases the AP current threshold
A Representative traces of single APs elicited by 20 ms current injections at P15. Injected current was increased in 10 pA increments to determine the current threshold. **B** Analysis of AP properties for threshold APs at P15 (Group 1). Deprived neurons had significantly lower current threshold, the voltage threshold was unchanged (unpaired *t*-test, current threshold **P* = 0.0148, voltage threshold *P* = 0.07 *n* = 15 cells for Ctrl, 18 cells for Dep). The AP half width and AP amplitude were also unchanged (unpaired *t*-test half width *P* = 0.201, AP amplitude *P* = 0.276, n = 15 cells for Ctrl, 20 cells for Dep) **C** Analysis of AP properties for threshold APs at P21 (group 1). Current threshold and voltage threshold were unchanged (unpaired *t*-test, current threshold *P* = 0.56, voltage threshold *P* = 0.41 *n* = 14 cells for Ctrl, 13 cells for Dep). The AP half width and AP amplitude were also unchanged (unpaired

t-test half width *P* = 0.98, AP amplitude P = 0.40, n = 14 cells for Ctrl, 13 cells for Dep). Parts of the figure modified from Jamann et al., 2020.

Based on these findings, it was hypothesized that AIS length selectively affects current threshold. To perform a correlation analysis between the two parameters, recorded neurons were filled with biocytin for 45 minutes after electrophysiological recordings and immunostained for βIV-spectrin so that AIS length could be determined for individual neurons (Fig. 21A). The measured current was then correlated with AIS length for each neuron. Intriguingly, there was a significant correlation between the parameters (Fig. 21B, linear regression **P* = 0.029). According to this analysis, AIS length is a predictor of current threshold, with longer AIS correlating with a lower threshold. Interestingly, although the number of measured values (n) is lower in electrophysiological studies due to the technical limitations, the structural differences were still preserved: AIS length of deprived neurons was significantly longer at P15 (mean AIS length 23.5 ± 3.6 µm (Ctrl) vs 27.35 ± 0.4 µm, Mann-Whitney test **P* = 0.03), supporting the hypothesis that deprivation triggers AIS elongation and therefore lowers current threshold.

Table 16 Passive properties are unchanged after deprivation

	P15 Ctrl (n=15)	**P15 Dep (n=17)**	**P**
RMP (mV)	-81.76 ± 3.8	-78.62 ± 5,13	0.056
R_N (MΩ)	303.12 ± 73.98	347.45 ± 72.02	0.092
R_s (MΩ)	14.88 ± 2.62	14.74 ± 5.04	0.922
	P21 Ctrl (n=14)	**P21 Dep (n=14)**	**P**
RMP (mV)	-82.22 ± 5.3	-83.65 ± 6.2	0.51
R_N (MΩ)	202.9 ± 69.22	237.1 ± 100.3	0.29
R_s (MΩ)	12.70 ± 5.2	12.66 ± 6.04	0.77

Abbreviations: RMP = resting membrane potential, R_N = Input resistance, R_S = Series resistance. Data are indicated as mean ± SD. P – values depict results of unpaired *t*-tests or Mann-Whitney tests.

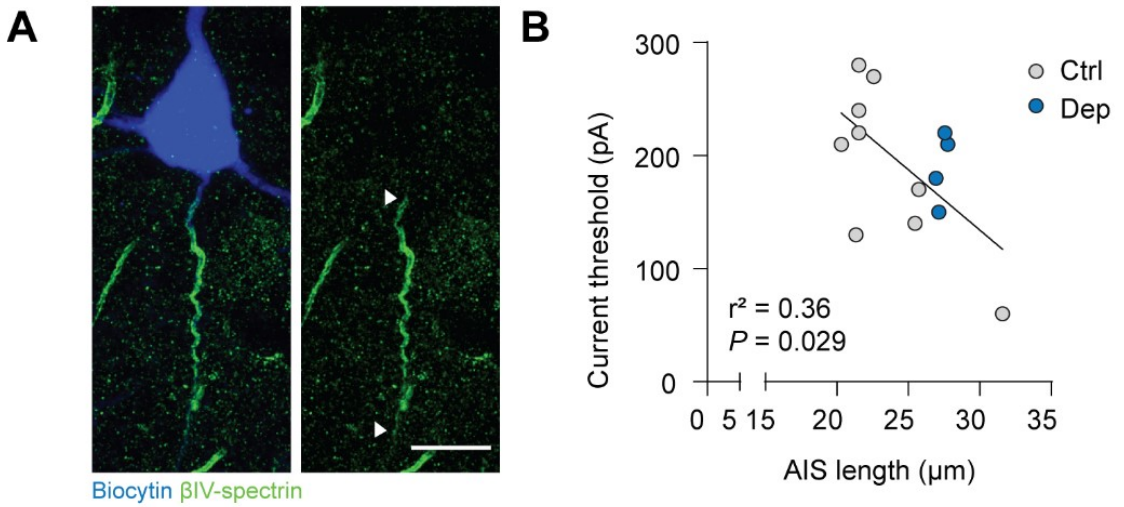

Figure 21 AIS length is a strong predictor of AP current threshold
A Representative confocal image of a neuron from the P15 deprivation group filled with biocytin (blue) for post-hoc determination of AIS length via labeling with βIV-spectrin (green). Arrows indicate start and end of AIS. Scale bar 10 µm. **B** Correlation analysis of the relationship between AIS length and current threshold. Results of linear regression analysis indicated in figure (*n* = 13 cells). Parts of the figure modified from Jamann et al., 2020.

During development, key features of AP shape such as the voltage threshold (Fig 11C) and the first and second peak in the phase plane plot (Fig. 12C, D) had been remarkably stable. Would they remain stable after long-term sensory deprivation? Indeed, there was no change in the AIS and soma peak of the AP phase plot, neither in the P15 nor in the P21 groups (Fig. 22A, B). This further supports the finding that AIS length changes will selectively influence current threshold, but not other AP parameters.

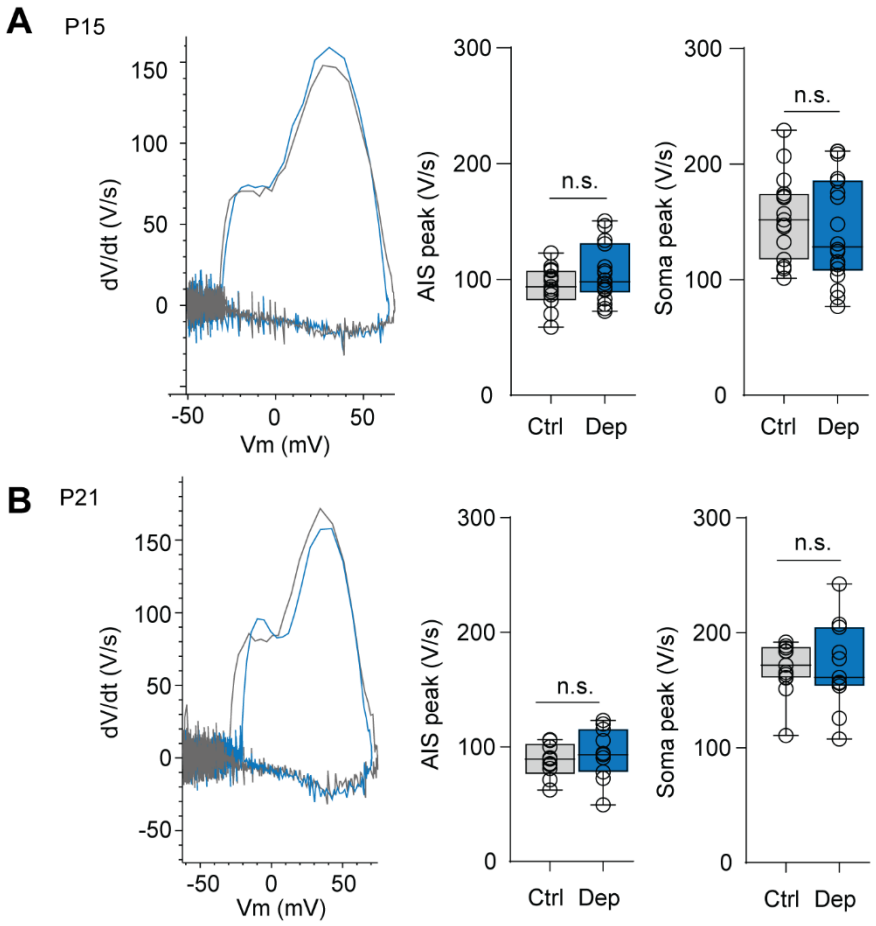

Figure 22 AP waveform is unaffected by sensory deprivation
A Phase plane plot analysis of Dep vs Ctrl APs at P15. *Left*: Representative phase plane plots of a Ctrl and Dep neuron demonstrate the similarity in AP shape. *Right*: Analysis of the first and second peak (AIS and soma peak respectively) of the phase plane plot reveals no significant difference between deprivation and control neurons at P21 (unpaired *t*-test AIS peak $P = 0.106$, soma peak $P = 0.443$, n = 18 cells Dep, n = 15 cells Ctrl). **B** Phase plane plot analysis of Dep vs Ctrl APs at P21. *Left*: Representative phase plane plots of a Ctrl and Dep neuron demonstrate the similarity in AP shape. *Right*: Analysis of the first and second peak (AIS and soma peak respectively) of the phase plane plot reveals no significant difference between deprivation and control neurons at P21 (unpaired *t*-test AIS peak $P = 0.44$, soma peak $P = 0.97$, n = 13 cells Dep, n = 11 cells Ctrl). Parts of the figure modified from Jamann et al., 2020.

Several studies had previously reported changes to synaptic connectivity and strength after sensory deprivation in the barrel cortex (Fox, 1992; Lee et al., 2009; Wimmer et al., 2010). To determine whether such changes would also occur in the current experimental paradigm, EPSCs in the control and deprived neurons were recoded (Fig. 23A, B). Strikingly, at P15, about twice as many EPSCs were recorded in deprived layer II/III neurons (Fig. 23A, mean frequency ~ 3.5 Hz (Dep) vs 1.7 Hz (Ctrl), unpaired

t-test ***P* = 0.004). At the same time, these events had an on average lower amplitude (unpaired *t*-test **P* = 0.035). Interestingly, this difference was no longer evident at P21, despite continuous deprivation (Fig. 23B). These results indicate that long-term deprivation not only triggers AIS plasticity, but also potentially induces simultaneous morphological and/or functional plasticity at synapses.

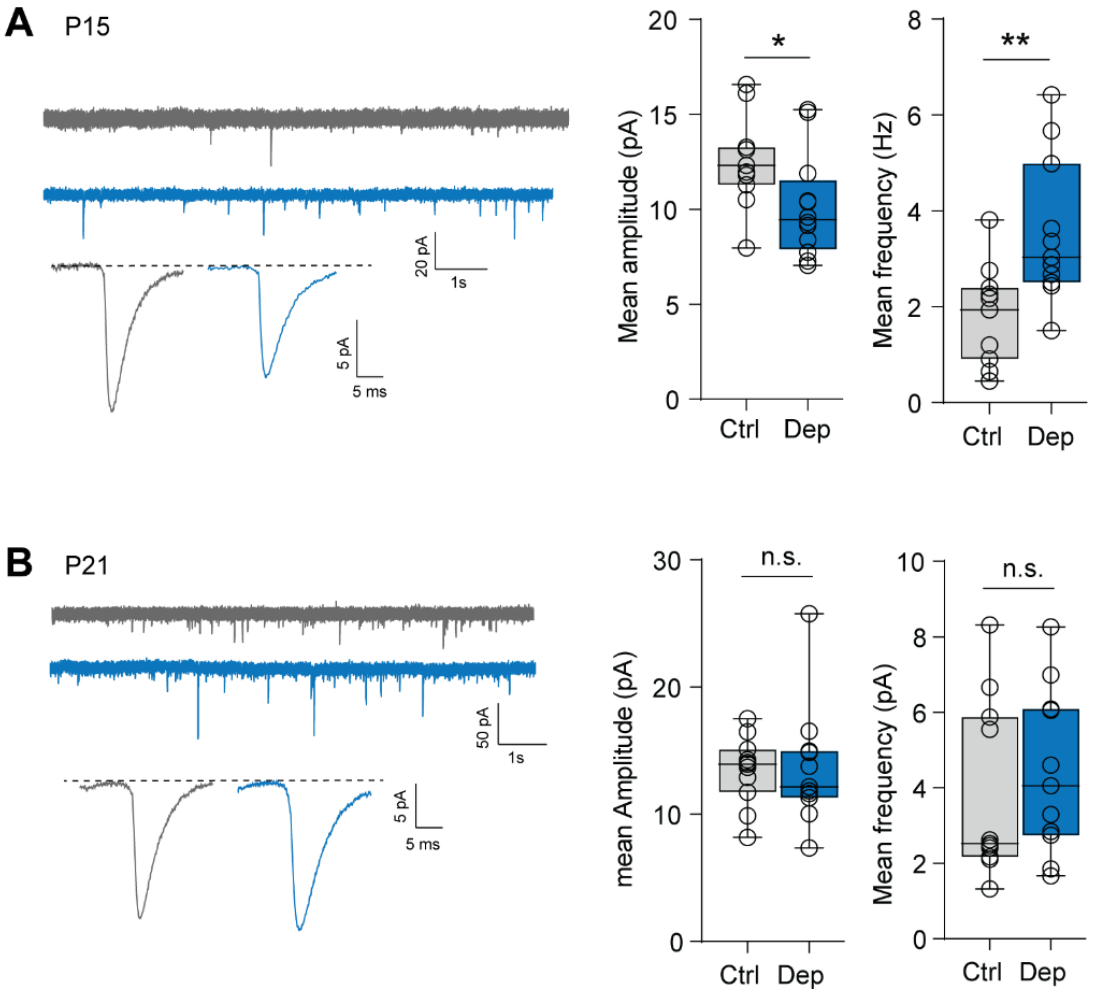

Figure 23 Frequency and strength of synaptic input is altered by sensory deprivation
A *Left*: Representative traces of EPSCs recorded at -70 mV in P15. Top trace shows 10 s of recording. Bottom trace depicts the averaged EPSCs across the entire recording session of 2 minutes for two sample cells. *Right*: Mean amplitude and frequency of EPSCs. Input onto deprived neurons had on average a lower amplitude and occurred at a significantly frequency (unpaired *t*-test, amplitude: **P* = 0.035, frequency: ***P* = 0.004, *n* = 11 cells for Dep and Ctrl). **B** *Left*: Representative traces of EPSCs recorded at -70 mV in P21. Top trace shows 10 s of recording. Bottom trace depicts the averaged EPSCs across the entire recording session of 2 minutes for two example cells. *Right*: Mean amplitude and frequency of EPSCs was not changed at P21 (unpaired *t*-test, amplitude: *P* = 0.70, frequency: *P* = 0.36, *n* = 11 cells for Dep and Ctrl). Parts of the figure modified from Jamann et al., 2020.

4 DISCUSSION

In this study investigating AIS plasticity in the developing and mature somatosensory barrel field, data show that (1) AIS length changes on a triphasic time scale during development, (2) AIS protein expression increases during development, (3) sensory deprivation alters the normal AIS developmental profile, and (4) deprivation leads to an increase in neuronal excitability.

4.1 AIS plasticity is a common feature during the development of sensory cortices

A starting point for this study was an observation made in the mouse primary visual cortex: Here, AIS length initially increased after birth and reached its maximum at around P15 (Gutzmann et al., 2014). After eye-opening, AIS length was dramatically reduced until P28. Subsequently, AIS length increased again to reach intermediate, “mature” levels at P45. When pups were deprived of visual input by rearing them in the dark, AIS length remained long, suggesting an activity-dependent AIS maturation (Gutzmann et al., 2014). Based on these findings, in the current study it was hypothesized that AIS plasticity occurs in all sensory areas of the cortex, since these regions typically undergo an increase of sensory input during development, which has been shown to be crucial for circuit maturation (Zhang and Poo, 2001). To expand on the current knowledge in sensory cortices, one of the best-studied and described sensory systems in the rodent brain was chosen, the somatosensory cortex barrel field (S1BF) (Yang et al., 2018). Here, the hypothesis that activity-dependent AIS plasticity occurs during development of S1BF was tested. Indeed, the results confirmed that AIS plasticity also occurs during the development of S1BF: From late embryonal stages (E20) to P15, a steady increase in AIS length both in layers II/III and V was observed (Fig. 6B). In fact, AIS maturation during S1BF development initially follows the time course of AIS length development in visual cortex (Gutzmann et al., 2014). However, after P15, the developmental profile diverges: in the visual cortex, AIS length dramatically decreases with a reduction of ~ 15 µm in both layers until P28. In the barrel cortex, a less pronounced, yet faster AIS length reduction was observed: AIS length shortens ~ 6 µm in layer II/III and ~ 5 µm in layer V, and reaches is minimum length already at P21. When comparing the AIS length between cortices both during development and in mature animals, it becomes evident that AIS in S1BF are a few µm shorter than in visual cortex (Supplementary Table 5).

In both studies, AIS of layer V neurons were on average 2-3 µm shorter than in layer II/III in mature animals. However, in S1BF, layer V AIS were initially longer after birth and only remained shorter than layer II/III after the second postnatal week. Interestingly, whereas in the visual cortex length reduction in both layers only began after P15, in the barrel cortex a shortening in layer V AIS already started to become apparent after P10 (Fig. 6B).

In conclusion, dynamic AIS length maturation seems to be a common theme in sensory cortices whereas it is most likely absent in other brain regions. For example, in primary motor cortex, cingulate cortex and the hippocampus, AIS length steadily increased and did not show a significant reduction at any point during development ((Gutzmann et al., 2014), Katgely and Engelhardt, Dannehl et al., unpublished data). In the prefrontal cortex of rhesus monkeys on the other hand, AIS length initially decreased during the first 6 postnatal months but remained stable in adult monkeys (Cruz et al., 2009). The hypothesis that AIS plasticity primarily occurs in sensory areas goes in line with the first description of *in vivo* AIS plasticity after sensory deprivation, which was made in the auditory brainstem nuclei of chicks whose cochlear was removed after birth (Kuba et al., 2010). Overall, current data indicates that activity-dependent developmental AIS plasticity is indeed a common feature of sensory cortices.

4.2 AIS heterogeneity

When comparing visual and barrel cortex, I focused on the mean AIS length at a given time point. Investigating the distribution of AIS length across the population, it was evident that in fact AIS length was highly heterogeneous, with lengths spanning a range of 10 to 60 µm within the same age group (Fig. 7). This observation agrees with previous findings in the visual cortex (Gutzmann et al., 2014). Additionally, this further supports studies providing evidence that baseline AIS length is highly diverse depending on species, neuronal cell type, and brain region (Bender et al., 2010; Kole et al., 2007; Kuba et al., 2010; Thome et al., 2014). When comparing length distribution profiles, AIS length overall followed a normal distribution so that a Gaussian curve could be fitted. However, the width of the Gaussian curves changed during development and following deprivation: During early development (P1) and at adult stages, the distribution was relatively narrow, indicating a more homogeneous population (Fig. 7). In contrast, at P15, there was a markedly higher range of AIS lengths. Interestingly, the heterogeneity was further increased by long-term deprivation

(Fig. 13E). This suggests that during periods of increased remodeling and plasticity, AIS length is more diverse. Hence, AIS length refinement during development was not only confined to overall shortening, but appeared to serve “homogenization” of AIS length to an intermediate, “ideal” length, which then was a defining feature of mature neurons. Interestingly, deprivation by whisker trimming did not affect this maturation of the population distribution, since at P21 the width was comparable to the control animals (Fig. 13F). This indicates that the narrowing of AIS length distribution after P15 was independent of sensory input.

4.3 AIS plasticity is layer-specific

In addition to the described difference in time course and baseline length of layer II/III and layer V AIS plasticity (Fig. 6), the deprivation experiments clearly show that plasticity induced by whisker trimming only resulted in AIS plasticity in layer II/III neurons (Fig. 13C). AIS length in layer V neurons remained stable (Fig. 13D). The same phenomenon was observed in adult mice, where remodeling in layer II/III could still be triggered, but not in layer V (Fig. 16).

What could be a possible explanation for this finding? One of the structural limitations of AIS plasticity in layer V might be the onset of the myelin sheath in close proximity to the distal end of the AIS. Myelination of the cortex is gradually achieved throughout development from infra- to supragranular layers, with an overall increased expression in layer V (Hamada and Kole, 2015; Tomassy et al., 2014). Additionally, layer V neurons have been shown to be myelinated directly adjacent to the onset of the AIS. This might explain why layer V neurons are left with no reserve space to extend their distal AIS any further as soon as myelination is completed. Layer II/III pyramidal neurons often exhibit a long section of axon that remains unmyelinated until the axon projects into deeper layers or along white fiber tracts intercortically. This is evident in a visible gap past the distal end of the AIS, and before myelin onset (Tomassy et al., 2014). Thus, this might be an explanation why AIS plasticity in form of an elongation at the distal end predominantly occurred in layer II/III. Another difference between the layers can be found at the circuit level. The main input layer in S1BF is layer IV, which receives direct input from the thalamus (Feldmeyer et al., 2013). The afferent thalamic signals are then transferred by layer IV neurons to layer II/III, forming the first intracortical connection. Subsequently, the information is transferred from layer II/III to layer V, the main output layer of the cortex. Due to intracortical processing and local

inhibition, there might be dampened synaptic input on the level of the second intracortical synapse, leading to a reduced drive for activity-dependent plasticity. Layer V has been reported to also receive a direct input from the thalamus (Bureau et al., 2006). More specifically, only a subset of neurons (layer Vb) receives this input from VPM, which is also slightly delayed and weaker compared to the layer IV input (Armstrong-James et al., 1992; Bureau et al., 2006). These anatomical scenarios might ultimately explain the lack of AIS plasticity in layer V.

Additionally, there might be a general ability of supragranular layers to retain plasticity beyond early development when compared to infragranular layers as reported previously for synaptic plasticity in S1Bf (Glazewski and Fox, 1996; Skibinska et al., 2000). Activity-dependent processes such as spine dynamics and synaptic plasticity were found to be layer specific (Bourg et al., 2016, 2019). Similar findings were made in other sensory cortices such as the visual cortex (Jiang et al., 2007).

Interestingly, there have been reports of layer-specific functional differences during development. Whisker-evoked spiking develops differently in both layers: The number of spikes evoked by whisker deflection decreases during the second and third postnatal week in layer II/III, whereas spike counts in layer V increase (Bourg et al., 2016). A response selectivity for a certain whisker movement (e.g. direction of whisker deflection) emerges in both layers around P14, which correlates with the onset of AIS shortening. Overall, the difference in developmental and activity-dependent plasticity of the AIS appears to be layer-specific in S1BF. The underlying regulatory mechanisms need to be elucidated by further studies.

4.4 AIS elongation in the context of early barrel cortex development

In order to elucidate the various factors that influence and promote the observed AIS remodelling during development and in the adult, it is important to analyse a time course that reflects the major stages of circuit maturation, spanning from the late embryonic period (E20) into full maturity (P180). As outlined in the introduction, various critical periods occur during S1BF development, during which important steps in establishment of the local connectivity are achieved. One noteworthy fact is that a great majority of long-range axonal connections in S1BF are already established during embryogenesis and are therefore already believed to be hardwired into the circuit at the time of birth (Erzurumlu and Gaspar, 2012). The whisker-to-barrel pathway is formed in a peripheral to central fashion: Initially, new-born neurons in the trigeminal nuclei elongate their axonal projections both toward the whisker pad, which they reach

around E10.5, as well as the brainstem, which they innervate by E12 (Ding et al., 2003; Stainier and Gilbert, 1990). Neurons in the principal nucleus of the trigeminus (PrV) start extending their axons toward the contralateral thalamus around E11 and reach VPM at E17 (Ding et al., 2003). VPM neurons begin to project towards the cortex at E16 (Erzurumlu and Gaspar, 2012). Around the same time, layer IV neurons are born (Rebsam et al., 2002). The thalamocortical afferents reach the cortex at around E20/P0 (Agmon et al., 1993). Interestingly, in a very similar way, the topographical organization at the different pathway relay stations is formed in a temporally subsequent manner: At P0, the first barrelettes in the brainstem become apparent (Ma and Woolsey, 1984). At P1 and P2, respectively, the axon terminals in VPM and the cortex start forming “rows”. They are the templates for barreloids and barrels, which form a few days later: VPM barreloids are detectable at P3 (Durham and Woolsey, 1984). Barrels only start forming between P5 – P7 (Rice et al., 1985). Between P1 and P7, the morphology of thalamocortical afferents changes from poorly branched axon terminals to highly branched axons that are spatially restricted to an individual barrel (Rebsam et al., 2002). Thus, the initial phase of AIS elongation falls into a phase where local cortical connectivity is still being established, whereas the pathway that conveys sensory information from the periphery has already been formed.

At the same time, clearly distinguishable cortical layers are still being established. At birth, the laminarization of the cortex is not yet fully formed. Instead, the cortex is divided into several plates: Closest to the pia is the marginal zone, which will later develop into layer I. Adjacent to it, the cortical plate will later form layers II to VIA. At P0, the cortical plate is still relatively thin and expands until P12, when full development of all cortical layers is achieved (Osterheld-Haas and Hornung, 1996). The subplate constitutes the innermost plate in the developing cortex and will later form layer VIB. It contains early born neurons that display fully mature firing properties at birth. They exhibit a burst firing pattern by which they mediate oscillatory activity in the cortical plate (Tolner et al., 2012). These synchronous network oscillations are characteristic for the new-born brain, as they can be found in rodent pups as well as premature born humans (Khazipov and Luhmann, 2006). After P5 in rodents, networks start to gradually desynchronize until the end of the second postnatal week (Golshani et al., 2009). In the first postnatal week, when cortical layers are not yet distinguishable and firing is synchronized, AIS appeared short and had a thin, contorted shape (Fig. 6A). With increasing postnatal age, AIS elongated and straightened in shape, following the

trajectory of cortical expansion (Fig. 6A). Taken together, postnatal AIS elongation occurs during a phase when mature cortical layering is being established, possibly reflecting an immature circuit.

4.5 A shift in the excitation-inhibition balance coincides with AIS shortening during development

The AIS shortening after P15 for layer II/III and P10 for layer V (Fig. 6) coincides with a phase of increased plasticity and several critical periods. A two-photon time-lapse study following the motility of small dendritic processes (spines and filopodia) *in vivo* in layer II/III rat barrel cortex found that motility is highly increased during the second postnatal week (Lendvai et al., 2000). Sensory deprivation led to a 40% reduction in motility at P11-P13, demonstrating a very brief critical period for sensory-dependent spine motility (Lendvai et al., 2000). Although intracortical connections are already forming before P10, there is an abrupt increase in the total number of putative synapses in the time window between P10 and P15 (Micheva and Beaulieu, 1996). This increase continues until P21 for excitatory synapses, after which total synapse numbers begin declining, indicating a possible refinement and pruning of the initially formed synaptic connections. At the same time, the number of inhibitory GABAergic synapses increases (Micheva and Beaulieu, 1996). However, after an initial steep increase from P10 to P15, the total number of GABAergic synapses reaches a plateau (Micheva and Beaulieu, 1996). The differential expression of synapses during this period of development might have major effects on the ratio of cortical cellular excitation to inhibition, in short termed the “excitation-inhibition balance”. Since cortical neurons have to integrate thousands of signals from both excitatory and inhibitory inputs, a balance of the net current is thought to be essential to maintain a physiological dynamic range (Yizhar et al., 2011). Between P15 and P21, the excitation-inhibition balance might be tilting towards an increased excitation, which could be one explanation for the onset of AIS shortening during this period. The resulting decrease in intrinsic excitability could homeostatically counteract the excitation-inhibition balance shift. Subsequently, the balance might reach a new equilibrium once excess excitatory synapses are being pruned, thus leading to the slight elongation after P21 (Fig. 6). Of note, the observed changes in synapse number occurred both in supra- and infragranular layers, thus explaining the decrease in AIS length for both layer II/III and V in the present study. An electrophysiological study by Stern at al. investigated the

maturation of receptive fields in layer II/III during this period. Interestingly, whereas synaptic responses were undetectable at P12, they were suddenly present at P14 and already resembled receptive field properties (Stern et al., 2001). At P20, neurons then showed mature receptive fields and firing rates. Thus, this study highlights the rapidity of circuit formation and maturation during the second and third postnatal week.

Another study demonstrated that indeed the critical periods of layer IV to layer II/III synapses as well as horizontal layer II/III to layer II/III coincide with the end of the second postnatal week: Wen and Bart used a plasticity paradigm in which all but one whisker is trimmed bilaterally ("single whisker experience") (Wen and Barth, 2011). 24 h after the trimming, induced postsynaptic potentials were measured in acute slices by stimulating in either layer IV or layer II/III. The authors found a strengthening of connections in the spared whisker between P12 and P14 for layer IV to layer II/III synapses and between P13 and P16 for layer II/III synapses (Wen and Barth, 2011). The overall increase in synaptic input during development is reflected in the studies recordings of spontaneous synaptic events, which increase in their frequency after P15 (Fig. 12E). The finding that synaptic amplitude is reduced at P28, is puzzling at first glance (Fig. 12F). However, the recordings were not done under pharmacological isolation of currents and the holding potential was relatively close to the chloride reversal potential. Therefore, excitatory and inhibitory inputs cannot be distinguished, which might be an explanation for this apparent discrepancy to previous studies.

Sensory deprivation between P9 and P14, but not from P15 – P20 alters the structure of layer II/III receptive fields (Stern et al., 2001). Consequently, the formation of synaptic connections in layer II/III highly depends on sensory input from P12 and P16. In the present study, I found a clear effect of sensory deprivation on presynaptic input to layer II/III neurons: Long-term deprivation from P0 to P15 increased the frequency and decreased the amplitude of EPSCs (Fig. 23A). Mice start actively whisking and exploring their environment during this period: Around P10, C57/Bl6 mice develop a strong increase in symmetric whisking behaviour (Arakawa and Erzurumlu, 2015). At P14, this whisking becomes "active", a term describing bundled, directed whisking movements towards an object that is being explored. It is likely that the resulting increase in activity from the periphery triggers synapse formation and strengthening of excitatory inputs in layer II/III.

Other structures that are most likely influential during AIS development are Chandelier cell (ChC) synapses. A recent study provided intriguing first evidence that formation of

ChC synapses onto the AIS of excitatory cortical neurons coincides with the AIS plasticity profile that was observed here: Using a transgenic mouse line, Pan-Vasquez et al. imaged ChCs *in vivo* over time during S1BF development (Pan-Vazquez et al., 2020). The authors uncovered a developmental window during which the typical cartridges of synaptic boutons onto the AIS of pyramidal neurons rapidly begin to emerge (P12-P18). Under conditions of increased network activity during this period, the number of synapses and the resulting postsynaptic responses decreased. If the same experiment was performed in older mice (P40-P46), it did not trigger any reduction of bouton numbers. Interestingly, the developmental period where these connections are formed and refined coincides with the period of AIS shortening that was observed in the present study (Fig. 6). This suggests a possible relationship between these two forms of homeostatic plasticity: The formation of ChC synapses might trigger AIS shortening or both processes might be driven by the same developmental program. However, it remains to be investigated in which way these AIS-centred mechanisms influence each other and how activity shapes the entire process. On a physiological level, the ChC study added to the mounting evidence that GABAergic synapses undergo a developmental switch from being excitatory during development to being inhibitory in the adult brain (Ben-Ari, 2002). This offers another compelling explanation for the AIS shortening observed in the present study. If ChC synapses rapidly start forming after P12 and are excitatory at first, this indicates a shift towards excitation. AIS shortening would counteract this shift in a homeostatic manner, since it would lower excitability levels and therefore normalize firing levels in light of the increased input.

Taken together, AIS shortening could be a result of the increase in overall excitation and sensory input in the maturing barrel cortex circuit.

4.6 AIS shortening is accompanied by a shift in intrinsic excitability in layer II//III

After uncovering that morphological alterations of the AIS coincided with a proposed shift in excitation/inhibition balance at network level, the next question was whether the change in AIS length would also be reflected in changes to intrinsic excitability of individual neurons at different ages. Strikingly, substantial changes in passive and active properties were observed when comparing electrophysiological parameters at P15, P21, and P28 (Fig. 10, 11, 12). These findings indicate that overall, RMP is slightly

hyperpolarized (Table 16), whereas the voltage threshold is remarkably stable over time (Fig. 11C), resulting in an increased current to threshold (Fig. 11B). Additionally, APs become slightly broader and their amplitude increases. However, the overall maximal kinetics of AP initiation are similar at P15 vs P28, as reflected by the unchanged phase plane plots (Fig. 12). As outlined in the introduction, AP shape is modulated by the presence and activation of K_vs such as K_v1 (Kole et al., 2007) and voltage threshold is determined by the activation kinetics of Na_vs at the AIS (Hu et al., 2009). In this study, the expression of ion channels over time was not investigated since reliable antibodies for quantitative approaches in immunofluorescence are lacking. In the future, possible alternative approaches using methods to genetically tag ion channels at the AIS might provide some insight into the pending question whether the ion channel composition at the AIS indeed mediates the observed changes in AP properties.

In a study that used similar paradigms and time points to the current study, Maravall et al. studied the intrinsic excitability of layer II/III neurons at the second and third postnatal week (Maravall et al., 2004) (Table 17). The authors measured firing properties of these neurons in acute slices at P12, P14, and P17 and found that over this time course, the spiking properties changed from phasic firing with rapid spike adaptation to regular spiking with little to no adaptation. Whereas at P12 only 20% of neurons were regular spiking, at P17 already 80% were regular spiking. Additionally, passive membrane properties and spiking properties changed: R_{In} decreased from ~250 MΩ to ~170 MΩ and voltage threshold decreased by about 2 mV. There was also a trend for an increase in the maximum slope of the I/f curve during development (Maravall et al., 2004). In the present study, electrophysiological properties of two developmental age groups (P13-P16 vs P19-P22) were measured. However, the time points were shifted a few days as compared to Maravall et al. Intriguingly, when comparing these time points, in the current study there is a trend towards altered excitability: RMP is reduced from ~ –82 mV to ~ –87 mV and R_{In} is reduced from ~ 300 MΩ to ~ 130 MΩ (Table 15). This is accompanied by a decrease in excitability as indicated by an increase in current threshold (Fig. 11A, B), and current at the maximum slope of the I/f curve (Fig. 10). These findings are supported by the Maravall et al study, which indicates that gradually, there is a shift towards reduced excitability during the second and third week of postnatal development.

4.7 Effect of sensory deprivation on barrel cortex development

Ever since the ground-breaking visual deprivation experiments of Hubel and Wiesel, we know that the correct development of sensory systems depends on input driven by sensory stimuli (Wiesel and Hubel, 1963). These early studies inspired deprivation studies in the S1BF, which intended to investigate experience-dependent plasticity in a comparable manner. As opposed to the visual cortex, however, where visual input was initially omitted by suturing of one eye, early deprivation studies in S1 often consisted of lesions to the whisker pad (Loos and Woolsey, 1973). This form of deprivation was not only completely blocking sensory dependent activity, but also spontaneous activity by damaging the afferent pathway. As a result, rather drastic morphological changes were observed, with entire barrel columns disappearing (Loos and Woolsey, 1973). Consequently, deprivation paradigms later shifted to less invasive methods like whisker plucking or trimming. In turn, this meant that the deprivation was only partial since pressure to the whisker pad during huddling and sucking activity would still elicit APs in the tactile receptors of the snout. Consequently, more subtle effects of deprivation on intracortical wiring and synaptic plasticity could be investigated. Critical periods for synaptic plasticity of individual layers were described (Fox, 1992; Wen and Barth, 2011). Additionally, it was discovered that the properties of the peripheral areas to which an individual neuron responds ("receptive fields") are determined during early development and shaped by sensory input (Lee et al., 2009; Shoykhet et al., 2005; Stern et al., 2001). Table 17 summarizes the most important findings from whisker deprivation studies conducted so far.

Table 17 Representative whisker deprivation studies

Authors	Species	Type of deprivation	Time points	Observation
(Loos and Woolsey, 1973)	mouse	Vibrissal injury	P0 to P12 - P43	Barrels of injured vibrissae disappear
(Fox, 1992)	rat	Whisker plucking All whiskers, D1 spared	From P2/P4/P7 to P20 or P90 (day of recording)	Critical period for layer IV synaptic plasticity from P0-P4, critical period for layer II/III until P7
(Stern et al., 2001)	rat	whisker trimming, unilateral	From P9, recording at P14 and P20	Reorganization of receptive fields, small amplitude centre, broad surround

(Maravall et al., 2004)	rat	Whisker trimming, unilateral	Trimming from P9 until P12, P14 and P17 respectively	Delayed maturation of intrinsic properties and spiking
(Shoykhet et al., 2005)	rat	Whisker trimming, unilateral	Trimming from either P0 or P12, for 40-45 days, followed by regrowth	Enlarged excitatory and weakened inhibitory receptive fields in layer IV
(Lee et al., 2009)	rat	Whisker trimming, bilateral	P0-P3, testing at P30	Receptive fields enlarged, larger dendritic tree, spine density increased
(Wimmer et al., 2010)	rat	Whisker trimming All whiskers, 1 – 3 spared on one side from C and D rows	Trimming from P0-7, P21, P42 and P96	Decreased thalamocortical innervation of deprived barrels, no critical period, reversibility of effect upon whisker regrowth
(Marik et al., 2010)	mouse	Whisker plucking, rows D and E	Plucking for various amounts of days	Reorganisation of excitatory and inhibitory axons in deprived columns
(Wen and Barth, 2011)	mouse	Whisker trimming, all but one whisker (SWE)	age P11 to P17, 24 h	Increased synaptic strength between P12 to P14 in layer II/III and IV

In summary, most studies so far focused the effect of deprivation on receptive field properties and synaptic strength, whereas studies on axonal compartments other than presynaptic boutons are rather sparse (Marik et al., 2010; Wimmer et al., 2010) (Table 17). In this context, the present study is to the best of my knowledge the first to investigate the effect of whisker deprivation on AIS morphology, providing correlation with neuronal function.

In the study already described under 5.5, Maravall et al. also investigated whether deprivation had any effect on the developmental changes in intrinsic excitability. Surprisingly, the authors did not find any changes in deprived neurons and thus suggested that instead of a dependence on sensory input, an independent, intrinsically mediated shift of excitability occurs (Maravall et al., 2004). However, one must consider two facts in this context. First, the authors only started the deprivation at P9. Data from this study indicates that deprivation just from P10 to P15 does not lead to any significant AIS length changes (Fig. 14). Thus, the length and time points of deprivation paradigms the authors used might have not been sufficient to trigger any detectable changes to intrinsic excitability. Second, as in the present study, the authors used the

paradigm of whisker trimming for sensory deprivation, which only reduces but not abolishes sensory input. Hence, the remaining sensory input might suffice to trigger the developmental shift in excitability. The same conclusion can be reached in the present study, since deprivation reduced, but not prevented the developmental AIS shortening. Yet, whereas at P15 differences in the firing properties of deprived neurons were detected, these differences were gone at P21 (Fig. 19, Fig. 20). This finding supports the notion that the shift in intrinsic excitability is independent of sensory input, and could be intrinsically regulated, e.g. via genetic programs. In the context of the literature cited here, an important factor to keep in mind is that most deprivation studies were conducted in rats (Table 17). In general, mice and rats have comparable cerebral developmental profiles, however, the time course and velocity of their profiles may not always overlap completely.

4.8 Reversibility of AIS plasticity under physiological conditions

Many studies have uncovered critical periods for developmental processes, during which sensory input it essential for normal development. If sensory input is taken away during these periods, the resulting alterations are irreversible and cannot be rescued by later restoration of sensory input.

It was initially hypothesized that deprivation during development might also trigger irreversible AIS remodeling during certain periods. Surprisingly, the findings show that even after long-term deprivation for 15 days, subsequent restoration of whisker input via regrowth of whiskers completely rescued AIS length (Fig. 15). In fact, shorter deprivation periods failed to even elicit any detectable AIS length changes (Fig. 14). The data suggests that a critical period for AIS plasticity does not exist in S1BF, as it does for the primary visual cortex (Gutzmann et al., 2014). This was further corroborated by experiments in adult animals (> P100), in which a period of 16 days of whisker trimming resulted in AIS length changes (Fig. 15). These relatively mild and reversible changes to AIS length are in opposition to previous studies, where AIS morphology was dramatically altered by experimental interventions (Baalman et al., 2013; Grubb and Burrone, 2010; Kuba et al., 2010). Upon closer examination, these experimental interventions were not reflecting a physiological brain state but came rather close to or even actively tried to mimic a pathological environment by permanent and severe alterations of activity (irreversible sensory deprivation, pathophysiological hyperexcitation). The whisker trimming paradigm that was employed here is far less

invasive in terms of altered neuronal function. In fact, it is something that will even occur during normal rodent behavior (known as “barbering”) by cage mates (Garner et al., 2004). Additionally, whisker trimming still preserves a partial sensory input since whisker follicles remain intact and are activated during huddling and sucking.
In summary, one can conclude that AIS tend to remain at a stable, intermediate length under physiological conditions. However, when sensory input is continuously reduced, AIS will elongate to stabilize neuronal excitability and input/output function. In this context, the present data provide compelling evidence for the hypothesis that AIS plasticity serves as a homeostatic mechanism to adapt to altered sensory input *in vivo*.

4.9 Mechanistic implications of developmental AIS plasticity

With this study, it was demonstrated that during cortical development *in vivo*, AIS plasticity occurs in the form of length changes. This adds to the increasing amount of evidence suggesting that *in vivo*, it is most likely the length rather than AIS position that is being altered, since a shift of the AIS onset has only been demonstrated *in vitro* so far (Evans et al., 2015; Grubb and Burrone, 2010). As outlined in section 1.5, the underlying mechanism for AIS plasticity remains elusive. Based on the current knowledge on AIS structure and assembly, one can only speculate how AIS elongation and shortening might be regulated during development. Since the structural markers for AIS length were either ßIV-spectrin or ankG, it is likely that the total amount of protein available will affect total AIS length. Indeed, as shown by Western blot data, changes in protein expression levels correlate to structural changes. Most notably, the expression profile of the giant isoform of ankG, previously termed the ‘master organizer’ of the AIS, follows the development profile of the AIS length: Initially, expression of all isoforms increases after birth. While the 190 kDa isoform further increases towards adulthood, the 480 kDa isoform is downregulated (Fig. 9E)
This could point towards a functional link. However, there are a few confounding factors. First, ankG is also expressed at noR (Jenkins et al., 2015; Kordeli et al., 1995). Thus, with increased myelination of the neocortex, as measured by an increase in MBP, ankG levels will also increase due to higher numbers of noR. Second, ankG is also expressed at synapses: The 190 kDa and 270 kDa have been found to be localized at spines, where they are important for AMPA receptor clustering (Smith et al., 2014). The giant isoform on the other hand forms nanodomains in the soma and dendritic shaft, where GABAergic synapses are localized (Tseng et al., 2015). Thus,

the variations in expressions could also be in part mediated by synapse formation or pruning. However, based on immunofluorescence, most proteins are probably present at the AIS due to its relatively large size and the high local density of the scaffold.
Interestingly, protein expression differed after deprivation. At P15, where AIS are elongated, expression of the 480 kDa isoform was reduced. However, over time, the expression increased significantly for both βIV-spectrin and 480 kDa ankG.
Another suggestion about the possible mechanism of AIS elongation comes from the analysis of the length histograms: When comparing the length profiles at P15 in controls and the deprivation group (Fig. 13E), it is evident that in the deprived group, the population distribution is broader, especially because of a subpopulation with extremely long AIS (>50 µm). This indicates that instead of all AIS elongating evenly, it seems that it is rather a subgroup of neurons undergoes extreme AIS remodeling while others keep their AIS length constant. Thus, AIS elongation occurs in a subset of neurons, most likely in those who are affected the most by sensory deprivation.
This study provides strong experimental support for the hypothesis that AIS plasticity is triggered by changes of neuronal activity, thereby contributing to the regulation of neuronal input-output relations. However, by which pathway these two are linked is elusive to date and remains a matter of speculation. One likely messenger is Calcium (Ca^{2+}). As outlined in section 1.5, both T- and L-type Ca_Vs have been identified at the AIS (Bender and Trussell, 2009). Evans et al. found that blocking the L-type Ca_V, as well as the Ca^{2+}-sensitive phosphatase Calcineurin, abolished activity-dependent plasticity *in vitro* (Evans et al., 2015). Additionally, the presence of calcium stores located at the AIS, termed the cisternal organelle (CO), increases the likelihood of Ca^{2+} playing a role in triggering or regulating AIS plasticity. The CO expresses the sarco/ER Ca^{2+} ATPase (SERCA) type 1 Ca^{2+} pump, the inositol 1,4,5-trisphosphate (IP3) receptor Ca^{2+} channel (IP3R), and the ryanodine receptor (Ry receptors), indicating that the CO is involved in Ca^{2+}-dependent Ca^{2+} release (Berridge, 1998). Intriguingly, the CO undergoes structural remodeling during visual cortex development and after sensory deprivation: During development, the number of CO clusters, as measured by expression of CO-specific protein synaptopodin (synpo), initially increase until P15, thus following the AIS lengthening during this period (Schlüter et al., 2017). Cluster size however stays stable. Remarkably, when mice are reared in the dark, the number of clusters remains unchanged, while cluster size is significantly increased, suggesting

an activity-dependent mechanism that regulates CO size and, potentially, calcium release (Schlüter et al., 2017).

4.10 AIS plasticity in the adult brain

One of the most surprising findings of this study was the fact that AIS plasticity could be induced in adult/mature brains. This is, to the best of my knowledge, the first direct evidence that AIS plasticity is not limited to development, but could be a physiological homeostatic mechanism in fully developed circuits in order to still be able to adapt to changes to sensory input. In the current literature, AIS plasticity is either described in dissociated or organotypic cultures *in vitro* on in developing brains *in vivo*. In dissociated hippocampal cultures, increased activity leads to AIS shortening (Evans et al., 2013; Grubb and Burrone, 2010), whereas in cultures of the olfactory bulb, dopaminergic interneurons show an inverted plasticity with AIS lengthening after an activity increase (Chand et al., 2015). *In vivo*, auditory deprivation in chickens, via removal of the cochlea, lead to an elongation of AIS in the auditory brainstem nuclei and an increased excitability, as well as altered K_v distribution (Kuba et al., 2010, 2015). However, the authors did not try to deprive adult chickens of auditory input in any of the follow up studies. In another study conducted in the auditory system, Kim et al. decided to test whether structural AIS plasticity would occur in the medial nucleus of the trapezoid body of adult mice when these experienced a sudden hearing loss by blast exposure (Kim et al., 2019). Indeed, AIS length was significantly elongated in these mice. However, this paradigm is again a relatively extreme, pathological insult to sensory input. When the authors applied more physiological stimuli such as mild sound stimulation for a week, no AIS plasticity was observed (Kim et al., 2019). Thus, it had not been demonstrated whether activity-dependent AIS plasticity was also a feature of mature cortices under physiological conditions and if so, to which extent.

As is true for other homeostatic mechanisms, plasticity in the adult brain is present, yet reduced in comparison to juvenile or immature brains. Here, whereas a period of 16 days of deprivation via daily whisker trimming led to an average increase of about 4 µm in new-born mouse pups (Fig. 13), the same amount of time only elicited a length change of 2.4 µm in adult mice (Fig. 16). This is in agreement with other structural changes in the somatodendritic and distal axonal compartment, where plasticity is reduced, but still detectable. For example, both bouton and spine dynamics markedly decrease with age (Jamann et al., 2018; Paola et al., 2006; Trachtenberg et al., 2002).

However, as this is the first evidence for adult AIS plasticity, and it only occurred in layer II/III, further studies are necessary to uncover in which other brain regions and layers and under which circumstances AIS plasticity is retained in adulthood.

4.11 Activity-dependent AIS plasticity and its effect on neuronal excitability

By correlating the observed structural changes to electrophysiological measurements of excitability, the data shows that altered AIS morphology is associated with neuronal firing properties. This is clearly in in accordance with the current literature and expands on the field by providing the first *in vivo* data in this context. As detailed in section 1.5, two hallmark studies were the first to describe this correlation (Grubb and Burrone, 2010; Kuba et al., 2010). Table 18 summarizes the findings of these two studies, which are placed in direct context of the present study. Remarkably, although overall results support each other, some noteworthy differences are apparent. In all three studies, current threshold and thus neuronal excitability is altered. However, in the initial studies, the changes to current threshold are more pronounced (30% vs 22% in the present study, Fig. 20B). One possible explanation could be that the methods used to induce AIS plasticity were far more drastic in the two studies: Grubb and Burrone used an *in vitro* model, which by its nature does not correspond to an intact circuit. Second, the neurons were subjected to a period of 12 h of sustained extracellular potassium levels to 15 mM, which is nonphysiological. Although the authors do not show the exact frequencies at which the neurons fire during this period, one can assume that they far exceed any physiological range *in vivo*. Kuba et al. on the other hand did use an *in vivo* system. However, sensory input was completely and irreversibly abolished by removing the avian cochlea after birth. In the present study a less invasive approach was chosen to reduce sensory input, which leaves the sensory pathway including the sensory receptors intact. Thus, a certain amount of activity (e.g. via pressure to the snout) could still be elicited. This in turn would explain why the observed changes to AIS plasticity and excitability are more subtle and therefore probably closer to a physiological situation. In the previous two studies, there were no indications if and how RMP was altered between groups. This could have major implications for firing properties, since depolarized neurons remain at a RMP closer to threshold and would therefore be more excitable. In the present study, although there was a trend towards a more depolarized RMP, no significant changes were detected in the deprived neurons (Table 16).

When comparing AP properties, Kuba et al. found strong alterations in AP shape: Voltage threshold was decreased and AP amplitude and max dV/dt were increased, with an especially strong effect on the amplitude, which nearly doubled. In the present study, no alterations of the AP waveform were observed (Fig. 22), which could again be due to the less invasive deprivation paradigm. In contrast, when looking at spontaneous EPSCs, Kuba et al. found no changes at the synaptic level. In the present study, synaptic frequency increased, whereas the amplitude of synaptic events decreased. Further studies will have to address if and when alterations to synaptic input correlate with AIS plasticity and how these two forms of homeostatic plasticity interact with each other.

Table 18 Comparison of changes of key electrophysiological parameters following AIS plasticity

	(Kuba et al., 2010)	**(Grubb and Burrone, 2010)**	**Present study: P15 Dep vs Ctrl**
RMP	n/A	n/A	no change
R_M	n/A	Decrease, ~150 MΩ	no change
Current threshold	Decrease, ~1000 pA (infinite step), ~30%	Increase, ~100 pA, ~30% (20 ms step)	Decrease, ~40 pA (20ms step), ~22%
Voltage threshold	Decrease, ~4 mV	n/A	no change
AP amplitude	Increase, ~1.8 x	n/A	no change
AP half width	n/A	n/A	no change
Firing frequency	n/A	n/A	Increased close to threshold, max difference at 100 pA, ~ 5 Hz
Max dV/dt (soma peak)	Increased, ~100 V/s	n/A	No change
sEPSCs amplitude	no change	n/A	Decrease, ~ 20 %
sEPSC frequency	no change	n/A	Increase, ~ 50 %

None of the original studies compared firing frequencies between control and treated neurons. Thus, the present study is the first to demonstrate that although the frequencies close to threshold are increased in deprived neurons, the maximum firing frequencies are not affected by AIS plasticity (Fig. 19). Finally, a correlation analysis of AIS length and current threshold found a significant correlation between the two

parameters (Fig. 21). This is a particularly exciting novel finding, since it indicates that current threshold is tightly controlled by AIS length. Therefore, this finding strongly supports the hypothesis that AIS plasticity serves to regulate neuronal excitability, acting as a homeostatic mechanism.

4.11.1 Axonal microdomain plasticity is crucial for network function

What do the present findings about AIS plasticity add to our understanding of how neurons work together in functional networks? Decades of research have mainly focused on neuronal “input” domains, namely spines and dendrites and how their function is essential for integration of a multitude of signals (Magee and Johnston, 2005; Nimchinsky et al., 2002). The AIS on the other hand is an axonal microdomain and the site of spike initiation. As such, it is the key “output” device for neuronal signaling. Thus, it is the prime location to directly influence and modify neuronal firing patterns. By shifting intrinsic excitability, AIS plasticity therefore shapes how neurons communicate with each other, which will have major implications for how neuronal networks function overall. In this context, the study’s findings add to the increasing amount of evidence that AIS plasticity actively shapes circuits in light of alterations to sensory or possibly also other forms of input. Most importantly, it could show that a moderate, physiological deprivation paradigm is sufficient to trigger sustained and substantial AIS plasticity in the form of AIS elongation (Fig. 13). Such forms of AIS plasticity might occur in the network as a whole to dampen overall excitability. On the other hand, AIS plasticity might also occur in a subset of neurons receiving increased input, which could serve to fine-tune local microcircuits and the role of their different players. Additionally, when AIS plasticity is perturbed in the context of disease, normal network function might be severely disrupted (Buffington and Rasband, 2011). This could explain why malfunction of AIS-specific channels or proteins are associated with such severe diseases as epilepsy, schizophrenia, and bipolar disorder (Ferreira et al., 2008; Schulze et al., 2008; Wimmer et al., 2010b). Overall, my thesis adds another layer of complexity to the question how neuronal input-output relations are regulated to ensure normal network function. Consequently, understanding and investigating AIS plasticity is and continues to be a fascinating and fundamental area of neurophysiological research.

5 SUMMARY

The axon initial segment (AIS) is an axonal microdomain characterized by its unique molecular composition of scaffolding proteins that tether voltage gated ion channels to the axonal membrane. Due to the resulting high density of sodium channels (Na_V), the AIS is the site of action potential initiation in neurons. In 2010, two hallmark studies were the first to demonstrate that AIS could shift in their position relative to the soma and vary their length. Electrophysiological experiments suggested that AIS plasticity occurred to enable neurons to homeostatically adapt to changes in synaptic input by adapting their intrinsic excitability. Experimental and modelling data indicated that longer and more proximal AIS would lead to a lowering of firing threshold and thus an increase in neuronal excitability. In a study conducted in the visual cortex AIS plasticity during development was investigated and a striking, triphasic pattern was observed: Initially, AIS length steadily increased after birth. After eye-opening at P14, AIS length rapidly shortened and later reached an intermediate length in mature animals. Rearing animals in the dark prevented developmental AIS shortening, suggesting an activity-dependent mechanism. It remained unclear however, whether developmental AIS plasticity could also be observed during the development in other sensory cortices. Furthermore, it was unclear whether the observed structural changes would also lead to changes in intrinsic excitability and firing properties of cortical pyramidal neurons. Thus, in the present study, it was aimed to characterize AIS plasticity during the development of the murine somatosensory barrel field (S1BF), the cortical area representing the whiskers on the contralateral snout. Because of its unique somatotopic organisation, where every whisker is represented in a separate cortical column, S1BF structure, function, and connectivity have been extremely well characterized. Here, a combination of immunofluorescence, confocal imaging, Western blotting, and electrophysiology was used to uncover if AIS structure and function change during S1BF development. Additionally, whisker deprivation experiments were employed to investigate whether the observed developmental changes were dependent on sensory input. A remarkable refinement of AIS structure during S1BF development was uncovered. Using antibodies against the main scaffolding proteins Ankyrin G (ankG) and ßIV-spectrin, AIS length changes and protein expression profiles in layer II/III and layer V of S1BF were traced during early development. It was found that AIS length initially increases in both layers. This was

accompanied by a significant increase of all three brain specific isoforms of ankG as well as ßIV-spectrin. After the onset of active whisking at P12, when pups start actively exploring their environment, a shortening of AIS length in both layers was observed. Subsequently, AIS length reached maturity around P45. Strikingly, all isoforms except the “giant” ankG isoform (480 kDa) were strongly upregulated after the second postnatal week, whereas 480 kDa isoform expression was downregulated, thus following the developmental length profile. On a functional level, AIS length reduction lead to an increase in firing threshold from P15 to P28 as reflected by a decrease of firing frequencies. Next, it was asked whether whisker trimming from birth would alter the observed developmental plasticity. Indeed, sensory deprivation elicited a significant increase in AIS length in layer II/III, but not layer V. This effect was more pronounced during early development and accompanied by a significant increase in excitability. Over time, AIS remained longer than the control group even at P45, although the length difference was not as pronounced as at earlier time points. This indicated a partial dependence of developmental AIS plasticity on sensory input. This was further supported by the fact that allowing whiskers to regrow after P21 restored mature AIS length, indicating that there is no critical period of AIS plasticity during development. Additionally, shorter periods of deprivation (5 days) did not elicit any detectable AIS length changed. Remarkably, when a two-week deprivation paradigm in adult animals was applied, a significant AIS length increase in layer II/III occurred, indicating that AIS plasticity is not confined to development but also a feature of mature cortical networks. Taken together, this study provides strong evidence that AIS plasticity in the form of length changes and protein expression alterations occurs during development, but also in the mature animal. Sensory deprivation lead to an increase in AIS length, which was accompanied by an increase in firing rates. Strikingly, the present study found a strong correlation between AIS length and AP current threshold, suggesting that AIS length is a strong predictor of AP threshold. The findings strongly support the hypothesis that AIS plasticity serves as a homeostatic mechanism to regulate neuronal excitability in response to prolonged changes in synaptic drive.

6 REFERENCES

Agmon, A., Yang, L., O'Dowd, D., and Jones, E. (1993). Organized growth of thalamocortical axons from the deep tier of terminations into layer IV of developing mouse barrel cortex. J Neurosci *13*, 5365–5382.

Aiken, S.P., Lampe, B.J., and Brown, B.S. (1995). Reduction of spike frequency adaptation and blockade of M-current in rat CA1 pyramidal neurones by linopirdine (DuP 996), a neurotransmitter release enhancer. Brit J Pharmacol *115*, 1163–1168.

Arakawa, H., and Erzurumlu, R.S. (2015). Role of whiskers in sensorimotor development of C57BL/6 mice. Behav Brain Res *287*, 146–155.

Armstrong-James, M., Fox, K., and Das-Gupta, A. (1992). Flow of excitation within rat barrel cortex on striking a single vibrissa. J Neurophysiol *68*, 1345–1358.

Baalman, K.L., Cotton, R.J., Rasband, S.N., and Rasband, M.N. (2013). Blast Wave Exposure Impairs Memory and Decreases Axon Initial Segment Length. J Neurotraum *30*, 741–751.

Battefeld, A., Tran, B.T., Gavrilis, J., Cooper, E.C., and Kole, M.H.P. (2014). Heteromeric Kv7.2/7.3 Channels Differentially Regulate Action Potential Initiation and Conduction in Neocortical Myelinated Axons. J Neurosci *34*, 3719–3732.

Ben-Ari, Y. (2002). Excitatory actions of gaba during development: the nature of the nurture. Nat Rev Neurosci *3*, 728–739.

Bender, K.J., and Trussell, L.O. (2009). Axon Initial Segment Ca2+ Channels Influence Action Potential Generation and Timing. Neuron *61*, 259–271.

Bender, K.J., Ford, C.P., and Trussell, L.O. (2010). Dopaminergic Modulation of Axon Initial Segment Calcium Channels Regulates Action Potential Initiation. Neuron *68*, 500–511.

Benned-Jensen, T., Christensen, R.K., Denti, F., Perrier, J.-F., Rasmussen, H.B., and Olesen, S.-P. (2016). Live Imaging of Kv7.2/7.3 Cell Surface Dynamics at the Axon Initial Segment: High Steady-State Stability and Calpain-Dependent Excitotoxic Downregulation Revealed. J Neurosci *36*, 2261–2266.

Bennett, V., and Baines, A.J. (2001). Spectrin and Ankyrin-Based Pathways: Metazoan Inventions for Integrating Cells Into Tissues. Physiol Rev *81*, 1353–1392.

Bennett, V., Baines, A.J., and Davis, J.Q. (1985). Ankyrin and synapsin: Spectrin-binding proteins associated with brain membranes. J Cell Biochem *29*, 157–169.

Berghs, S., Aggujaro, D., Dirkx, R., Maksimova, E., Stabach, P., Hermel, J.-M., Zhang, J.-P., Philbrick, W., Slepnev, V., Ort, T., et al. (2000). βiv Spectrin, a New Spectrin Localized at Axon Initial Segments and Nodes of Ranvier in the Central and Peripheral Nervous System. J Cell Biology *151*, 985–1002.

Berridge, M.J. (1998). Neuronal Calcium Signaling. Neuron *21*, 13–26.

Beurel, E., Grieco, S.F., and Jope, R.S. (2015). Glycogen synthase kinase-3 (GSK3): Regulation, actions, and diseases. Pharmacol Therapeut *148*, 114–131.

Blythe, S.N., Wokosin, D., Atherton, J.F., and Bevan, M.D. (2009). Cellular Mechanisms Underlying Burst Firing in Substantia Nigra Dopamine Neurons. J Neurosci *29*, 15531–15541.

Boiko, T., Rasband, M.N., Levinson, S.R., Caldwell, J.H., Mandel, G., Trimmer, J.S., and Matthews, G. (2001). Compact Myelin Dictates the Differential Targeting of Two Sodium Channel Isoforms in the Same Axon. Neuron *30*, 91–104.

Boiko, T., Wart, A.V., Caldwell, J.H., Levinson, S.R., Trimmer, J.S., and Matthews, G. (2003). Functional Specialization of the Axon Initial Segment by Isoform-Specific Sodium Channel Targeting. J Neurosci *23*, 2306–2313.

Bourg, A. van der, Yang, J.-W., Reyes-Puerta, V., Laurenczy, B., Wieckhorst, M., Stüttgen, M.C., Luhmann, H.J., and Helmchen, F. (2016). Layer-Specific Refinement of Sensory Coding in Developing Mouse Barrel Cortex. Cereb Cortex.

Bourg, A. van der, Yang, J., Stüttgen, M.C., Reyes-Puerta, V., Helmchen, F., and Luhmann, H.J. (2019). Temporal refinement of sensory-evoked activity across layers in developing mouse barrel cortex. Eur J Neurosci *50*, 2955–2969.

Bréchet, A., Fache, M.-P., Brachet, A., Ferracci, G., Baude, A., Irondelle, M., Pereira, S., Leterrier, C., and Dargent, B. (2008). Protein kinase CK2 contributes to the organization of sodium channels in axonal membranes by regulating their interactions with ankyrin G. J Cell Biology *183*, 1101–1114.

Brette, R. (2013). Sharpness of Spike Initiation in Neurons Explained by Compartmentalization. Plos Comput Biol *9*, e1003338.

Buffington, S.A., and Rasband, M.N. (2011). The axon initial segment in nervous system disease and injury. Eur J Neurosci *34*, 1609–1619.

Bureau, I., Paul, F. von S., and Svoboda, K. (2006). Interdigitated Paralemniscal and Lemniscal Pathways in the Mouse Barrel Cortex. Plos Biol *4*, e382.

Byers, T.J., and Branton, D. (1985). Visualization of the protein associations in the erythrocyte membrane skeleton. Proc National Acad Sci *82*, 6153–6157.

Cajal, S.R. y (1911). Histologie du système nerveux de l'homme et des vertébrés.

Callewaert, G., Eilers, J., and Konnerth, A. (1996). Axonal calcium entry during fast 'sodium' action potentials in rat cerebellar Purkinje neurones. J Physiology *495*, 641–647.

Catterall, W. (1981). Localization of sodium channels in cultured neural cells. J Neurosci *1*, 777–783.

Catterall, W.A. (2011). Voltage-Gated Calcium Channels. Csh Perspect Biol *3*, a003947.

Catterall, W.A., Goldin, A.L., and Waxman, S.G. (2005). International Union of Pharmacology. XLVII. Nomenclature and Structure-Function Relationships of Voltage-Gated Sodium Channels. Pharmacol Rev *57*, 397–409.

Chand, A.N., Galliano, E., Chesters, R.A., and Grubb, M.S. (2015). A Distinct Subtype of Dopaminergic Interneuron Displays Inverted Structural Plasticity at the Axon Initial Segment. J Neurosci *35*, 1573–1590.

Chen, S., Owens, G.C., Makarenkova, H., and Edelman, D.B. (2010). HDAC6 Regulates Mitochondrial Transport in Hippocampal Neurons. Plos One *5*, e10848.

Chernoff, G.F. (1981). Shiverer: an autosomal recessive mutant mouse with myelin deficiency. J Hered *72*, 128–128.

Cotel, F., Exley, R., Cragg, S.J., and Perrier, J.-F. (2013). Serotonin spillover onto the axon initial segment of motoneurons induces central fatigue by inhibiting action potential initiation. Proc National Acad Sci *110*, 4774–4779.

Cruz, D.A., Lovallo, E.M., Stockton, S., Rasband, M., and Lewis, D.A. (2009). Postnatal development of synaptic structure proteins in pyramidal neuron axon initial segments in monkey prefrontal cortex. J Comp Neurol *514*, 353–367.

Davis, J.Q., and Bennett, V. (1994). Ankyrin binding activity shared by the neurofascin/L1/NrCAM family of nervous system cell adhesion molecules. J Biological Chem *269*, 27163–27166.

Davis, L.H., and Bennett, V. (1990). Mapping the binding sites of human erythrocyte ankyrin for the anion exchanger and spectrin. J Biological Chem *265*, 10589–10596.

D'Este, E., Kamin, D., Göttfert, F., El-Hady, A., and Hell, S.W. (2015). STED Nanoscopy Reveals the Ubiquity of Subcortical Cytoskeleton Periodicity in Living Neurons. Cell Reports *10*, 1246–1251.

Devaux, J.J., Kleopa, K.A., Cooper, E.C., and Scherer, S.S. (2004). KCNQ2 Is a Nodal K+ Channel. J Neurosci *24*, 1236–1244.

Ding, Y.-Q., Yin, J., Xu, H.-M., Jacquin, M.F., and Chen, Z.-F. (2003). Formation of Whisker-Related Principal Sensory Nucleus-Based Lemniscal Pathway Requires a Paired Homeodomain Transcription Factor, Drg11. J Neurosci *23*, 7246–7254.

Dodson, P.D., Barker, M.C., and Forsythe, I.D. (2002). Two Heteromeric Kv1 Potassium Channels Differentially Regulate Action Potential Firing. J Neurosci *22*, 6953–6961.

Doyle, D.A., Cabral, J.M., Pfuetzner, R.A., Kuo, A., Gulbis, J.M., Cohen, S.L., Chait, B.T., and MacKinnon, R. (1998). The Structure of the Potassium Channel: Molecular Basis of K+ Conduction and Selectivity. Science *280*, 69–77.

Duflocq, A., Bras, B.L., Bullier, E., Couraud, F., and Davenne, M. (2008). Nav1.1 is predominantly expressed in nodes of Ranvier and axon initial segments. Mol Cell Neurosci *39*, 180–192.

Durham, D., and Woolsey, T.A. (1984). Effects of neonatal whisker lesions on mouse central trigeminal pathways. J Comp Neurology *223*, 424–447.

Engelhardt, M., Vorwald, S., Sobotzik, J.-M., Bennett, V., and Schultz, C. (2013). Ankyrin-B structurally defines terminal microdomains of peripheral somatosensory axons. Brain Struct Funct *218*, 1005–1016.

Engelhardt, M., Jamann, N., and Wefelmeyer, W. (2019). Small domain, large consequences: the axon initial segment as a key player in neuronal excitability. Neuroforum *25*, 49–60.

Erzurumlu, R.S., and Gaspar, P. (2012). Development and critical period plasticity of the barrel cortex. Eur J Neurosci *35*, 1540–1553.

Evans, M.D., Sammons, R.P., Lebron, S., Dumitrescu, A.S., Watkins, T.B.K., Uebele, V.N., Renger, J.J., and Grubb, M.S. (2013). Calcineurin Signaling Mediates Activity-Dependent Relocation of the Axon Initial Segment. J Neurosci *33*, 6950–6963.

Evans, M.D., Dumitrescu, A.S., Kruijssen, D.L.H., Taylor, S.E., and Grubb, M.S. (2015). Rapid Modulation of Axon Initial Segment Length Influences Repetitive Spike Firing. Cell Reports *13*, 1233–1245.

Feldmeyer, D., Brecht, M., Helmchen, F., Petersen, C.C.H., Poulet, J.F.A., Staiger, J.F., Luhmann, H.J., and Schwarz, C. (2013). Barrel cortex function. Prog Neurobiol *103*, 3–27.

Ferreira, M.A.R., O'Donovan, M.C., Meng, Y.A., Jones, I.R., Ruderfer, D.M., Jones, L., Fan, J., Kirov, G., Perlis, R.H., Green, E.K., et al. (2008). Collaborative genome-wide association analysis supports a role for ANK3 and CACNA1C in bipolar disorder. Nat Genet *40*, 1056–1058.

Fox, K. (1992). A critical period for experience-dependent synaptic plasticity in rat barrel cortex. J Neurosci *12*, 1826–1838.

Fried, S.I., Lasker, A.C.W., Desai, N.J., Eddington, D.K., and Rizzo, J.F. (2009). Axonal Sodium-Channel Bands Shape the Response to Electric Stimulation in Retinal Ganglion Cells. J Neurophysiol *101*, 1972–1987.

Gallo, G. (2013). More than one ring to bind them all: Recent insights into the structure of the axon. Dev Neurobiol *73*, 799–805.

Garner, J.P., Dufour, B., Gregg, L.E., Weisker, S.M., and Mench, J.A. (2004). Social and husbandry factors affecting the prevalence and severity of barbering ('whisker trimming') by laboratory mice. Appl Anim Behav Sci *89*, 263–282.

Garver, T.D., Ren, Q., Tuvia, S., and Bennett, V. (1997). Tyrosine Phosphorylation at a Site Highly Conserved in the L1 Family of Cell Adhesion Molecules Abolishes Ankyrin Binding and Increases Lateral Mobility of Neurofascin. J Cell Biology *137*, 703–714.

Gentet, L.J., and Williams, S.R. (2007). Dopamine Gates Action Potential Backpropagation in Midbrain Dopaminergic Neurons. J Neurosci *27*, 1892–1901.

Glazewski, S., and Fox, K. (1996). Time course of experience-dependent synaptic potentiation and depression in barrel cortex of adolescent rats. J Neurophysiol *75*, 1714–1729.

Goethals, S., and Brette, R. (2020). Theoretical relation between axon initial segment geometry and excitability. Elife *9*, e53432.

Goldberg, E.M., Clark, B.D., Zagha, E., Nahmani, M., Erisir, A., and Rudy, B. (2008). K+ Channels at the Axon Initial Segment Dampen Near-Threshold Excitability of Neocortical Fast-Spiking GABAergic Interneurons. Neuron *58*, 387–400.

Goldin, A.L., Barchi, R.L., Caldwell, J.H., Hofmann, F., Howe, J.R., Hunter, J.C., Kallen, R.G., Mandel, G., Meisler, M.H., Netter, Y.B., et al. (2000). Nomenclature of Voltage-Gated Sodium Channels. Neuron *28*, 365–368.

Golshani, P., Gonçalves, J.T., Khoshkhoo, S., Mostany, R., Smirnakis, S., and Portera-Cailliau, C. (2009). Internally Mediated Developmental Desynchronization of Neocortical Network Activity. J Neurosci *29*, 10890–10899.

Grubb, M.S., and Burrone, J. (2010). Activity-dependent relocation of the axon initial segment fine-tunes neuronal excitability. Nature *465*, 1070.

Gulbis, J.M., Zhou, M., Mann, S., and MacKinnon, R. (2000). Structure of the Cytoplasmic β Subunit--T1 Assembly of Voltage-Dependent K+ Channels. Science *289*, 123–127.

Gulledge, A.T., and Bravo, J.J. (2016). Neuron Morphology Influences Axon Initial Segment Plasticity. Eneuro *3*, ENEURO.0085-15.2016.

Gutman, G.A., Chandy, K.G., Adelman, J.P., Aiyar, J., Bayliss, D.A., Clapham, D.E., Covarriubias, M., Desir, G.V., Furuichi, K., Ganetzky, B., et al. (2003). International Union of Pharmacology. XLI. Compendium of Voltage-Gated Ion Channels: Potassium Channels. Pharmacol Rev *55*, 583–586.

Gutzmann, A., Ergül, N., Grossmann, R., Schultz, C., Wahle, P., and Engelhardt, M. (2014). A period of structural plasticity at the axon initial segment in developing visual cortex. Front Neuroanat *8*, 11.

Hamada, M.S., and Kole, M.H.P. (2015). Myelin Loss and Axonal Ion Channel Adaptations Associated with Gray Matter Neuronal Hyperexcitability. J Neurosci *35*, 7272–7286.

Hamada, M.S., Goethals, S., Vries, S.I. de, Brette, R., and Kole, M.H.P. (2016). Covariation of axon initial segment location and dendritic tree normalizes the somatic action potential. Proc National Acad Sci *113*, 14841–14846.

Hanemaaijer, N.A., Popovic, M.A., Wilders, X., Grasman, S., Arocas, O.P., and Kole, M.H. (2020). Ca2+ entry through NaV channels generates submillisecond axonal Ca2+ signaling. Elife *9*, e54566.

Harterink, M., Vocking, K., Pan, X., Jerez, E.M.S., Slenders, L., Fréal, A., Tas, R.P., Wetering, W.J. van de, Timmer, K., Motshagen, J., et al. (2019). TRIM46 Organizes Microtubule Fasciculation in the Axon Initial Segment. J Neurosci *39*, 4864–4873.

Häusser, M., Stuart, G., Racca, C., and Sakmann, B. (1995). Axonal initiation and active dendritic propagation of action potentials in substantia nigra neurons. Neuron *15*, 637–647.

He, J., Zhou, R., Wu, Z., Carrasco, M.A., Kurshan, P.T., Farley, J.E., Simon, D.J., Wang, G., Han, B., Hao, J., et al. (2016). Prevalent presence of periodic actin–spectrin-based membrane skeleton in a broad range of neuronal cell types and animal species. Proc National Acad Sci *113*, 6029–6034.

Hedstrom, K.L., Ogawa, Y., and Rasband, M.N. (2008). AnkyrinG is required for maintenance of the axon initial segment and neuronal polarity. J Cell Biology *183*, 635–640.

Hensch, T.K. (2005). Critical period plasticity in local cortical circuits. Nat Rev Neurosci *6*, 877–888.

Höfflin, F., Jack, A., Riedel, C., Mack-Bucher, J., Roos, J., Corcelli, C., Schultz, C., Wahle, P., and Engelhardt, M. (2017). Heterogeneity of the Axon Initial Segment in Interneurons and Pyramidal Cells of Rodent Visual Cortex. Front Cell Neurosci *11*, 332.

Howard, A., Tamas, G., and Soltesz, I. (2005). Lighting the chandelier: new vistas for axo-axonic cells. Trends Neurosci *28*, 310–316.

Hu, W., Tian, C., Li, T., Yang, M., Hou, H., and Shu, Y. (2009). Distinct contributions of Nav1.6 and Nav1.2 in action potential initiation and backpropagation. Nat Neurosci *12*, 996–1002.

Hund, T.J., Koval, O.M., Li, J., Wright, P.J., Qian, L., Snyder, J.S., Gudmundsson, H., Kline, C.F., Davidson, N.P., Cardona, N., et al. (2010). A βIV-spectrin/CaMKII signaling complex is essential for membrane excitability in mice. J Clin Invest *120*, 3508–3519.

Inda, M.C., DeFelipe, J., and Muñoz, A. (2006). Voltage-gated ion channels in the axon initial segment of human cortical pyramidal cells and their relationship with chandelier cells. P Natl Acad Sci Usa *103*, 2920–2925.

Jamann, N., Jordan, M., and Engelhardt, M. (2018). Activity-dependent axonal plasticity in sensory systems. Neuroscience *368*, 268–282.

Jamann, N., Dannehl, D., Wagener, R., Corcelli, C., Schultz, C., Staiger, J., Kole, M.H.P., and Engelhardt, M. (2020). Sensory input drives rapid homeostatic scaling of the axon initial segment in mouse barrel cortex. Biorxiv 2020.02.27.968065.

Jarnot, M.D., and Corbett, A.M. (1995). High titer antibody to mammalian neuronal sodium channels produces sustained channel block. Brain Res *674*, 159–162.

Jenkins, S.M., and Bennett, V. (2001). Ankyrin-G coordinates assembly of the spectrin-based membrane skeleton, voltage-gated sodium channels, and L1 CAMs at Purkinje neuron initial segments. J Cell Biology *155*, 739–746.

Jenkins, P.M., Kim, N., Jones, S.L., Tseng, W.C., Svitkina, T.M., Yin, H.H., and Bennett, V. (2015). Giant ankyrin-G: A critical innovation in vertebrate evolution of fast and integrated neuronal signaling. Proc National Acad Sci *112*, 957–964.

Jiang, B., Trevino, M., and Kirkwood, A. (2007). Sequential Development of Long-Term Potentiation and Depression in Different Layers of the Mouse Visual Cortex. J Neurosci *27*, 9648–9652.

Khazipov, R., and Luhmann, H.J. (2006). Early patterns of electrical activity in the developing cerebral cortex of humans and rodents. Trends Neurosci *29*, 414–418.

Khirug, S., Yamada, J., Afzalov, R., Voipio, J., Khiroug, L., and Kaila, K. (2008). GABAergic Depolarization of the Axon Initial Segment in Cortical Principal Neurons Is Caused by the Na–K–2Cl Cotransporter NKCC1. J Neurosci *28*, 4635–4639.

Kim, E.J., Feng, C., Santamaria, F., and Kim, J.H. (2019). Impact of Auditory Experience on the Structural Plasticity of the AIS in the Mouse Brainstem Throughout the Lifespan. Front Cell Neurosci *13*, 456.

Knaus, H.-G., Eberhart, A., Glossmann, H., Munujos, P., Kaczorowski, G.J., and Garcia, M.L. (1994). Pharmacology and structure of high conductance calcium-activated potassium channels. Cell Signal *6*, 861–870.

Kobayashi, T., Storrie, B., Simons, K., and Dotti, C.G. (1992). A functional barrier to movement of lipids in polarized neurons. Nature *359*, 647–650.

Kole, M.H., and Brette, R. (2018). The electrical significance of axon location diversity. Curr Opin Neurobiol *51*, 52–59.

Kole, M.H.P., and Stuart, G.J. (2012). Signal Processing in the Axon Initial Segment. Neuron *73*, 235–247.

Kole, M.H.P., Letzkus, J.J., and Stuart, G.J. (2007). Axon Initial Segment Kv1 Channels Control Axonal Action Potential Waveform and Synaptic Efficacy. Neuron *55*, 633–647.

Kole, M.H.P., Ilschner, S.U., Kampa, B.M., Williams, S.R., Ruben, P.C., and Stuart, G.J. (2008). Action potential generation requires a high sodium channel density in the axon initial segment. Nat Neurosci *11*, 178–186.

Kordeli, E., Lambert, S., and Bennett, V. (1995). Ankyrin A NEW ANKYRIN GENE WITH NEURAL-SPECIFIC ISOFORMS LOCALIZED AT THE AXONAL INITIAL SEGMENT AND NODE OF RANVIER. J Biol Chem *270*, 2352–2359.

Kosaka, T. (1983). Axon initial segments of the granule cell in the rat dentate gyrus: synaptic contacts on bundles of axon initial segments. Brain Res *274*, 129–134.

Kress, G.J., Dowling, M.J., Eisenman, L.N., and Mennerick, S. (2010). Axonal sodium channel distribution shapes the depolarized action potential threshold of dentate granule neurons. Hippocampus *20*, 558–571.

Kuba, H., and Ohmori, H. (2009). Roles of axonal sodium channels in precise auditory time coding at nucleus magnocellularis of the chick. J Physiology *587*, 87–100.

Kuba, H., Ishii, T.M., and Ohmori, H. (2006). Axonal site of spike initiation enhances auditory coincidence detection. Nature *444*, 1069.

Kuba, H., Oichi, Y., and Ohmori, H. (2010). Presynaptic activity regulates Na+ channel distribution at the axon initial segment. Nature *465*, 1075.

Kuba, H., Yamada, R., Ishiguro, G., and Adachi, R. (2015). Redistribution of Kv1 and Kv7 enhances neuronal excitability during structural axon initial segment plasticity. Nat Commun *6*, 8815.

Kunimoto, M. (1995). A neuron-specific isoform of brain ankyrin, 440-kD ankyrinB, is targeted to the axons of rat cerebellar neurons. J Cell Biology *131*, 1821–1829.

Laatsch, R.H., and Cowan, W.M. (1966). Electron microscopic studies of the dentate gyrus of the rat. I. Normal structure with special reference to synaptic organization. J Comp Neurol *128*, 359–395.

Lee, L.-J., Chen, W.-J., Chuang, Y.-W., and Wang, Y.-C. (2009). Neonatal whisker trimming causes long-lasting changes in structure and function of the somatosensory system. Exp Neurol *219*, 524–532.

Leite, S.C., and Sousa, M.M. (2016). The neuronal and actin commitment: Why do neurons need rings? Cytoskeleton *73*, 424–434.

Leite, S.C., Sampaio, P., Sousa, V.F., Nogueira-Rodrigues, J., Pinto-Costa, R., Peters, L.L., Brites, P., and Sousa, M.M. (2016). The Actin-Binding Protein α-Adducin Is Required for Maintaining Axon Diameter. Cell Reports *15*, 490–498.

Lendvai, B., Stern, E.A., Chen, B., and Svoboda, K. (2000). Experience-dependent plasticity of dendritic spines in the developing rat barrel cortex in vivo. Nature *404*, 876–881.

León-Espinosa, G., Antón-Fernández, A., Tapia-González, S., DeFelipe, J., and Muñoz, A. (2018). Modifications of the axon initial segment during the hibernation of the Syrian hamster. Brain Struct Funct *223*, 4307–4321.

Leterrier, C., Potier, J., Caillol, G., Debarnot, C., Rueda Boroni, F., and Dargent, B. (2015). Nanoscale Architecture of the Axon Initial Segment Reveals an Organized and Robust Scaffold. Cell Reports *13*, 2781–2793.

Lewis, D.A., Hashimoto, T., and Volk, D.W. (2005). Cortical inhibitory neurons and schizophrenia. Nat Rev Neurosci *6*, nrn1648.

Loos, H.V.D. (1976). Barreloids in mouse somatosensory thalamus. Neurosci Lett *2*, 1–6.

Loos, H.V. der, and Woolsey, T.A. (1973). Somatosensory Cortex: Structural Alterations following Early Injury to Sense Organs. Science *179*, 395–398.

Lorincz, A., and Nusser, Z. (2008). Cell-Type-Dependent Molecular Composition of the Axon Initial Segment. J Neurosci *28*, 14329–14340.

Lübke, J., Egger, V., Sakmann, B., and Feldmeyer, D. (2000). Columnar Organization of Dendrites and Axons of Single and Synaptically Coupled Excitatory Spiny Neurons in Layer 4 of the Rat Barrel Cortex. J Neurosci *20*, 5300–5311.

Ma, P.M., and Woolsey, T.A. (1984). Cytoarchitectonic correlates of the vibrissae in the medullary trigeminal complex of the mouse. Brain Res *306*, 374–379.

Magee, J.C., and Johnston, D. (2005). Plasticity of dendritic function. Curr Opin Neurobiol *15*, 334–342.

Maravall, M., Stern, E.A., and Svoboda, K. (2004). Development of Intrinsic Properties and Excitability of Layer 2/3 Pyramidal Neurons During a Critical Period for Sensory Maps in Rat Barrel Cortex. J Neurophysiol *92*, 144–156.

Marik, S.A., Yamahachi, H., McManus, J.N.J., Szabo, G., and Gilbert, C.D. (2010). Axonal Dynamics of Excitatory and Inhibitory Neurons in Somatosensory Cortex. Plos Biol *8*, e1000395.

Martinello, K., Huang, Z., Lujan, R., Tran, B., Watanabe, M., Cooper, E.C., Brown, D.A., and Shah, M.M. (2015). Cholinergic Afferent Stimulation Induces Axonal Function Plasticity in Adult Hippocampal Granule Cells. Neuron *85*, 346–363.

McEwen, D.P., and Isom, L.L. (2004). Heterophilic Interactions of Sodium Channel β1 Subunits with Axonal and Glial Cell Adhesion Molecules. J Biol Chem *279*, 52744–52752.

Meza, R.C., López-Jury, L., Canavier, C.C., and Henny, P. (2018). Role of the Axon Initial Segment in the Control of Spontaneous Frequency of Nigral Dopaminergic Neurons In Vivo. J Neurosci *38*, 733–744.

Michaely, P., and Bennett, V. (1992). The ANK repeat: a ubiquitous motif involved in macromolecular recognition. Trends Cell Biol *2*, 127–129.

Michaely, P., and Bennett, V. (1993). The membrane-binding domain of ankyrin contains four independently folded subdomains, each comprised of six ankyrin repeats. J Biological Chem *268*, 22703–22709.

Michaely, P., and Bennett, V. (1995). Mechanism for Binding Site Diversity on Ankyrin:: COMPARISON OF BINDING SITES ON ANKYRIN FOR NEUROFASCIN AND THE Cl/HCO 3 ANION EXCHANGER. J Biol Chem *270*, 31298–31302.

Micheva, K.D., and Beaulieu, C. (1996). Quantitative aspects of synaptogenesis in the rat barrel field cortex with special reference to GABA circuitry. J Comp Neurology *373*, 340–354.

Nimchinsky, E.A., Sabatini, B.L., and Svoboda, K. (2002). Structure and Function of Dendritic Spines. Annu Rev Physiol *64*, 313–353.

Osterheld-Haas, M.C., and Hornung, J.P. (1996). Laminar development of the mouse barrel cortex: effects of neurotoxins against monoamines. Exp Brain Res *110*, 183–195.

Palay, S.L., Sotelo, C., Peters, A., and Orkand, P.M. (1968). THE AXON HILLOCK AND THE INITIAL SEGMENT. J Cell Biology *38*, 193–201.

Pan, Z., Kao, T., Horvath, Z., Lemos, J., Sul, J.-Y., Cranstoun, S.D., Bennett, V., Scherer, S.S., and Cooper, E.C. (2006). A Common Ankyrin-G-Based Mechanism Retains KCNQ and NaV Channels at Electrically Active Domains of the Axon. J Neurosci *26*, 2599–2613.

Pan-Vazquez, A., Wefelmeyer, W., Sabater, V.G., Neves, G., and Burrone, J. (2020). Activity-Dependent Plasticity of Axo-axonic Synapses at the Axon Initial Segment. Neuron *106*, 265-276.e6.

Paola, V.D., Holtmaat, A., Knott, G., Song, S., Wilbrecht, L., Caroni, P., and Svoboda, K. (2006). Cell Type-Specific Structural Plasticity of Axonal Branches and Boutons in the Adult Neocortex. Neuron *49*, 861–875.

Peters, A. (1966). THE NODE OF RANVIER IN THE CENTRAL NERVOUS SYSTEM. Q J Exp Physiol Cms *51*, 229–236.

Peters, A., Proskauer, C.C., and Kaiserman-Abramof, I.R. (1968). THE SMALL PYRAMIDAL NEURON OF THE RAT CEREBRAL CORTEX The Axon Hillock and Initial Segment. J Cell Biology *39*, 604–619.

Pierret, T., Lavallée, P., and Deschênes, M. (2000). Parallel Streams for the Relay of Vibrissal Information through Thalamic Barreloids. J Neurosci *20*, 7455–7462.

Rasband, M.N. (2010). The axon initial segment and the maintenance of neuronal polarity. Nat Rev Neurosci *11*, 552.

Rasband, M.N., Trimmer, J.S., Schwarz, T.L., Levinson, S.R., Ellisman, M.H., Schachner, M., and Shrager, P. (1998). Potassium Channel Distribution, Clustering, and Function in Remyelinating Rat Axons. J Neurosci *18*, 36–47.

Rebsam, A., Seif, I., and Gaspar, P. (2002). Refinement of Thalamocortical Arbors and Emergence of Barrel Domains in the Primary Somatosensory Cortex: A Study of Normal and Monoamine Oxidase A Knock-Out Mice. J Neurosci *22*, 8541–8552.

Rice, F.L., Gomez, C., Barstow, C., Burnet, A., and Sands, P. (1985). AComparative analysis of the development of the primary somatosensory cortex: Interspecies similarities during barrel and laminar development. J Comp Neurology *236*, 477–495.

Royeck, M., Horstmann, M.-T., Remy, S., Reitze, M., Yaari, Y., and Beck, H. (2008). Role of Axonal NaV1.6 Sodium Channels in Action Potential Initiation of CA1 Pyramidal Neurons. J Neurophysiol *100*, 2361–2380.

Sanchez-Ponce, D., Muñoz, A., and Garrido, J.J. (2011). Casein kinase 2 and microtubules control axon initial segment formation. Mol Cell Neurosci *46*, 222–234.

Schafer, D.P., Jha, S., Liu, F., Akella, T., McCullough, L.D., and Rasband, M.N. (2009). Disruption of the Axon Initial Segment Cytoskeleton Is a New Mechanism for Neuronal Injury. J Neurosci *29*, 13242–13254.

Schlüter, A., Turco, D.D., Deller, T., Gutzmann, A., Schultz, C., and Engelhardt, M. (2017). Structural Plasticity of Synaptopodin in the Axon Initial Segment during Visual Cortex Development. Cereb Cortex *27*, 4662–4675.

Schlüter, A., Rossberger, S., Dannehl, D., Janssen, J.M., Vorwald, S., Hanne, J., Schultz, C., Mauceri, D., and Engelhardt, M. (2019). Dynamic Regulation of Synaptopodin and the Axon Initial Segment in Retinal Ganglion Cells During Postnatal Development. Front Cell Neurosci *13*, 318.

Schulze, T.G., Detera-Wadleigh, S.D., Akula, N., Gupta, A., Kassem, L., Steele, J., Pearl, J., Strohmaier, J., Breuer, R., Schwarz, M., et al. (2008). Two variants in Ankyrin 3 (ANK3) are independent genetic risk factors for bipolar disorder. Mol Psychiatr *14*, mp2008134.

Shah, M.M., Migliore, M., Valencia, I., Cooper, E.C., and Brown, D.A. (2008). Functional significance of axonal Kv7 channels in hippocampal pyramidal neurons. Proc National Acad Sci *105*, 7869–7874.

Shavkunov, A.S., Wildburger, N.C., Nenov, M.N., James, T.F., Buzhdygan, T.P., Panova-Elektronova, N.I., Green, T.A., Veselenak, R.L., Bourne, N., and Laezza, F. (2013). The Fibroblast Growth Factor 14·Voltage-gated Sodium Channel Complex Is a New Target of Glycogen Synthase Kinase 3 (GSK3). J Biol Chem *288*, 19370–19385.

Shoykhet, M., Land, P.W., and Simons, D.J. (2005). Whisker Trimming Begun at Birth or on Postnatal Day 12 Affects Excitatory and Inhibitory Receptive Fields of Layer IV Barrel Neurons. J Neurophysiol *94*, 3987–3995.

Skibinska, A., Glazewski, S., Fox, K., and Kossut, M. (2000). Age-dependent response of the mouse barrel cortex to sensory deprivation: a 2-deoxyglucose study. Exp Brain Res *132*, 134–138.

Smith, K.R., Kopeikina, K.J., Fawcett-Patel, J.M., Leaderbrand, K., Gao, R., Schürmann, B., Myczek, K., Radulovic, J., Swanson, G.T., and Penzes, P. (2014). Psychiatric Risk Factor ANK3/Ankyrin-G Nanodomains Regulate the Structure and Function of Glutamatergic Synapses. Neuron *84*, 399–415.

Sobotzik, J.-M., Sie, J.M., Politi, C., Turco, D.D., Bennett, V., Deller, T., and Schultz, C. (2009). AnkyrinG is required to maintain axo-dendritic polarity in vivo. Proc National Acad Sci *106*, 17564–17569.

Somogyi, P. (1977). A specific ‘axo-axonal’ interneuron in the visual cortex of the rat. Brain Res *136*, 345–350.

Somogyi, P., Smith, A., Nunzi, M., Gorio, A., Takagi, H., and Wu, J. (1983). Glutamate decarboxylase immunoreactivity in the hippocampus of the cat: distribution of immunoreactive synaptic terminals with special reference to the axon initial segment of pyramidal neurons. J Neurosci *3*, 1450–1468.

Soriano, E., and Frotscher, M. (1989). A GABAergic axo-axonic cell in the fascia dentata controls the main excitatory hippocampal pathway. Brain Res *503*, 170–174.

Srinivasan, J., Schachner, M., and Catterall, W.A. (1998). Interaction of voltage-gated sodium channels with the extracellular matrix molecules tenascin-C and tenascin-R. Proc National Acad Sci *95*, 15753–15757.

Staiger, J.F., Bisler, S., Schleicher, A., Gass, P., Stehle, J.H., and Zilles, K. (2000). Exploration of a novel environment leads to the expression of inducible transcription factors in barrel-related columns. Neuroscience *99*, 7–16.

Stainier, D.Y., and Gilbert, W. (1990). Pioneer neurons in the mouse trigeminal sensory system. Proc National Acad Sci *87*, 923–927.

Stern, E.A., Maravall, M., and Svoboda, K. (2001). Rapid Development and Plasticity of Layer 2/3 Maps in Rat Barrel Cortex In Vivo. Neuron *31*, 305–315.

Stuart, G.J., and Häusser, M. (2001). Dendritic coincidence detection of EPSPs and action potentials. Nat Neurosci *4*, 63–71.

Szabadics, J., Varga, C., Molnár, G., Oláh, S., Barzó, P., and Tamás, G. (2006). Excitatory Effect of GABAergic Axo-Axonic Cells in Cortical Microcircuits. Science *311*, 233–235.

Szwed, M., Bagdasarian, K., and Ahissar, E. (2003). Encoding of Vibrissal Active Touch. Neuron *40*, 621–630.

Tapia, M., Wandosell, F., and Garrido, J.J. (2010). Impaired Function of HDAC6 Slows Down Axonal Growth and Interferes with Axon Initial Segment Development. Plos One *5*, e12908.

Tapia, M., Puerto, A.D., Puime, A., Sánchez-Ponce, D., Fronzaroli-Molinieres, L., Pallas-Bazarra, N., Carlier, E., Giraud, P., Debanne, D., Wandosell, F., et al. (2013). GSK3 and β-catenin determines functional expression of sodium channels at the axon initial segment. Cell Mol Life Sci *70*, 105–120.

Thome, C., Kelly, T., Yanez, A., Schultz, C., Engelhardt, M., Cambridge, S.B., Both, M., Draguhn, A., Beck, H., and Egorov, A.V. (2014). Axon-Carrying Dendrites Convey Privileged Synaptic Input in Hippocampal Neurons. Neuron *83*, 1418–1430.

Tolner, E.A., Sheikh, A., Yukin, A.Y., Kaila, K., and Kanold, P.O. (2012). Subplate Neurons Promote Spindle Bursts and Thalamocortical Patterning in the Neonatal Rat Somatosensory Cortex. J Neurosci *32*, 692–702.

Tomassy, G.S., Berger, D.R., Chen, H.-H., Kasthuri, N., Hayworth, K.J., Vercelli, A., Seung, H.S., Lichtman, J.W., and Arlotta, P. (2014). Distinct Profiles of Myelin Distribution Along Single Axons of Pyramidal Neurons in the Neocortex. Science *344*, 319–324.

Trachtenberg, J.T., Chen, B.E., Knott, G.W., Feng, G., Sanes, J.R., Welker, E., and Svoboda, K. (2002). Long-term in vivo imaging of experience-dependent synaptic plasticity in adult cortex. Nature *420*, 788–794.

Trunova, S., Baek, B., and Giniger, E. (2011). Cdk5 Regulates the Size of an Axon Initial Segment-Like Compartment in Mushroom Body Neurons of the Drosophila Central Brain. J Neurosci *31*, 10451–10462.

Tseng, W.C., Jenkins, P.M., Tanaka, M., Mooney, R., and Bennett, V. (2015). Giant ankyrin-G stabilizes somatodendritic GABAergic synapses through opposing endocytosis of GABAA receptors. Proc National Acad Sci *112*, 1214–1219.

Tsushima, H., Emanuele, M., Polenghi, A., Esposito, A., Vassalli, M., Barberis, A., Difato, F., and Chieregatti, E. (2015). HDAC6 and RhoA are novel players in Abeta-driven disruption of neuronal polarity. Nat Commun *6*, 7781.

Vacher, H., Yang, J.-W., Cerda, O., Autillo-Touati, A., Dargent, B., and Trimmer, J.S. (2011). Cdk-mediated phosphorylation of the Kvβ2 auxiliary subunit regulates Kv1 channel axonal targeting. J Cell Biology *192*, 813–824.

Veinante, P., and Deschênes, M. (1999). Single- and Multi-Whisker Channels in the Ascending Projections from the Principal Trigeminal Nucleus in the Rat. J Neurosci *19*, 5085–5095.

Veinante, P., Lavallée, P., and Deschênes, M. (2000). Corticothalamic projections from layer 5 of the vibrissal barrel cortex in the rat. J Comp Neurol *424*, 197–204.

Wart, A.V., Trimmer, J.S., and Matthews, G. (2007). Polarized distribution of ion channels within microdomains of the axon initial segment. J Comp Neurol *500*, 339–352.

Wefelmeyer, W., Cattaert, D., and Burrone, J. (2015). Activity-dependent mismatch between axo-axonic synapses and the axon initial segment controls neuronal output. Proc National Acad Sci *112*, 9757–9762.

Wen, J.A., and Barth, A.L. (2011). Input-Specific Critical Periods for Experience-Dependent Plasticity in Layer 2/3 Pyramidal Neurons. J Neurosci *31*, 4456–4465.

Westrum, L.E. (1966). Synaptic Contacts on Axons in the Cerebral Cortex. Nature *210*, 1289.

Wiesel, T.N., and Hubel, D.H. (1963). SINGLE-CELL RESPONSES IN STRIATE CORTEX OF KITTENS DEPRIVED OF VISION IN ONE EYE. J Neurophysiol *26*, 1003–1017.

Wimmer, V.C., Broser, P.J., Kuner, T., and Bruno, R.M. (2010a). Experience-induced plasticity of thalamocortical axons in both juveniles and adults. J Comp Neurology *518*, 4629–4648.

Wimmer, V.C., Reid, C.A., Mitchell, S., Richards, K.L., Scaf, B.B., Leaw, B.T., Hill, E.L., Royeck, M., Horstmann, M.-T., Cromer, B.A., et al. (2010b). Axon initial segment dysfunction in a mouse model of genetic epilepsy with febrile seizures plus. J Clin Invest *120*, 2661–2671.

Winckler, B., Forscher, P., and Mellman, I. (1999). A diffusion barrier maintains distribution of membrane proteins in polarized neurons. Nature *397*, 698.

Woodruff, A.R., Anderson, S.A., and Yuste, R. (2010). The Enigmatic Function of Chandelier Cells. Front Neurosci-Switz *4*, 201.

Woodruff, A.R., McGarry, L.M., Vogels, T.P., Inan, M., Anderson, S.A., and Yuste, R. (2011). State-Dependent Function of Neocortical Chandelier Cells. J Neurosci *31*, 17872–17886.

Woolsey, T.A., and Loos, H.V. der (1970). The structural organization of layer IV in the somatosensory region (S I) of mouse cerebral cortex. Brain Res *17*, 205–242.

Woolsey, T.A., and Wann, J.R. (1976). Areal changes in mouse cortical barrels following vibrissal damage at different postnatal ages. J Comp Neurology *170*, 53–66.

Xu, K., Zhong, G., and Zhuang, X. (2013). Actin, Spectrin, and Associated Proteins Form a Periodic Cytoskeletal Structure in Axons. Science *339*, 452–456.

Yang, J.-W., Kilb, W., Kirischuk, S., Unichenko, P., Stüttgen, M.C., and Luhmann, H.J. (2018). Development of the whisker-to-barrel cortex system. Curr Opin Neurobiol *53*, 29–34.

Yellen, G. (2002). The voltage-gated potassium channels and their relatives. Nature *419*, 35.

Yin, L., Rasch, M.J., He, Q., Wu, S., Dou, F., and Shu, Y. (2017). Selective Modulation of Axonal Sodium Channel Subtypes by 5-HT1A Receptor in Cortical Pyramidal Neuron. Cereb Cortex *27*, 509–521.

Yizhar, O., Fenno, L.E., Prigge, M., Schneider, F., Davidson, T.J., O'Shea, D.J., Sohal, V.S., Goshen, I., Finkelstein, J., Paz, J.T., et al. (2011). Neocortical excitation/inhibition balance in information processing and social dysfunction. Nature *477*, 171–178.

Yoshimura, T., Kawano, Y., Arimura, N., Kawabata, S., Kikuchi, A., and Kaibuchi, K. (2005). GSK-3β Regulates Phosphorylation of CRMP-2 and Neuronal Polarity. Cell *120*, 137–149.

Yu, J., Fischman, D.A., and Steck, T.L. (1973). Selective solubilization of proteins and phospholipids from red blood cell membranes by nonionic detergents. J Supramol Str Cell *1*, 233–248.

Yu, Y., Maureira, C., Liu, X., and McCormick, D. (2010). P/Q and N Channels Control Baseline and Spike-Triggered Calcium Levels in Neocortical Axons and Synaptic Boutons. J Neurosci *30*, 11858–11869.

Yue, C., and Yaari, Y. (2004). KCNQ/M Channels Control Spike Afterdepolarization and Burst Generation in Hippocampal Neurons. J Neurosci *24*, 4614–4624.

Zhang, L.I., and Poo, M. (2001). Electrical activity and development of neural circuits. Nat Neurosci *4*, 1207–1214.

Zhang, X., and Bennett, V. (1996). Identification of O-Linked N-Acetylglucosamine Modification of AnkyrinG Isoforms Targeted to Nodes of Ranvier. J Biol Chem *271*, 31391–31398.

Zhou, D., Lambert, S., Malen, P.L., Carpenter, S., Boland, L.M., and Bennett, V. (1998). AnkyrinG Is Required for Clustering of Voltage-gated Na Channels at Axon Initial Segments and for Normal Action Potential Firing. J Cell Biology *143*, 1295–1304.

7 OWN PUBLICATIONS

Parts of this thesis are included in the following publications or are in preparation for publication.

7.1 Publications in peer-reviewed journals

Jamann, N., Dannehl, D., Lehmann, N., Wagener, R., Corcelli, C., Schultz, C., Staiger, J., Kole, M.H.P., and Engelhardt, M. (2020). Sensory input drives rapid homeostatic scaling of the axon initial segment in mouse barrel cortex. Biorxiv 2020.02.27.968065. In revision.

Engelhardt, M., **Jamann, N**., Wefelmeyer, W. (2019) Small domain, large consequences: the axon initial segment as a key player in neuronal excitability [published online ahead of print,15.12.2018]. Neuroforum. DOI: https://doi.org/10.1515/nf-2018-0023

Jamann, N.*, Jordan, M.*, and Engelhardt, M. (2018). Activity-dependent axonal plasticity in sensory systems. Neuroscience 368, 268–282. Shared authorship. Add https://doi.org/10.1016/j.neuroscience.2017.07.035

Engelhardt, M., Hamad, M., Jack, A., Ahmed, K., König, J., Rennau, L., **Jamann, N.**, Räk, A., Schönfelder, S., Riedel, C., Wirth, M.J., Grabert, J., Patz, S., Wahle, P. (2018) Interneuron synaptopathy in developing rat cortex induced by the pro-inflammatory cytokine LIF. Experimental Neurology 302:169-180 https://doi.org/10.1016/j.expneurol.2017.12.011

7.2 Conference Presentations

10/2018	Poster: Jamann, N., Dannehl, D., Maurer, J., Wagener, R., Kaiser, M., Corcelli, C., Schultz, C., Staiger, J., Engelhardt, M. A role for the axon initial segment in rapid modulation of neuronal input-output parameters in mouse barrel cortex. Axons in the Hills, Heidelberg, Germany.
11/2017	Poster: Jamann, N., Kaiser, M., Wagener, R., Maurer J., Corcelli, C., Staiger, J., Schultz, C., Engelhardt, M. Rapid and slow axon initial segment plasticity in the rodent somatosensory cortex. SfN Meeting, Washington, D.C., USA
09/2016	Talk: Short- and long-term plasticity of the axon initial segment in the mouse barrel cortex. International meeting of the German Anatomical Society, Göttingen, Germany
07/2016	Poster: Wahle, P., Hamad, M., Patz, S., Wirth, MJ., Grabert, J., König, J., Jamann, N., Jack, A., di Cristo, G., Maffei, L., Berardi, N., Engelhardt, M. Interneuron synaptopathy induced by the pro-inflammatory cytokine LIF in developing neocortex. 10th FENS Forum of Neuroscience, Copenhagen, Denmark

05/2016	Junior Talk: Plasticity of the axon initial segment in the mouse barrel cortex. Barrel Cortex Function, Amsterdam, The Netherlands
10/2015	Poster: Jamann, N., Corcelli, C., Schultz, C., Engelhardt, M. Structural plasticity of the axon initial segment after sensory deprivation in mouse somatosensory cortex. Neuroscience 2015, annual meeting of the Society for Neuroscience, Chicago, IL, USA
09/2015	Poster: Jamann, N., Corcelli, C., Schultz, C., Engelhardt, M. Structural plasticity of the axon initial segment during early development of the mouse somatosensory cortex. 110th annual meeting of the Anatomische Gesellschaft, Würzburg, Germany

8 SUPPLEMENTARY TABLES

Supplementary Table 1 P-values of multiple comparisons for AIS length during layer II/III development. ** indicates *P* < 0.0001.**

vs.	E20	P1	P3	P7	P10	P13	P15	P21	P28	P35	P45	P180
E20												
P1	0.836											
P3	0.826	0.985										
P7	0.003	****	****									
P10	****	****	****	****								
P13	****	****	****	****	0.022							
P15	****	****	****	****	0.003	0.966						
P21	****	****	****	****	0.566	****	****					
P28	****	****	****	****	0.966	0.005	0.0006	0.823				
P35	****	****	****	****	0.966	0.003	0.0004	0.836	0.985			
P45	****	****	****	0.029	0.007	****	****	0.554	0.027	0.037		
P180	****	****	****	0.566	****	****	****	0.022	0.0004	0.0006	0.8005	

Supplementary Table 2 *P*-values of multiple comparisons for AIS length during layer V development. ** indicates *P* < 0.0001. Significant results (*P* < 0.05 are marked in bold font).**

vs.	E20	P1	P3	P7	P10	P13	P15	P21	P28	P35	P45	P180
E20		0.0004	****	****	****	****	****	****	****	****	****	0.010
P1			0.918	****	****	****	****	0.528	0.373	0.088	0.984	0.984
P3				0.01	****	0.0002	0.0005	0.984	0.984	0.849	0.984	0.306
P7					0.003	0.984	0.984	0.056	0.096	0.373	0.003	****
P10						0.029	0.014	****	****	****	****	****
P13							0.984	0.002	0.004	0.029	****	****
P15								0.004	0.0089	0.054	****	****
P21									0.984	0.984	0.984	0.065
P28										0.984	0.983	0.035
P35											0.576	0.005
P45												0.538
P180												

Supplementary Table 3 P-values of multiple comparisons of protein expression during development.

	AnkG 190 kDa	**AnkG 270 kDa**	**AnkG** 480 kDa	**βIV-spectrin**
E20 vs. P1	0.9890	0.9930	0.8733	0.9589
E 20 vs. P3	0.9682	0.7633	0.6510	>0.9999
E20 vs. P7	>0.9999	0.9809	0.9155	0.9708
E20 vs. P10	>0.9999	>0.9999	0.6225	0.2882
E20 vs. P13	0.7608	0.3319	0.0486	0.0013
E20 vs. P15	0.1882	0.0805	0.0013	0.0016
E20 vs. P21	0.0650	0.0218	0.0302	<0.0001
E20 vs. P45	<0.0001	0.0002	0.0823	<0.0001
P1 vs. P3	>0.9999	0.9952	>0.9999	0.9788
P1 vs. P7	0.9991	>0.9999	>0.9999	>0.9999
P1 vs. P10	0.9709	0.9791	0.9999	0.8949
P1 vs. P13	0.2618	0.0785	0.5068	0.0133
P1 vs. P15	0.0343	0.0148	0.0238	0.0168
P1 vs. P21	0.0104	0.0038	0.3745	<0.0001
P1 vs. P45	<0.0001	<0.0001	0.6715	<0.0001
P3 vs. P7	0.9952	0.9988	0.9997	0.9860
P3 vs. P10	0.9330	0.6698	>0.9999	0.3455
P3 vs. P13	0.1970	0.0159	0.7577	0.0016
P3 vs. P15	0.0240	0.0028	0.0553	0.0020
P3 vs. P21	0.0072	0.0007	0.6186	<0.0001
P3 vs. P45	<0.0001	<0.0001	0.8868	<0.0001
P7 vs. P10	>0.9999	0.9544	0.9995	0.8690
P7 vs. P13	0.5937	0.0591	0.4401	0.0116
P7 vs. P15	0.1143	0.0109	0.0187	0.0147
P7 vs. P21	0.0372	0.0028	0.3176	<0.0001
P7 vs. P45	<0.0001	<0.0001	0.6016	<0.0001
P10 vs. P13	0.8411	0.4155	0.7830	0.1845
P10 vs. P15	0.2442	0.1091	0.0606	0.2232
P10 vs. P21	0.0880	0.0303	0.6471	0.0002
P10 vs. P45	<0.0001	0.0002	0.9040	<0.0001
P13 vs. P15	0.9634	0.9937	0.6905	>0.9999
P13 vs. P21	0.7354	0.8401	>0.9999	0.0655
P13 vs. P45	0.0002	0.0242	>0.9999	0.0006
P15 vs. P21	0.9995	0.9987	0.8199	0.0524
P15 vs. P45	0.0020	0.1219	0.5259	0.0004
P21 vs. P45	0.0066	0.3571	0.9998	0.3680

Supplementary Table 4 P-values of multiple comparisons of the input-frequency curves during development.

	P15 vs. P21	**P15 vs. P28**	**P21 vs. P28**
0 pA	>0.9999	>0.9999	>0.9999
50 pA	>0.9999	>0.9999	>0.9999
100 pA	0.6669	0.0010	0.0519
150 pA	0.1955	<0.0001	<0.0001
200 pA	0.1696	<0.0001	<0.0001

250 pA	0.1245	<0.0001	0.0001
300 pA	0.1029	<0.0001	0.0268
350 pA	0.3699	0.0131	0.3903
400 pA	0.4585	0.2299	>0.9999
450 pA	0.7038	>0.9999	>0.9999

Supplementary Table 5 Comparison of AIS length in V1 and S1 during development.

	Visual cortex		**Barrel cortex**	
	LII/III	**LV**	**LII/III**	**LV**
E20	25.03 ± 0.5	-	15.21 ± 1.42	-
P1	25.35 ± 2.23	22.77 ± 2.10	13.86 ± 0.65	20.49 ± 1.86
P3	26.24 ± 1.39	24.62 ± 1.62	14.01 ± 1.42	22.02 ± 2.11
P7	28.42 ± 2.04	25.45 ± 1.12	19.74 ± 1.14	26.39 ± 1.16
P10	37.59 ± 1.56	35.03 ± 2.78	27.24 ± 1.64	31.26 ± 1.10
P15	37.48 ± 2.76	33.57 ± 2.32	31.51 ± 1.72	27.24 ± 1.64
P21	31.30 ± 2.67	29.00 ± 3.79	25.29 ± 2.11	22.75 ± 1.87
P28	22.75 ± 2.58	20.61 ± 3.11	26.72 ± 1.85	23.02 ± 2.68
P35	30.52 ± 3.76	26.65 ± 1.77	26.56 ± 2.66	23.75 ± 2.39
>P45	30.44 ± 3.03	29.53 ± 1.67	23.29 ± 2.53	21.59 ± 2.42
>P180	30.69 ± 2.71	26.91 ± 1.34	21.76 ± 1.15	19.35 ± 1.31

Data are indicated as mean ± SD

Supplementary Table 6 Equipment Immunofluorescence

Equipment	**Name/Specification**	**Source**
Microscope 1	Confocal Microscope Laser wavelengths: 488 nm; 548 nm; 642 nm Objectives: Nikon Plan Apo VC 20x NA 0.75 oil immersion Nikon Plan Apo VC 60x NA 1.4 oil immersion	Nikon Instruments Europe, Düsseldorf, Germany
Microscope 2	Confocal Microscope Laser wavelengths: Ar 488 nm/ 20 mW and 514 nm / 20 mW, DPSS 561 nm/ 20 mW, HeNe 633 nm /10 mW Objective: VC 63x NA 1.4 oil immersion	Leica Biosystems, Wetzlar, Germany
Cryostat	Microm HM 550	Thermo Scientific, Waltham, USA

Glass slides	SuperFrost™	Thermo Scientific, Waltham, USA

Abbreviations: NA = numerical aperture

Supplementary Table 7 Equipment Western Blot

Equipment	Name	Source
Bradford essay plate reader	Infinite 200 PRO	Tecan Trading AG, Männedorf, Switzerland
Electrophoresis chamber	PerfectBlue Twin S dual gel system	VWR International, Vienna, Austria
Blotting chamber	Mini Trans-Blot™ Cell	BioRad, Hercules, USA
Acquisition chamber	Fusion Solo Chemiluminescence 4M	Vilber Lourmat, Eberhardzell, Germany
Acquisition software	Fusion solo	Vilber Lourmat, Eberhardzell, Germany

Supplementary Table 8 Equipment Electrophysiology

Equipment	Name	Source
Amplifier	EPC 10 USB	HEKA electronics GmbH, Lambrecht/Pfalz, Germany
Amplifier Software	PatchMaster 2x90	HEKA electronics GmbH, Lambrecht/Pfalz, Germany
Pipette Puller	P-97 Flaming/Brown micropipette puller	Sutter Instruments, Novato, USA
Vibratome	VT 1200 S	Leica Biosystems, Wetzlar, Germany
Microscope	ECLIPSE FN1 upright microscope, IR-DIC 10x objective water immersion NA 0.10, WD 3.5mm 40x objective, water immersion NA 0.80, WD 3.5mm	Nikon Instruments Europe, Düsseldorf, Germany
Camera	OrcaFlash 4.0 LT Scientific CMOS Microscopy Camera FL400-Sensor with 4.0 megapixels	Hamamatsu Photonics, Hamamatsu City, Japan
Light source	Photofluor LM-75	89 North, Williston, USA
Micromanipulator	Sensapex piezo-driven micromanipulator, SMX series	Sensapex, Oulu, Finland
XY Microscope Stage	MT-1000	Sutter Instruments, Novato, USA
Peristaltic pump	Reglo analog	Ismatec, Wertheim, Germany
Bath chamber	RC-27, rectangular ope bath chamber	Warner Instruments, Hamden, USA
Glass capillaries	GB 150F-10 0.86x1.50x100 mm Borosilicate glass with filament	Science products, Hofheim, Germany
Harp	HSG-5F harp slice grid	ALA Scientific Instruments, New York, USA

Supplementary table 9 Analysis and statistics software

Application	Software	Source
AIS length analysis	ImageJ 1.51	Wayne Rasband, NIH, USA
Image processing	Adobe Photoshop CS4	Adobe Inc., San José, USA
Western blot quantification	ImageJ 1.51	Wayne Rasband, NIH, USA
Electrophysiology data	FitMaster 2x90 Origin 8.0 Pro AxoGraph 1.7.2	HEKA electronics GmbH, Lambrecht/Pfalz, Germany OriginLab, Northampton, USA AxoGraph Scientific, John Clements, USA
Statistical analysis	SigmaPlot 12.5	Systat Software GmbH, Erkrath, Germany
Graphs	GraphPad Prism 5.0	GraphPad Software, San Diego, USA
Illustrations	Adobe Illustrator CS4	Adobe Inc., San José, USA
Citation manager	EndNote X9 ReadCube Papers	Clarivate Analytics, Jersey, USA ReadCube, Boston, USA

9 CURRICULUM VITAE

Personal details

Name: Nora Sophie Jamann
Father: Wolfgang Jamann
Mother: Christine Jamann

Date of Birth: May 8, 1992
Place of Birth: Berlin
Nationality: German

Education

10/2011 – 11/2018	Medical Studies, Heidelberg University, Medical Faculty Mannheim
11/2018	Third state examination, grade 2.0
10/2017	Second state examination, grade 2.0
10/2013	First state examination, grade 2.0
2002-2010	Christian-Wirth-School, Usingen
06/2010	German High-School Degree (Abitur), Grade 1.1
1999-2002	Grundschule “Am Hasenberg”, Neu-Anspach
1998-1999	Kenton College Preparatory School, Nairobi, Kenya

Professional experience and scientific education

02/2019 – present	PhD thesis Netherlands Institute for Neuroscience (NIN), Amsterdam Department of Cell biology, University of Utrecht Supervisor: Prof. Maarten Kole
2015-2020	MD thesis Mannheim Centre for Translational Neuroscience (MCTN) Institute for Neuroanatomy, Supervisors: Professor Christian Schultz, MD, Maren Engelhardt, PhD
2014/2015	Member of the “Junior Scientific Masterclass”, extracurricular courses for further training of scientifically interested and gifted students
2015-2018	Member of the College Journal Club, Mannheim
09/2014-12/2014	Three-month laboratory internship at the Centre for

	Biomedical Research, University Andres Bello, Santiago, Chile, Supervisor: Brigitte van Zundert, PhD
06/2012-01/2014	Student assistant in the research group „Genetic Epidemiology in Psychiatry", Central Institute for Mental Health, Mannheim

Grants and Awards

09/2016	1st place, Young Investigator Award, international meeting of the German Anatomical Society, Göttingen, Germany
10/2015	Travel grant, GlaxoSmithKline Foundation, SfN Meeting Chicago, IL, USA

10 ACKNOWLEDGEMENTS

First and foremost, I would like to thank Dr. Maren Engelhardt for her supervision during my thesis. Maren, you not only sparked my interest for axonal plasticity but also kept it alive through the amazing opportunities you provided me with and through your constant mental and advisory support. This project would not have been this unique learning experience without your guidance. Thank you for standing behind all my crazy ideas and wishes, taking me to 2 SfN meetings which were absolute bliss, and encouraging me to give talks and poster presentations. You are and continue to be an inspiration as a scientist and as a mentor and I hope our paths cross again many more times!

Thank you to Prof. Christian Schultz for giving me the opportunity to conduct the project in his lab and for providing me with funding to establish and learn several new techniques including an entire patch-clamp setup. Thank you also for the financial support for the participation in several national and international conferences, which were a great academic and personal experience for me.

Corinna and Silke, you were not also the best technicians one could wish for but also great company during the many hours at the bench. Thank you for teaching me how to work in the lab and thank you for your amazing support! I could never have done this thesis without your help. In addition, it was always great fun to come to the lab and listen to “Les Misérables” when Silke was in charge of the music or to have a chat during incubation times. I will greatly miss you and hope we stay in touch!

To the rest of the lab, the famous “Neuroschweine” group. Needless to say, how much fun it was to be part of this crazy lot and how much I enjoyed our lab outings, going to parties and many “Examensbälle” together and our skiing trip to Austria. Special thanks go to Dominik for patching the EE neurons, Merryn for taking over the VPA project and Johannes for programming the AISuite. I hope there are many more Neuroschweine adventures to come.

Lastly, I want to thank my family for always being by my side and giving me the opportunity to pursue my dream of becoming a neuroscientist. Mum and dad, you

always believed in my abilities and did not hesitate to finance my free semesters that I took to carry out the experiments full time. I am very lucky to have such supportive and loving parents and of course Leon, the best brother in the world.